An Early-Stage Decision-Making Framework for Mission-Oriented Offshore Patrol Vessel Hull Design Using Comparative Scaling Techniques and Multi-Objective Optimisation

MScThesis

Avishai Horsky

TU Delft

Thesis for the degree of MSc in Marine Technology in the specialization of Ship Design

An Early-Stage Decision-Making Framework for Mission-Oriented Offshore Patrol Vessel Hull Design Using Comparative Scaling Techniques and Multi-Objective Optimisation

MScThesis

by

Avishai Horsky

This thesis (MT.25/26.005.M) is classified as confidential in accordance with the general conditions for projects performed by the TUDelft.

to obtain the degree of Master of Science at the Delft University of Technology to be defended publicly on October 6, 2025

Student number:	6021514	
Place:	Faculty of Mechanical Engineering, Delft	
Chair:	Dr. A.A. Kana	TU Delft
Thesis committee:	Dr. A.A. Kana	TU Delft
	Dr.-Ing. C.Thill	TU Delft
	Z.P. Oikonomou	TU Delft
Project Duration:	December, 2024 - October, 2025	

An electronic version of this thesis is available at `http://repository.tudelft.nl/`.

TU Delft Delft University of Technology

Preface

This thesis marks the culmination of my Master of Science studies in Marine Technology at Delft University of Technology. The work presented here was carried out between December 2024 and October 2025 and reflects both an academic and a personal journey.

The research focuses on developing a mission-oriented decision-making framework for scaling Offshore Patrol Vessels (OPVs) using Multi-Objective Optimisation (MOO). The motivation stems from the increasing demand for versatile, efficient, and scalable naval platforms that can adapt to diverse missions and operational constraints. Throughout the project, I sought to bridge the gap between traditional scaling approaches and modern optimisation techniques, ultimately contributing to more robust early-stage design methodologies.

This thesis would not have been possible without the guidance and support of many people. I am deeply grateful to my supervisors, Dr. A.A. Kana and Dr.-Ing. C. Thill, for their invaluable feedback, encouragement, and patience throughout the research process. Their expertise in ship design and optimisation provided direction and clarity whenever challenges arose.

Having worked for the last seven years at Israel Shipyards Ltd. (ISL), I would like to express my sincere gratitude to the company and, in particular, to Daniel Charsky, Nir Almany, Shiran Purvin (Vice President Engineering), and Eitan Zucker (CEO), for their trust and belief in my capabilities. Without their support, this adventure would not have been possible.

Finally, I wish to thank my family. To my two children, Nim Raveh and Kfir Raveh, thank you for keeping me company through the many long nights of work. To my partner, Ofrat Raveh, I am deeply grateful for your patience, love, and unwavering support throughout these two intense years—you made this journey bearable and meaningful.

Acknowledgements

During the preparation of this work, the author used artificial intelligence (AI) assisted tools (including Claude, ChatGPT, Litmaps, Elicit) in order to manage and find relevant literature, refine technical explanations, refine writing and enhance readability. All content generated with the assistance of these tools was carefully reviewed and edited by the author, who takes full responsibility for the final content of this publication.

Abstract

This thesis develops and demonstrates a mission-oriented, early-stage design framework for mid-size (40–90 [m]) Offshore Patrol Vessels (OPVs). The approach integrates hybrid scaling (geometric and targeted parametric variation) with multi-objective optimisation (MOO) in a Systems Engineering / Set-Based Design (SE–SBD) workflow. A parametric parent-hull model was implemented in CAESES and varied in principal dimensions and selected hull parameters. Performance was evaluated using Holtrop–Mennen resistance, intact-stability (GZ) analysis, and strip-theory RAOs aggregated into a multi-heading Seakeeping Index (SKI). The optimisation process combines Design of Experiments (DoE), surrogate modelling, and a MOGA-based global search. Objectives reflect key drivers (SKI, Stability Index (SI), total resistance R_T, and lightweight LWT), while feasibility is enforced through GM/B limits, roll-period (T_{roll}), and a range constraint.

Verification through hypervolume convergence and trend analysis confirmed robust optimisation behaviour, while validation against tank, CFD, and stability booklet data for a 45 [m] reference OPV demonstrated geometric fidelity and early-stage accuracy. The framework efficiently generates Pareto sets that reveal trade-offs between endurance, comfort, stability, resistance, and weight, supporting mission-aligned design choices.

The main contribution of this work is the development of a robust, adaptive, and mission-driven optimisation framework for OPVs. It explicitly integrates nonlinear scaling effects, dynamic stability criteria, and mission requirements within a single optimisation envelope. Beyond reproducing established naval-architectural behaviour, the framework advances early-stage practice by treating SKI and SI as explicit optimisation objectives and by embedding range and T_{roll} as feasibility constraints. Its adaptive structure allows objectives, variables, and constraints to be tailored flexibly to owner, shipyard, or designer requirements, making it a practical decision-support tool for concept design.

Keywords: Offshore Patrol Vessels (OPVs); early-stage ship design; hybrid scaling; parametric modelling; Systems Engineering (SE); Set-Based Design (SBD); multi-objective optimisation (MOO); Pareto analysis; seakeeping; SKI; stability; SI; resistance; lightweight; decision-support framework

Nomenclature

List of Abbreviations

AUV Autonomous Underwater Vehicle

AVS Angle of Vanishing Stability

CAESES Computer-Aided Engineering Software for Simulation-Driven Design

CAPEX Capital Expenditures

CBD Concept Baseline Design

CFD Computational Fluid Dynamics

COB Center of Buoyancy

COG Center of Gravity

DBB Design-Based Budget

DoE Design of Experiments

DoF Degrees of Freedom

EEZ Exclusive Economic Zone

EP Endurance Profile

ESD Energy Saving Device

FEA Finite Element Analysis

FFD Free-Form Deformation

GA Genetic Algorithm

GHG Greenhouse Gas

H&M Holtrop-Mennen

HV Hypervolume

IMDC Initial Minimum Design Condition

IMO International Maritime Organization

KPI Key Performance Indicator

LARS Launch and Recovery System

LHS Latin Hypercube Sampling

MDO Multidisciplinary Design Optimization

MOGA Multi-Objective Genetic Algorithm

MOGO Multi-Objective Global Optimization

MOO Multi-Objective Optimization

MOPSO Multi-Objective Particle Swarm Optimization

MOSA Multi-Objective Simulated Annealing

MSI Motion Sickness Index

MSLE Mission-Specific Lifecycle Evaluation

NBI Normal Boundary Intersection

NSGA_II Non-dominated Sorting Genetic Algorithm II

NURBS Non-Uniform Rational B-Splines

OMOE Overall Measure of Effectiveness

OPC Offshore Patrol Cutter

OPEX Operational Expenditures

OPV	Offshore Patrol Vessel
ORI	Operability Reliability Index
OSV	Offshore Support Vessel
RAO	Response Amplitude Operator
RBF	Radial Basis Function
RHIB	Rigid Hull Inflatable Boat
RSM	Response Surface Methodology
SA	Simulated Annealing
SAR	Search and Rescue
SBD	Ship Baseline Design
SE	Structural Efficiency
SFC	Specific Fuel Consumption
SGISC	Ship Geometry Input Scaling Coefficient
SS	Sea State
TLCC	Total Life Cycle Cost
USV	Unmanned Surface Vehicle
WL	Waterline

List of Roman symbols

A_M	Midship section area [m²]
A_W	Waterplane area [m²]
B	Beam [m]
B_{OA}	Beam Overall
B_{WL}	Beam at Waterline [m]
BM	Metacentric radius [m]
C_B	Block coefficient
C_M	Midship section coefficient
C_O	Operational coefficient
C_P	Prismatic coefficient
C_S	Stability coefficient
C_{power}	Power coefficient
C_{DL}	Design load coefficient
C_{WP}	Waterplane coefficient
D	Depth [m]
DWT	Deadweight tonnage [Ton]
g	Acceleration due to gravity [m/s^2]
GM	Metacentric height [m]
KB	Keel to center of buoyancy [m]
KG	Keel to center of gravity [m]
L	Length [m]
L/B	Length-to-beam ratio
L/H	Length-to-height ratio
L_{OA}	Length Overall
L_{PP}	Length Between Perpendiculars
L_{WL}	Length at Waterline
LCB	Longitudinal Center of Buoyancy [m]
LCG	Longitudinal Center of Gravity [m]
LWT	Lightweight tonnage [Ton]
P_E	Effective power [kW]
R	Resistance [N]
R_A	Added resistance [N]
R_B	Bulbous bow resistance [N]

R_C	Correlation resistance [N]
R_F	Frictional resistance [N]
R_T	Total resistance [N]
SI	Stability index
SKI	Seakeeping index
T	Draft [m]
T_{roll}	roll period [s]

List of Greek Symbols

α	Fuel-power scaling coefficient
Δ	Displacement mass [Ton]
η_{prop}	Propeller efficiency
λ	Geometric scaling factor
μ	Mean value
∇	Displacement volume [m^3]
ϕ	Heel angle or roll angle
ρ	Water density [kg/m^3]
σ	Variance
θ	Heel angle [deg]

Contents

List of Figures

List of Tables

1

Introduction

1.1. Introduction

Offshore Patrol Vessels (OPVs) are small surface vessels that serve as versatile maritime assets for navies and coast guards. They are used for missions such as search and rescue, exclusive economic zone (EEZ) monitoring, law enforcement, and counter-piracy operations. OPVs vary in size and capability, typically classified into three length categories: vessels under 50 [m], 50–90 [m], and those exceeding 90 [m] [1, 2, 3].

As operational demands evolve, navies and coast guards often require modifications to existing OPV designs to meet new mission profiles and technologies. Changes in operational range, payload capacity, seakeeping performance, or endurance may necessitate adjustments in a vessel's size and proportions, which must balance versatility, cost-efficiency, and performance across diverse maritime conditions. Expanding a proven hull form to accommodate new requirements, whether for increased autonomy, improved habitability, or better hydrodynamic efficiency, is a common practice in naval architecture [4].

Naval architects frequently rely on parent hulls and regression-based models to determine new main dimensions and optimise designs to meet specific requirements. These approaches often involve scaling techniques such as Geometric (Linear) Scaling and Parametric Scaling. However, scaling introduces significant challenges due to the non-linear interactions among key design factors, including resistance, stability, seakeeping, powering and cost [5].

Traditional ship design methods, such as the design spiral, rely heavily on iterative, experience-driven processes, which can be both time-consuming and costly. These conventional approaches often limit the scope of design space exploration and miss the optimal solution. In contrast, modern computational techniques—including parametric modelling, surrogate modelling, and multi-objective optimisation (MOO) enable broader and more efficient design evaluations. These methods allow for extensive parametric variation and mission-specific performance optimisation at the early design stage [5, 6, 7].

1.2. Motivation

There remains a gap in linking mission-specific performance requirements (e.g., specific sea states, seakeeping characteristics, operational speeds, endurance, cost, and range) directly to vessel geometry, including both principal dimensions and full 3D hull form. Current scaling methods do not effectively integrate these factors into the early-stage design process, leading to suboptimal trade-offs between vessel size and operational performance [7]. This thesis therefore, focuses on mid-size OPVs in the 40–90 [m] range, which represent the majority of existing designs with comparable semi-displacement hull forms and multi-mission roles such as EEZ surveillance, SAR, and law enforcement [4, 8]. MOO is increasingly used in modern ship design to address complex and often conflicting performance requirements. Designers can generate an optimal set of alternatives that reflect different trade-offs, supporting more informed and data-driven decision-making. Unlike traditional scaling methods that rely on designer intuition or simplistic geometric transformations, an MOO-based decision-making framework allows for a systematic exploration of vessel dimensions while considering the complex inter-dependencies between key performance parameters [5, 7, 9].

1.3. Research Objectives

The objective of this thesis is to develop an MOO-based decision-making framework for mid-size (40–90 [m]) multi-purpose OPVs. The study focuses on exploring scaling methods to establish preferred scaling relations based on performance trade-offs. It aims to identify how different scaling methods impact key performance areas, including hydrodynamic and hydrostatic performance, seakeeping, propulsion, and overall vessel efficiency. Through this analysis, the research seeks to develop a framework for rapid and cost-effective design scaling, ensuring optimised designs that meet both performance and operational requirements.

1.3.1. Main Research Question

"*How can scaling and mission-oriented Multi-Objective Optimisation (MOO) be integrated into an early-stage design framework that addresses the nonlinear effects of scaling, enhances operational flexibility, and performance of multipurpose OPVs?*"

1.3.2. Research sub-question

1. "*How do the fundamental characteristics, mission roles, and design drivers of multi-purpose Offshore Patrol Vessels (OPVs) influence their key design and mission requirements, and in turn shape overall vessel performance and operational effectiveness?*"
2. "*Do contemporary ship-design and scaling methodologies—including geometric, parametric, and hybrid approaches—adequately capture the non-linear interactions between key hull parameters (length, beam, draft, block coefficient) and performance indicators (resistance, stability, seakeeping,*

propulsion efficiency), and if so, how can they support optimisation in the early stages of design?"

3. "*What is the current state-of-the-art in design optimisation frameworks for early-stage ship design, and based on this, what are the requirements for a Multi-Objective Optimisation (MOO)-based decision-making framework suitable for OPV scaling?*"
4. "*What components are required for the proposed framework, and how can the setup be structured to support early-stage OPV design?*"
5. "*How can the effectiveness of an integrated scaling and mission-oriented MOO framework be verified and validated to ensure robust and reliable early-stage OPV design decisions?*"

1.4. Thesis Road Map

This thesis is structured to systematically address the research sub–questions and, ultimately, the main research question. The literature review provides a foundation by analysing existing research on OPVs, ship design processes, scaling techniques, parametric modelling, and optimisation methods, while subsequent chapters build and validate the proposed framework.

- **Chapter 2** provides an overview of Offshore Patrol Vessels (OPVs), their roles, and design drivers, addressing sub–question 1.
- **Chapter 3** reviews ship design processes, scaling techniques, and parametric modelling approaches, addressing sub–question 2.
- **Chapter 4** presents multi–objective optimisation (MOO) methods and outlines the requirements for a new framework based on parent–hull scaling, addressing sub–question 3.
- **Chapter 5** describes the methodology of the proposed design framework, detailing its components and setup, thereby addressing sub–question 4.
- **Chapter 6** validates the framework against parent–hull reference data (hydrostatics, resistance, stability, seakeeping), thereby addressing the validation part of sub–question 5.
- **Chapter 7** verifies the framework through trend consistency checks and convergence analysis, and demonstrates its application in a representative OPV case study, thereby addressing the verification part of sub–question 5.
- **Chapter 8** concludes the thesis with a discussion of findings, limitations, and recommendations for future research.

2

Offshore Patrol Vessel (OPV)

This chapter presents the fundamental characteristics, mission roles, and design drivers of OPVs. By examining their operational requirements, regulatory constraints, and cost considerations, it addresses the research question 1: "*How do the fundamental characteristics, mission roles, and design drivers of multi-purpose Offshore Patrol Vessels (OPVs) influence their key design and mission requirements, and in turn shape overall vessel performance and operational effectiveness?*".

2.1. Overview of OPVs

OPVs serve as cost-effective, multi-role assets in modern naval and coast guard operations, designed for a wide range of missions. OPVs provide a cost-effective solution for navies and coastguards, bridging the gap between smaller coastal patrol craft and larger combat ships such as corvettes and frigates. OPVs are primarily used for missions such as Exclusive Economic Zone (EEZ) surveillance, Environmental Protection (EP), search and rescue (SAR), counter-piracy, and law enforcement.

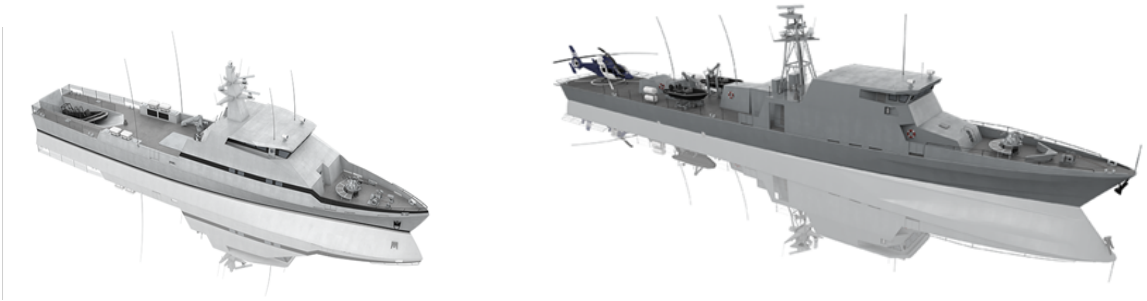

(a) OPV 45m – Multi-mission vessel. **(b)** OPV 62m – Naval Operations vessel

Figure 2.1: Examples of OPV configurations by Israel Shipyards Ltd. (ISL), illustrating differences in size, capabilities, and mission orientation [10]

Figure 2.1 presents two OPV configurations, highlighting their variations in size, operational capabilities, and mission focus. The OPV 45 [m] (2.1a) is designed primarily for as a multi-mission vessel including maritime security, border patrol and search and rescue operations, while the OPV 62 [m] (2.1b) features a naval operations configuration, tailored for enhanced combat and strategic naval Operations.

2.1.1. Missions and Mission Requirements for OPVs' Operational Roles

OPVs address multiple operational tasks, categorised by their intended purpose. Tasks can be divided specifically for Coast Guard or Navy operations or grouped by broader roles, such as SAR, EP, or Naval Operations. Many roles overlap in practice, demonstrating the versatility and multi-mission capabilities of OPVs. Table 2.1 summarises these mission requirements by classifying OPV operational roles based on their primary tasks and associated key features [2, 4, 11]

Table 2.1: Classification of OPVs Based on Missions and Operational Roles.

Operational Role	Primary Tasks	Key Features[1]
Maritime Security and Law Enforcement (MSLE)	Maritime Border Patrol and Surveillance Countering Criminal Law Enforcement Anti-Terrorism	Maximum continuous speed: 20–28 [knots] Operation Speed: 15–18 [knots] (Patrol), 10–12 [knots] (Surveillance) Endurance: 3,500–6,000 [nm], 15–25 [days] Sea State: Operable up to sea state (SS) 5 Equipped with radar, Surveillance systems, Small-calibre weapons space for boarding operations
Search and Rescue (SAR)	Search and Rescue (SAR) Humanitarian Assistance and Disaster Relief	Operation Speed: 18–22 [knots] (SAR) Endurance: 2,000–4,500 [nm], 10–20 [days] Sea State: Operable up to SS6 High manoeuvrability and towing capability Medical facilities and evacuation decks Accommodation for rescued personnel
Environmental Protection (EP)	Environmental Protection	Operation Speed: 12–16 [knots] Endurance: 3,000–5,000 [nm], 14–28 [days] Sea State: Operable up to SS5 Advanced sensors for environmental monitoring Oil spill cleanup equipment Systems for environmental compliance
Naval Operations (NO)	Escort Duties Mine Countermeasure Operations Support for Special Operations	Maximum continuous speed: 20–26 [knots] Endurance: 5,000–8,500 [nm], 20–35 [days] Sea State: Operable up to SS6+ Heavier armament (e.g., missiles, torpedoes) Integrated communication systems for fleet coordination Wartime adaptability

[1] Source: Adapted from [2, 11, 4, 12].

2.1.2. Existing Vessels and Case Studies

Existing OPVs vary in size, capabilities, and configurations, depending on the operational requirements of the owner. Table 2.2 showcases the versatility of OPVs by presenting a range of existing OPV designs. It is based both on an overview of current OPV specifications shown in Table A.1 [10, 13, 14, 15], and findings from existing studies [2, 11, 12]. In Figure 2.2, a heat map was created showing that most existing OPV designs are *MSLE* and *SAR* operations oriented. These analyses provide a basis for developing design requirements tailored to meet both operational and financial constraints. While existing OPV designs span a length range of approximately 40–120 [m], this thesis focuses on the mid-size segment between 40–90 [m], which encompasses the majority of multi-mission OPVs with comparable hull forms and operational profiles (see Section 1.2 Motivation).

Table 2.2: Main characteristics and equipment of OPVs based on market research and literature

Design Aspect	Key Features [2]
L_{OA}[3]	40 to 120 [m]
breadth[3]	10 to 15 [m]
draft[3]	3.25 to 4.55 [m]
beam-to-draft ratio (B/T)[2]	2.88 to 4.3
volumetric coefficient (C_v)[1,2]	2.7 to 4.3
Displacement[3]	300 to 2,500 [Ton]
Hull Form	C-SHARP hull design
Propulsion	Diesel Mechanical CODAE
Autonomy [3]	21 to 40 [days]
Range [3]	3,000 to 10,000 [nm]
Maximum continuous Speed[3]	22 to 30 [knots]
Sea-State	Operational up to Sea-State 5–6
Mission Adaptability	Flexible and Reconfigurable: - Mission bays - Autonomous Underwater Vehicle (AUV) and Unmanned Surface Vehicle (USV) Launch-and-Recovery System (LARS) - Helicopter operations - Medical & Humanitarian aid - Combat modules Mission containers for ecological protection Diving operations Rigid Hull Inflatable Boats (RHIBs) Helicopter accommodations (small, medium, or heavy)
Combat Capabilities	20–76 mm automatic cannons Configurable weapon systems per mission

[2]The data in this table are compiled from a structured review of publicly available specifications from shipbuilders (Appendix A), along with findings from academic and technical literature [2, 11, 12].

[3]This range represents the most common size and displacement for OPVs. However, there are OPVs that exceed or fall below this range depending on specific operational requirements and national naval strategies.

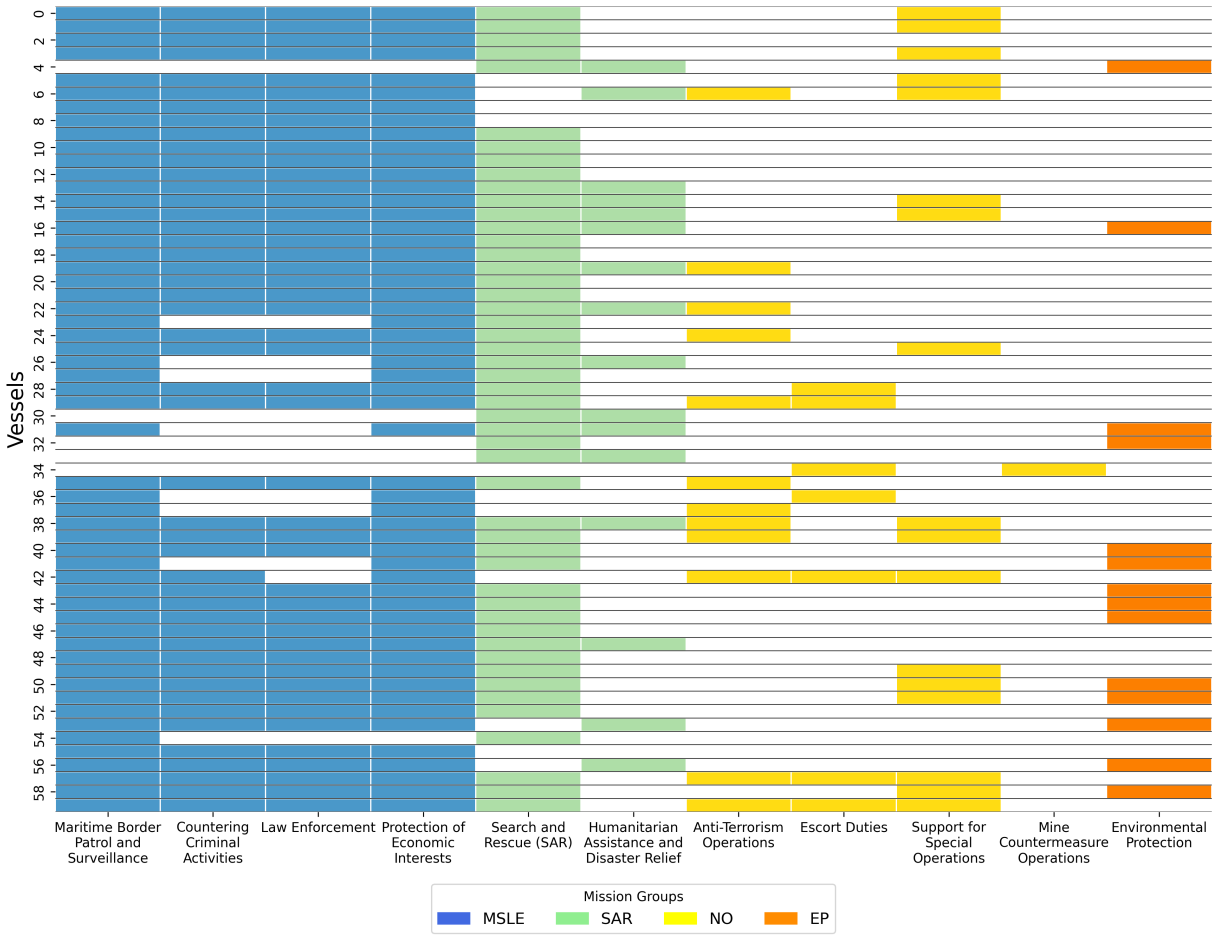

Figure 2.2: Heatmap of OPV Mission Groups distribution base on the table A.1 in Appendex A Overview of existing OPVs designs.

Figures 2.3 and 2.4, based on Table A.1, illustrate the diversity of OPVs in terms of length, range, endurance, and Froude number (Fn). The majority of vessels operate within the semi-displacement regime, with Fn values ranging between 0.4-0.6, and fall within the typical length range of 40–90 [m].

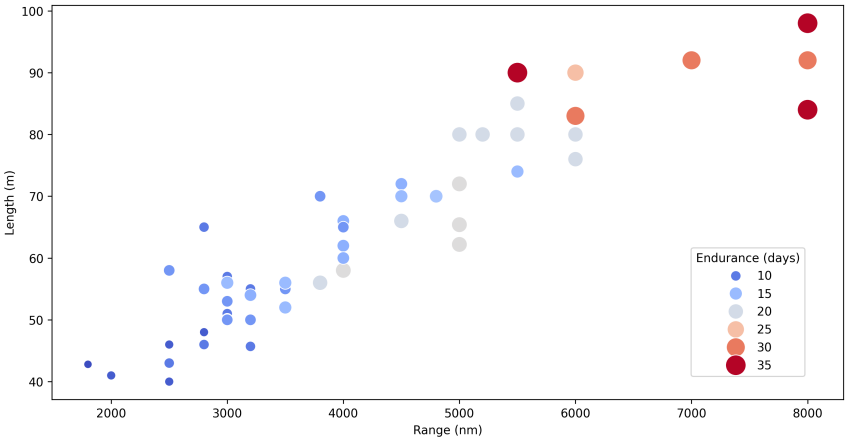

Figure 2.3: Length [m] vs Range [nm] with Endurance Representation

Figure 2.4 includes a fitted trend line illustrating a negative correlation between the L/B ratio and the Froude number (Fn). However, the relatively low coefficient of determination ($R^2 = 0.45$) indicates only a moderate correlation, suggesting that the trend line should be interpreted cautiously as an indicative representation of the general pattern rather than as a reliable predictive model. While classical theory suggests that vessels designed for higher Fn would typically employ more slender hulls to minimise resistance, the observed inverse trend reflects the operational context of OPVs, where maximum speeds are relatively fixed across vessels and variations in Fn are primarily driven by differences in hull length. Consequently, longer vessels, despite higher L/B ratios, operate at lower Fn due to their increased length rather than hydrodynamic optimisation for speed. The data points are colour-coded by vessel length to emphasise this hull-scaling effect. A complementary analysis using the hull-based Froude number ($F_{n,h}$), defined by $L \cdot B$, is provided in Appendix A, showing a slightly stronger correlation ($R^2 = 0.51$). Together, the figures highlight that endurance is closely tied to absolute vessel length: longer OPVs operating at the same mission speeds achieve lower Froude numbers and greater endurance, whereas shorter OPVs operate at higher Froude numbers and can attain higher relative speeds but at the expense of range. This reinforces the presence of design trade-offs and the diversity of OPV design approaches shaped by differing operational requirements and mission profiles.

2.1.3. OPV Hull Design

Offshore Patrol Vessels (OPVs) typically adopt a semi-displacement, round-bilge hull form, which offers a balanced compromise between hydrodynamic efficiency and operability. While many performance attributes such as moderate resistance, fuel efficiency, and manoeuvrability can also be achieved with

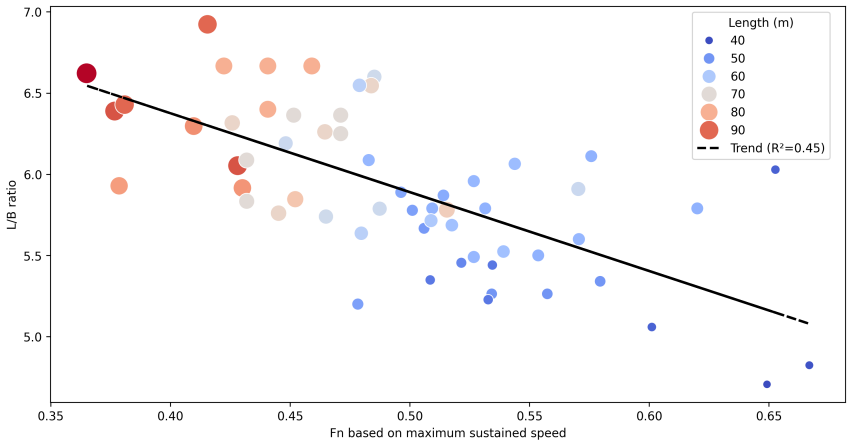

Figure 2.4: Length-to-Beam (L/B) Ratio vs Froude Number (Fn) with Length colour code Representation

hard-chine semi-displacement designs, the round-bilge configuration provides more favourable seakeeping performance, making it well-suited for long-duration patrol missions [8, 11, 16].

From a dimensional perspective, OPVs generally employ a L/B between 4 and 7, reflecting the trade-off between slenderness for resistance reduction and beam for transverse stability. The latter is especially critical for ensuring weapon accuracy, safe helicopter operations, and overall crew comfort. Similarly, a B/T between 2.5 and 4.5 is commonly adopted, while C_B typically range from 0.30 to 0.60, balancing endurance, payload capacity, and hydrodynamic performance. [4]

To mitigate roll motions and enhance operability across a wide range of SS, OPVs are often fitted with bilge keels, active stabilisers, or moderate keel lines. Depending on vessel size, speed, and mission profile, some designs also integrate a bulbous bow, although its adoption is influenced by construction simplicity and cost considerations.

In terms of operational profiles, OPVs are designed to operate across a broad speed envelope, with sprint speeds of 20–28 knots for interception and rapid-response missions. However, they typically spend the majority of their operational life—up to 80% of the time—at lower transit speeds of 20 knots or less, where endurance and fuel economy dominate performance requirements [12].

2.2. Design drivers

2.2.1. Total Life Cycle Cost (TLCC)

Total Life Cycle Cost (TLCC) is a critical factor in the design and procurement of OPVs, which are typically government-funded and acquired as part of fleet modernisation programs involving multiple vessels. Schmitz et al. [4] described the United States Coast Guard Offshore Patrol Cutter (OPC) program, which aimed to modernise the U.S. Coast Guard's surface fleet with 25 new cutters at an average unit cost of $329 million, emphasising cost as a design driver. However, OPV acquisition costs can vary widely

[4] The data in this table are compiled from a structured review of publicly available specifications from shipbuilders (Appendix A), along with findings from academic and technical literature [2, 11, 12].

depending on vessel size, mission capability, outfitting level, and regional procurement policies [1].

Like all maritime assets, OPV TLCC are evaluated using standard financial frameworks divided into:

- Capital Expenses (CAPEX), Costs related to materials, fabrication, and onboard systems. These are commonly estimated using regression analyses relating Lightship weight (LWT) and propulsion power to construction costs [17, 18].
- Operational Expenses (OPEX), Recurring costs such as fuel consumption, maintenance, crew salaries, and training, which play a key role in long-term cost efficiency [1, 17, 19].

2.2.2. Endurance and Range

Section 2.1 and Table 2.2 present the endurance and range requirements for OPV operations. These requirements are governed by the vessel's Deadweight Tonnage (DWT), primarily comprising fuel and consumables in the case of OPVs [20, 21], as well as propulsion efficiency, both of which are directly influenced by hull design [18, 22]. Consequently, endurance and range are established as key design drivers with significant implications for hull form and overall vessel configuration.

2.2.3. Ship Resistance

Ship resistance (R_T) is a fundamental performance parameter that directly determines the effective power (P_E) required, as expressed in Equation 2.1, where V_s is the ship speed. Effective power in turn defines the installed propulsion capacity, influencing fuel consumption, emissions, operational endurance, range, and ultimately both OPEX and CAPEX [12, 19, 23].

$$P_E = R_T \cdot V_s \tag{2.1}$$

Studies demonstrate that variations in key design parameters—such as length-to-beam ratio (L/B), prismatic coefficient, and the presence of a bulbous bow—significantly affect the resistance profile of patrol vessels [7, 8, 19, 24, 25]. Beyond hull-form optimisation, navies have also employed energy-saving devices (ESDs), including stern flaps, wedges, hull-mounted foils and fins, propeller ducts, and energy-saving rudders, These devices generate some additional drag themselves but improve overall resistance by influencing vessel trim, wake flow, and propulsion efficiency. Nevertheless, they cannot substitute the dominant influence of hull geometry on overall hydrodynamic performance [26, 27].

Although the International Maritime Organization (IMO) does not currently impose greenhouse gas (GHG) reduction requirements on military vessels [28], increasing environmental awareness and national policy frameworks encourage navies and coast guards to adopt emission-reduction strategies [29]. Reducing hull resistance directly contributes to lowering fuel consumption, emissions, and associated operating costs. Taken together, the mixed-speed operational profile of OPVs, coupled with growing environmental pressures and the strong influence of endurance, range, and TLCC in early-stage design, establishes resistance as one of the most critical design drivers in OPV development.

Resistance prediction methods can be broadly categorised into high-fidelity approaches (e.g., CFD simulations, towing tank experiments) and low-fidelity approaches (e.g., empirical formulas, regression methods, and systematic series). For early-stage OPV design, low-fidelity methods provide practical estimates to compare multiple hull candidates before committing to more computationally expensive simulations [8, 18].

2.2.4. Stability

Stability is a fundamental requirement in naval architecture, ensuring that a vessel can recover from heeling moments and return to an upright condition, thereby maintain safe operations under varying loads and environmental conditions. Stability analysis is conducted in calm water at zero speed, providing a baseline measure of how the ship responds to heeling forces. However, OPVs must remain operational in more demanding environments. For this reason, strong initial stability is essential to prevent excessive heeling and dynamic rolling, thereby ensuring safe and comfortable operations. At higher speeds and in rougher seas, seakeeping analysis is performed to evaluate dynamic responses such as motions, accelerations, and overall operability. International regulations define criteria for both intact and damage stability (Equation 2.2). The righting arm curve (GZ) provides an evaluation of a vessel's stability characteristics; however, its accurate calculation requires a fully defined 3D hull geometry and a sufficiently detailed estimate of weight distribution, which is typically only available in later design stages.

$$GZ(L, B, D, T, C_B, KG) \geq GZ_{IMO} \tag{2.2}$$

In early-stage design, detailed information about weight distribution and internal configuration is limited. Since the vertical centre of gravity (KG) is the main factor governing stability, designers rely on approximate assumptions for KG and use the metacentric height (GM) as a practical proxy for assessing initial stability at small heel angles.

2.2.5. Seakeeping

Seakeeping directly impacts the operability, habitability, safety, and mission effectiveness of a vessel in varying sea conditions. This is particularly relevant for OPVs, which frequently operate in SS5 or 6 while conducting surveillance, SAR, boarding operations, launch and recovery tasks, and helicopter deployments [4]. Additionally, OPVs must sustain operational effectiveness during high-speed transits, tactical manoeuvres, and dynamic operations such as RHIB deployments and flight deck operations. These tasks require a stable platform capable of mild pitch, roll, and heave motions while ensuring endurance over long missions [30]. To ensure safety, operational effectiveness, and crew endurance, OPVs must be designed with careful consideration of their seakeeping capabilities. However, this presents a complication, as seakeeping analysis requires a detailed 3D hull representation, which is typically available only in later design stages. In the early phases of ship design, empirical formulas and simplified 2D models can be used to estimate seakeeping behaviour. These methods, while useful for initial decision-making, lack the

accuracy required to fully capture complex hydrodynamic interactions [22, 31].

The ship's motion response is defined by amplitude, velocity, and acceleration across all six degrees of freedom (DoF), though not all are equally critical in every operational context. Seakeeping performance is largely influenced by hull geometry, centre of gravity, and displacement, making early-stage design considerations critical. While damping systems can support achieving desired performance levels, the hull geometry is the primary element considered in early-stage optimisation, as it provides the foundation for any additional motion control systems. Neglecting seakeeping in the early design phases can result in Performance issues that are difficult or, in some cases, impossible to correct later without significant redesign and cost [4].

Optimising seakeeping performance ensures that OPVs function efficiently in adverse weather conditions, keeping vessel motions and derived responses within acceptable limits. Understanding how vessel dimensions, hull form, and loading conditions affect wave-induced responses is essential for evaluating overall mission success. Gutsch et al. [30] emphasise that achieving optimal seakeeping requires a comprehensive design approach, integrating computational analysis, tank testing, and the development of key performance indicators (KPIs) for seakeeping assessment.

2.2.6. Seakeeping Criteria and Motion Limits

Various standards define acceptable motion limits for different operational profiles, including those set by the USCGC, NORDFORSK (1987), NATO STANAG 4154, ISO 2631-1, and IMO Second Generation Intact Stability Criteria (SGISC). Studies conducted by Cruickshank, Tasaki, and Tello et al. further support these standards. Among them, the USCGC and NORDFORSK (1987) criteria are particularly relevant for OPVs, as they establish motion limits that directly influence operational effectiveness [32].

Table 2.3: Comparison of key limiting factors in well-established seakeeping criteria for OPVs.

Criterion	USCGC	NORDFORSK	NATO STANAG 4154
Roll Angle	$4°$ (bridge)	$4°$ (naval)	Mission-dependent
Accelerations	$0.2g$ (vertical)	$0.275g$ (vertical FP)	$0.4g$ (pilot house)
Slamming	20 slams/hr	0.03 probability	Mission thresholds
Pitch	$1.5°$	-	$3°$-$9°$

2.2.7. Vessel size

The size of an OPV is determined by a combination of mission requirements, operational constraints, and design trade-offs. Larger OPVs generally offer greater endurance, improved habitability, and increased payload capacity, while smaller OPVs benefit from enhanced agility, reduced fuel consumption, and lower acquisition costs. The vessel must provide adequate space for machinery, equipment, crew accommodations, and mission-specific systems while maintaining seakeeping performance, fuel efficiency, and manoeuvrability. During the concept design phase, naval architects define minimum and maximum size

boundaries based on mission profiles, payload requirements, and regulatory constraints. Vessel size influences stability, endurance, resistance, and modular flexibility, making it a key parameter in OPV optimisation. [19]

2.2.8. Manoeuvrability

Manoeuvrability influences an OPV's ability to perform diverse missions, including search and rescue, interception, and escort operations. It is primarily affected by hull form, propulsion system, steering devices configuration, and control automation. Although manoeuvrability is a critical operational capability, it is generally addressed in the later stages of the design process, once propulsion and control systems are defined in detail. In the context of this thesis, which focuses on early-stage hull scaling and optimisation, manoeuvrability is excluded due to its limited sensitivity to geometric scaling and its dependence on detailed subsystem design. [11, 18].

2.2.9. Structural Integrity and Survivability

OPVs must be designed to withstand damage and maintain operational capability, particularly for security and naval operations. Survivability measures are critical to ensure that vessels can operate even in hostile or high-risk environments [11]. Survivability features, such as compartmentalised hulls, reinforced bulkheads, and redundancy systems, are typically addressed in later design stages, requiring detailed internal layout modelling. As this thesis focuses on early-stage hull form scaling, where internal arrangements are not yet defined, survivability aspects are beyond the scope of the current methodology. Nevertheless, for variants exceeding 79 meters, subdivision requirements as per SOLAS 2020 are acknowledged [33]. While internal subdivision is not assessed, the hull scaling maintains a constant freeboard-to-depth ratio (F/D), ensuring consistent floodable length characteristics and preserving feasibility for future compliance with the required subdivision index R [34]. For an OPV treated as a cargo ship under SOLAS 2020, the Required Subdivision Index R is a function of the subdivision length L_s. For $80 \leq L_s < 100$ m, SOLAS applies a continuity formula referenced to the 100 m value R_0:

$$R_0 = 1 - \frac{128}{100 + 152} = 0.492 \tag{2.3}$$

Approximating $L_s \approx 90$ m for the scaled OPV:

$$R = 1 - \frac{1}{1 + 0.01\, L_s \frac{R_0}{1-R_0}} \quad \Rightarrow \quad R \approx 0.466 \tag{2.4}$$

Thus, the design must achieve:

$$A \geq 0.466 \tag{2.5}$$

table 2.4 Required subdivision index R for 80-90 feasible design will require meeting this criterion will require detailed subdivision modelling, which is beyond the scope of this thesis.

Table 2.4: Required subdivision index R for different subdivision lengths L_s (cargo ships, SOLAS 2020).

L_s [m]	80	85	90
R_0 at 100 m	0.492	0.492	0.492
R ($80 \leq L_s < 100$)	0.437	0.452	0.466

2.3. Criticality of Key Performance Indicators (KPIs)

While multiple KPIs influence OPV performance, their relative importance varies significantly depending on the mission profile, operational environment, and stakeholder priorities. Table 2.5 presents a qualitative ranking of KPI criticality across representative OPV mission profiles, using three levels: High (H), Medium (M), and Low (L). The rankings are based on the findings presented in this chapter.

Table 2.5: Qualitative ranking of KPI criticality across representative OPV mission profiles.

KPI	MSLE	SAR	EP	MO
Resistance	H	M	H	M
Endurance / Range	H	M	H	H
Maximum Speed	H	H	L	H
Seakeeping (SS5–6)	M	H	H	H
Stability	H	H	H	H
Total Life Cycle Cost (TLCC)	H	M	H	M

2.4. Related Work

OPV design presents conflicting requirements such as high endurance and range while maintaining low cost, low resistance versus high range and good seakeeping, and balancing good seakeeping with cost efficiency. Additionally, trade-offs between ship size and range affect operability and mission performance, necessitating a multi-objective design framework.

Schmitz et al. [4] analyse seakeeping and affordability but rely on regression models and Monte Carlo simulations that lack a direct correlation between hull form and operational performance. Their approach highlights the difficulty of linking cost considerations with operability criteria, yet also underscores the need for design frameworks that explicitly integrate hull-form parameters with mission-specific performance metrics.

Winyall et al. [8], utilised Design Synthesis combined with 3D parametric modelling and MOO for OPV hull-form design, integrating 33 design variables such as L/B, B/T, and curvature. Performance metrics included resistance and seakeeping, assessed using the Seakeeping Index (SKI) in SS5, focusing on heave, pitch, and vertical displacements at critical locations in head seas. However, the study did not address scalability or clear correlations between design parameters and performance, limiting fleet-wide application.

Rahmaji et al. [35], applied regression analysis to evaluate hydrodynamic performance, focusing

on resistance, stability, and seakeeping of fast patrol boats with hard-chine, V-shaped planing hulls. Key variables included DWT and main dimensions (L, B, D, T). Using Maxsurf® (a commercial naval architecture software for hydrostatics, resistance, and seakeeping simulations), the study assessed resistance through the Savitsky method [36], stability via GZ curves, and seakeeping using strip-theory-based RAOs (heave, pitch, roll), Motion Sickness Index, slamming, and deck wetness probabilities. While this approach is valid for hard-chine planing craft, the original Savitsky formulation is not applicable to round-bilge or displacement-type OPVs considered in this thesis. Moreover, specific inconsistencies arise between the stated methodology and the reported data: the regression is based on only five hulls with very low R^2 values, yet is treated as predictive; resistance analysis at $Fn = 0.5$ reports zero values for some regression hulls while others show non-zero results, which is physically implausible; the scaling method claims C_B was fixed, yet Table 5 (in Rahmaji et al. [35] reports) shows variation (0.454–0.435); and claims of scaling superiority rely on highlighting a maximum similarity value, even though the average similarity is lower than that of the regression method. These issues require a cautious interpretation of the study findings.

Yurdakul et al. [7] utilised Pareto frontier optimisation for principal dimensions of planning craft and destroyers. Variables included beam, deadrise angle, speed, Longitudinal Centre of Buoyancy (LCB), and Block coefficient (C_B). For the planing craft, the longitudinal centre of gravity (LCG) was treated as a variable because it directly affects the trim equilibrium and wetted length, which in turn determine resistance and the vertical acceleration at the centre of gravity, as expressed in Savitsky's acceleration formulation. For the destroyer case, the performance criteria focused instead on effective power and pitch acceleration at the bridge. Geometry variations were generated using MATLAB® and Maxsurf® and evaluated through nuShallo™ (a non-linear potential-flow solver developed by HSVA, Hamburg), combined with strip-theory-based seakeeping methods. While demonstrating effective early-stage optimisation, the study lacked comprehensive parametric control and relied on mid-fidelity hydrodynamic tools.

De Gaaij [37] conducted a parametric optimisation study on naval support vessels, integrating a CAESES (CAE Software for Engineering Simulations developed by FRIENDSHIP-Systems), based parametric model with resistance prediction methods and simplified seakeeping calculations. Resistance was estimated using RAPID® (a non-linear potential-flow solver developed by MARIN [38]) in combination with the empirical Holtrop-Mennen (H&M)method [39], while motions were evaluated through linear strip theory. Design variables included T,L_{OA},B, Entrance Angle at WL, Stem distance, and frame indication factors. Constraints included minimum volume and a Beam-to-Draft ratio (B/T). Optimisation utilised a genetic algorithm by DAKOTA (Design Analysis Kit for Optimization and Terascale Applications, developed by Sandia National Laboratories [40]) to minimise resistance and vertical bow displacement. Resistance predictions were validated against towing tank experiments, while seakeeping performance was checked through Maxsurf® evaluations (Bentley Systems) of vertical bow acceleration. In total, seakeeping validation was performed on 16 design variants (4 cases for 4 different ship types).

MacPherson et al. [41] present a practical case study demonstrating how a coupled optimisation

approach using CAESES (for geometry and optimisation) and NavCad® (HydroComp, Inc., Durham, NH, USA is a commercial software environment for ship resistance and propulsion analysis), can effectively address performance deficiencies in patrol craft design. The study involved a patrol craft initially unable to achieve its required contract speed of 26 knots, only reaching approximately 23 knots. The design variables were L_{WL}, Beam at Waterline (B_{WL}), Transom immersion, Transom deadrise angle, C_P, LCB, and Displacement. This outcome illustrated how early-stage parametric optimisation, combined with accurate performance prediction, can lead to significant lifecycle cost savings and improved mission capability.

Two related studies by Ljulj et al. [3, 11], present a multi-attribute design synthesis framework for early-stage naval vessel design, integrating decision-making based on TLCC and Overall Measure of Effectiveness (OMOE). The approach employs a self-balancing concept model with 20 variables, including hull form parameters (e.g., C_P, C_M, C_{DL}, B/T, L/H), propulsion, autonomy, and mission range. "Monako PRB" (software developed for the multi-attribute concept design procedure of naval vessels) generates feasible candidates filtered via Pareto optimisation. Though effective for early-stage analysis, it lacks parametric geometry control and high-fidelity simulations.

Sariöz [42], proposes a method to determine the minimum ship size required to meet specified seakeeping performance at a given speed and SS. Using linear motion theory and RAO-based evaluations (pitch, roll, vertical acceleration), the study applies geometric scaling (50%–150%) to assess how size affects performance. This approach helps identify the smallest viable hull for given seakeeping criteria, enabling early trade-offs between performance, speed, and vessel size.

Brown and Salcedo [22], presented a total-ship design synthesis framework employing Multi-Objective Genetic Optimisation (MOGO) to explore 26 design variables, including hull geometry, propulsion, manning, and combat systems. Performance metrics—cost, risk, and mission effectiveness—were combined into an OMOE, supported by resistance (Gertler/Taylor series) and seakeeping (McCreight Index [43]) evaluations. This approach enables a balanced early-stage trade-off analysis in naval designs.

Martin Gutsch et al. [30], introduced the Operability Robustness Index (ORI), evaluating seakeeping under variable SS. Analysing L (80–160 [m]) and variations in B, T, and GM ≥2.0 [m], the study highlighted ORI's effectiveness in balancing resistance, cost, and motion performance. The results emphasised the non-linear relationship between dimensions and seakeeping,

Other studies [2, 16, 17, 35, 44, 45] do not comprehensively explore the design space within a multi-objective optimisation framework.

2.4.1. Important Dimensions for OPV

Figure 2.5 visualises the relationship between hull design parameters and KPIs relevant to OPVs. The heat map aggregates the frequency and strength of each parameter's appearance across multiple studies and performance criteria, including resistance, stability, seakeeping, range, and cost.

Each cell in the heatmap represents the number of times a given hull parameter was explicitly linked to a specific performance indicator in the reviewed literature. For each paper analysed (see Section 2.4), occurrences were recorded when a study either directly varied or optimised the parameter in relation to the performance metric, or reported a quantified or described influence of that parameter on the KPI. If multiple studies made similar links, their counts were summed, resulting in the values shown. For example, the value 13 in the cell for L/B Ratio vs. Resistance means that 13 instances were identified across the reviewed studies where the L/B ratio was connected to resistance performance. Darker colours indicate stronger support or more frequent association in the literature.

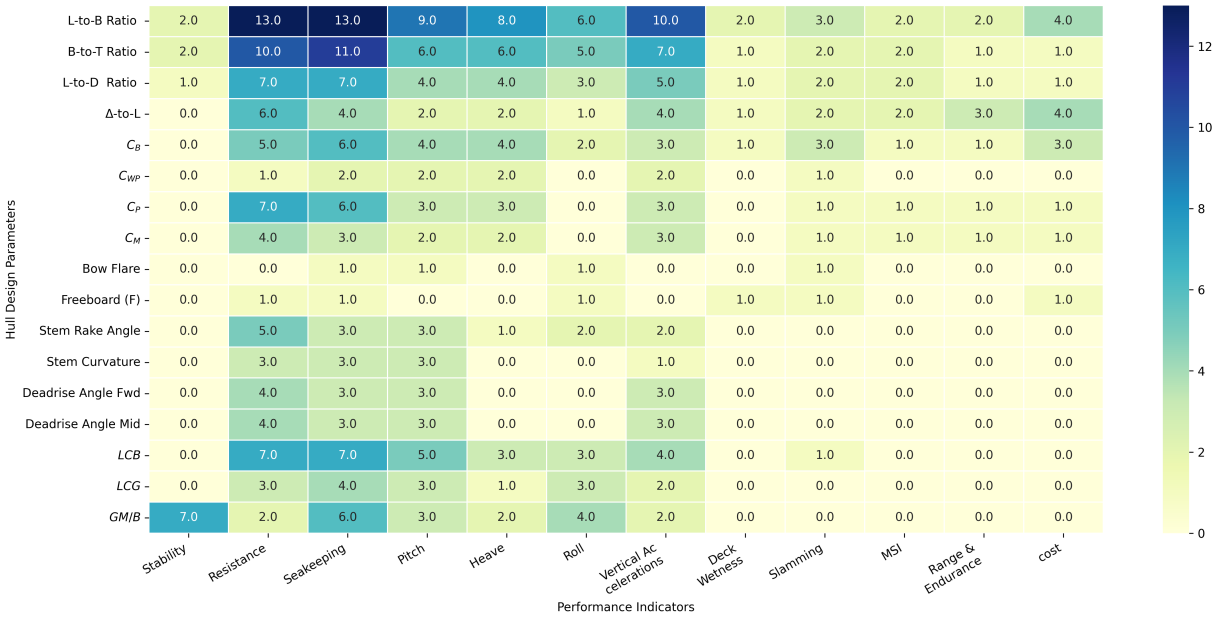

Figure 2.5: Heat-map of Hull Parameters vs Performance Indicators in OPV Literature

Key hull parameters have consistently emerged as highly influential in ship design, including:

- L/B ratio - influence resistance and stability
- B/T ratio - influence on seakeeping and stability
- C_B– influence resistance, range and endurance
- C_P, C_M - influence resistance and seakeeping
- Deadrise angle - influence seakeeping
- LCB - influence seakeeping
- Stem rake and curvature - influence seakeeping

It is important to note that the correlation discussed here is based on a limited number of studies relevant to this thesis. Most of these studies focus primarily on the main geometric parameters (L, B, T, C_B), while other influential parameters are often held constant to reduce complexity and focus the optimisation process, making it difficult to establish a direct correlation to key KPIs [7, 19, 22, 46]. Furthermore, analytic and

regression-based methods are more commonly used than full parametric or surrogate-based modelling [4, 11, 22]. It should also be acknowledged that interdependencies exist among nearly all hull parameters, and many can be defined in multiple valid ways. Finally, it should be noted that these parameter relationships are not unique to OPVs; however, the relevance of a given configuration is driven by the OPV specific performance matrix. In particular, range and cost are strongly linked to displacement, highlighting the need to consider these trade-offs early in the design process.

2.5. Research gap

Despite the growing use of multi-objective optimisation in ship design, existing studies often treat critical performance metrics such as endurance, range, and seakeeping in isolation or as fixed inputs. There remains a need for an integrated approach that dynamically connects hull form and principal dimensions to mission-specific performance demands. Addressing this gap requires a mission-driven, parametric optimisation framework that systematically links vessel geometry to key design drivers, enabling balanced trade-offs between endurance, resistance, cost, and seakeeping during the early design phase.

2.6. Conclusions

This chapter establishes a foundation for OPV design by outlining its fundamental characteristics, mission roles, and key design considerations. Through an analysis of existing OPV configurations and operational constraints, it addresses Sub-question 1:

"*How do the fundamental characteristics, mission roles, and design drivers of multi-purpose Offshore Patrol Vessels (OPVs) influence their key design and mission requirements, and in turn shape overall vessel performance and operational effectiveness?*"

The findings show that OPVs operate across a broad mission spectrum (Fig. 2.2, Table 2.2), including MSLE, SAR, EP, and NO. These roles impose partly conflicting requirements: high endurance for long patrols, sprint capability for rapid response, robust stability and seakeeping up to SS6, payload flexibility, and strict cost and weight limits. Such demands translate into trade-offs that directly shape hull geometry, propulsion configuration, and payload capacity.

Literature trends confirm that principal hull parameters (L, B, T, C_B) strongly influence OPV performance, with relationships such as L/B ratio affecting resistance and stability, B/T ratio influencing seakeeping and stability, and C_P shaping resistance and endurance (Fig. 2.5). OPVs therefore commonly adopt semi-displacement, round-bilge hull forms as a compromise between efficiency, operability, and mission flexibility. Addressing these trade-offs systematically is essential to ensure mission effectiveness and cost-efficiency.

Despite the growing adoption of Multi-Objective Optimisation (MOO) in naval architecture, existing OPV studies often lack integration between mission-specific requirements and parameterised hull form models. This gap limits the ability to quantify how geometric variations influence performance, underlining the need

for a framework that explicitly couples mission demands, operational constraints, and hull geometry from the earliest stages of conceptual design.

The next chapter builds on this foundation by reviewing ship design methodologies, scaling frameworks, and parametric modelling, thereby providing the methodological basis for developing an early-stage design framework.

3

Ship Design, Scaling Methodology

This chapter reviews the principles of early-stage ship design. It first outlines the classical *design-spiral* workflow, then compares geometric, parametric and hybrid scaling methods together with modern parametric-modelling tools. By evaluating the strengths and limitations of these approaches, the chapter addresses research question 2: "*How do contemporary ship-design and scaling methodologies—including geometric, parametric and hybrid approaches—capture the non-linear interactions between key hull parameters (length, beam, draft, block coefficient) and performance indicators (resistance, stability, seakeeping, propulsion efficiency), and thereby support optimisation in the early stages of design?*".

While this chapter establishes the conceptual basis for the non-linear interactions between principal hull parameters and key performance metrics, quantitative verification of these relationships will be presented in the subsequent research and results chapters.

3.1. Ship Design

Ship design is an inherently complex process, influenced by the growing demands for efficiency, sustainability, and multi-mission adaptability [31]. The hull form is a fundamental determinant of ship performance, impacting resistance, seakeeping, and manoeuvrability. Consequently, optimizing the hull design early in the process is critical, as later modifications can lead to significant cost escalations, as illustrated in Figure 3.1 [47].

3.1.1. Design Spiral

When considering ship design, one typically refers to the *Design Spiral* as illustrated in Figure 3.2, which represents a traditional iterative refinement process. The Design Spiral remains fundamental in modern shipbuilding due to its structured framework for integrating hydrodynamic, structural, and economic considerations, among others. The process begins with defining the ship's requirements, typically based

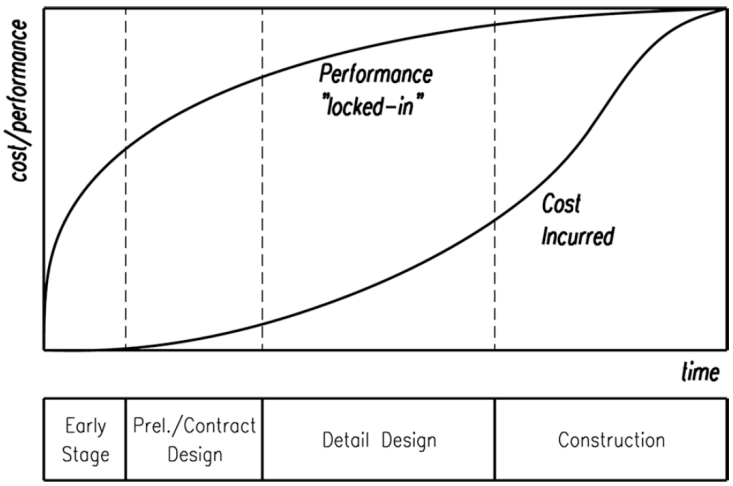

Figure 3.1: Cost vs performance during the ship design and construction phases [47]

on the client's needs. This is followed by iterative refinements of main dimensions, hull form, arrangement, resistance, propulsion, structural integrity, cost, and other parameters [20, 48].

As the design progresses through these stages, more technical and cost-related data become available, yet modifications become increasingly expensive. In the earlier conceptual and preliminary design stages, there is more flexibility to make adjustments without significant cost implications. As the design matures, incorporating higher-fidelity analyses such as Computational Fluid Dynamics (CFD) simulations, towing tank testing, and structural integrity assessments becomes necessary [24, 34].

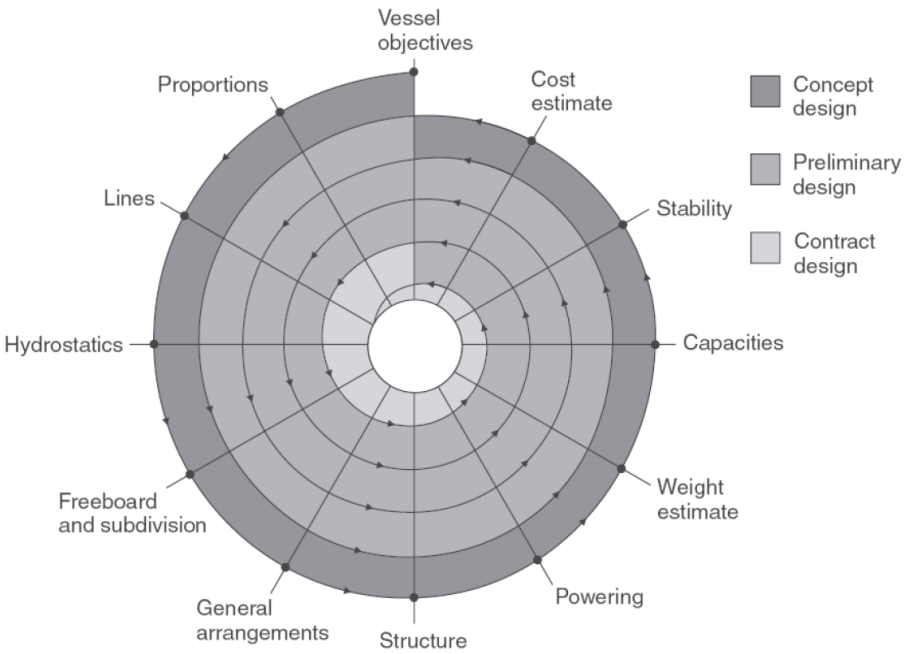

Figure 3.2: The Design Spiral [49]

3.1.2. The Evolution Towards Modern Design Methods

Historically, ship design has often been guided by proven design precedents, where empirical formulas and regression-based methods dictated hull dimensions and performance predictions. While this approach ensures reliability and predictability, it also imposes constraints on innovations and optimisation, especially when multiple, competing performance criteria must be balanced [5, 31].

As ships have become more complex, modern design approaches have blurred rigid phase boundaries, embracing an integrated, system-level framework. Recent advancements in Multi-disciplinary Design Optimisation (MDO) and knowledge management systems allow shipbuilders to optimise designs more holistically, balancing hydrodynamics, structure, and propulsion within a unified process [5].

A key development in this evolution is the adoption of multi-objective optimisation-based decision making, which enables designers to explore trade-offs between competing factors [22]. For instance, improving seakeeping might lead to increased fuel consumption, but Pareto analysis helps identify optimal compromises without overly sacrificing performance in any domain.

3.1.3. State-of-the-Art Design Approaches

The design spiral remains a foundational approach in ship design, but recent developments have placed greater emphasis on optimisation during the early design stages, enabling the creation of more efficient and refined design concepts. The 2022 State-of-the-Art report by Erikstad and Lagemann [50] introduced several evolutionary tracks as alternatives to the conventional design spiral, including a systems engineering-based approach, a set-based strategy, and a holistic optimisation strategy.

A Systems Engineering-Based Approach

The Systems Engineering (SE) -Based Approach is a structured, top-down process that integrates methodologies, tools, guidelines, and principles to ensure that all subsystems (hull, propulsion, structure, electronics, etc.) function cohesively within the overall ship system. This approach emphasises defining both the correct requirements and measurable performance criteria at the early concept stage, involving collaboration between the client and the designer. This approach acknowledges that there is no single optimal design, but rather a trade-off-based design process that balances competing requirements. Figure 3.3 visualizes SE activities throughout the life cycle stages, emphasising the validation process from left to right, with an increasing level of design detail [51]

A Set-Based Design (SBD) Strategy

A SBD Strategy employs a parallel exploration of multiple design options within design disciplines instead of focusing on a single ship design iteration. The design space is progressively refined based on performance metrics, constraints, and trade-offs, allowing for informed decision-making before committing to a final design [52]. Figure 3.4 illustrates the SBD Strategy, showing how multiple design disciplines are explored independently and gradually refined through an iterative convergence process. This approach minimises design risk by avoiding premature convergence on a suboptimal solution. However, the broad design space

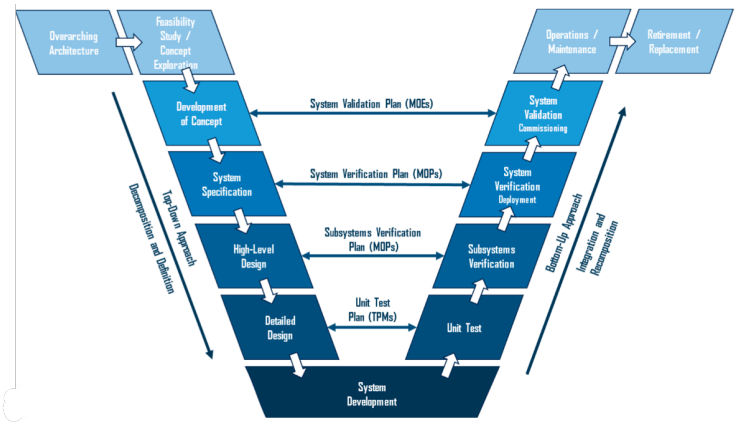

Figure 3.3: The Systems Engineering V-Model [51]

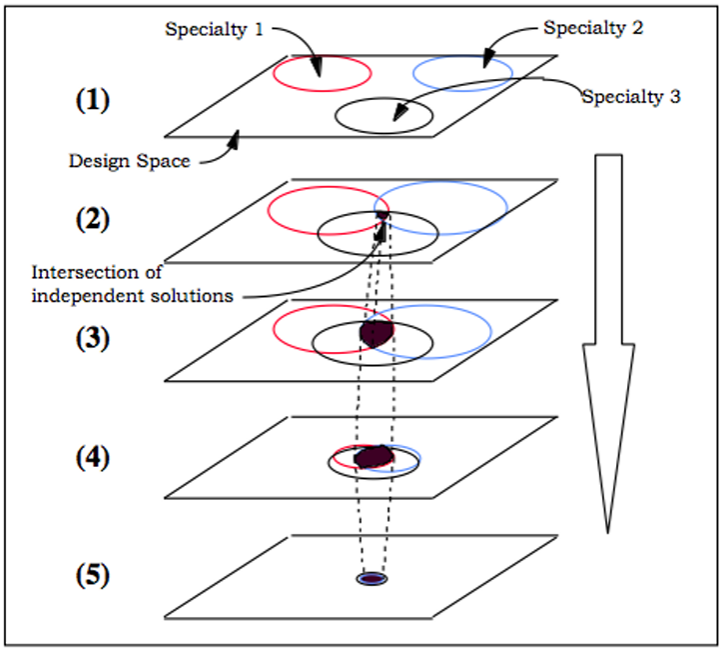

Figure 3.4: Set-Based Design process

and complex decision-making structure of SBD can increase project uncertainty and demand significant computational resources, especially in the early stages [52]. While this approach can lengthen early-stage development time, when well-managed, the up-front investment can shorten overall time-to-market, it offers greater flexibility and efficiency in the long run, particularly when requirements evolve during the design process. For example, evaluating multiple hull forms, propulsion configurations, and layout arrangements early on enables designers to identify robust solutions and avoid costly redesigns later, supporting an optimised OPV design.

A Holistic Optimisation

Holistic Optimisation Strategy views ship design as an interconnected system, optimising multiple parameters (e.g., hydrodynamics, stability, propulsion) simultaneously rather than focusing on individual

components in isolation. Using MOO to balance trade-offs between performance, cost, and sustainability. Figure 3.5 visualises this approach.[6]

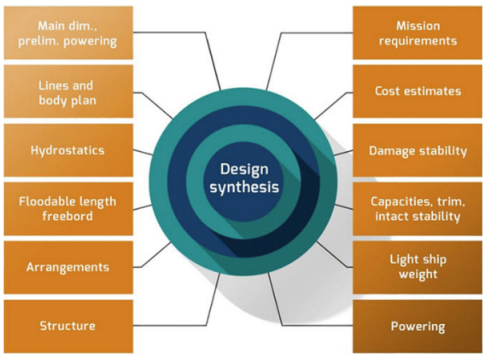

Figure 3.5: HOLISHIP design cycle - Holistic approach

Design Synthesis in Early-Stage Ship Design

While not a standalone methodology, design synthesis is worth mentioning as it is often applied in early-stage studies to simplify the design problem [3, 11]. Traditional synthesis approaches, such as rule-based or library-based combinations of global parameters (e.g., length, beam, draft), support early trade-off decisions but typically lack geometric flexibility and rely on simplified performance predictions [22]. Although useful for feasibility assessments, these methods lack precision as they do not explicitly model the hull geometry and, therefore, cannot capture detailed hydrodynamic or seakeeping effects.

Andrews et al. [5] emphasise that no one-size-fits-all approach exists in ship design, highlighting the need for frameworks tailored to specific ship types, companies, clients, or even individual designers. This is particularly relevant for OPVs, which are often built to order for multi-mission roles, underscoring the importance of flexible design frameworks capable of adapting to diverse scaling scenarios rather than applying a single predefined method.

3.2. Scaling Approaches

3.2.1. Geometric Scaling

Geometric scaling is a fundamental approach in ship design where all primary dimensions, including length, beam, and draft, are resized proportionally using a uniform scale factor (λ). This method maintains the hull form and shape characteristics while preserving geometric similarity. The simplicity of this approach allows for quick estimations of key ship parameters, making it a helpful tool in preliminary design. However, while geometric scaling offers consistency, it does not inherently optimise performance. The assumption that hydrodynamic, structural, and stability effects scale proportionally often does not hold due to non-linear interactions between wave resistance, structural loads, and propulsion efficiency [5, 31].

Mathematically, geometric scaling follows well-established proportional relationships. The primary dimensions length, beam, and draft scale linearly with the factor λ, Consequently, surface areas are scaled

quadratically with λ^2, while volumes and, by extension, displacement are scaled cubically with λ^3.

$$L_{new} = \lambda L_{parent}, \quad B_{new} = \lambda B_{parent}, \quad T_{new} = \lambda T_{parent}, \quad A_{new} = \lambda^2 A_{parent}. \quad \nabla_{new} = \lambda^3 \nabla_{parent} \tag{3.1}$$

Hydrodynamic coefficients such as the block coefficient (C_B), prismatic coefficient (C_P), water-plane coefficient (C_{WP}) and Mid-section coefficient shown in equation 3.2 remain constant since they are dimensionless and represent the overall shape of the hull rather than its absolute size.

$$C_B = \frac{\nabla}{L \cdot B \cdot T} \quad C_P = \frac{\nabla}{L \cdot A_M} \quad C_{WP} = \frac{A_W}{L \cdot B} \quad C_M = \frac{A_M}{B \cdot T} \tag{3.2}$$

Ship speed, when preserving the Froude number ($Fr = U/\sqrt{gL}$), follows a square root scaling:

$$U' = \sqrt{\lambda} U.$$

Stability characteristics such as the KB, BM, and LCB are geometric properties defined by the centroid of the submerged volume, and under geometric similarity, they scale proportionally with the factor λ. In contrast, the KG depends on weight distribution. For early-stage design, it can be approximated as a fraction of the moulded depth, under the assumption of similar internal arrangements. The LCG is required for seakeeping analysis as it governs trim and pitch. The LCB is a geometric property of the hull form and cannot be altered without changing the hull design. For equilibrium, the LCG must align with the LCB (no-trim condition).In early-stage design, when weight distribution is not yet known in detail, it is common to assume $LCG = LCB$, which holds consistently across all designs. As the design progresses, improved weight estimates may shift the assumed LCG, requiring reassessment of the initial balance with the hull's fixed LCB. This highlights how proportional scaling provides useful first-order estimates, but practical considerations such as machinery layout and outfitting can lead to departures from strict geometric similarity.

While geometric scaling provides a straightforward method for resizing vessels, it does not fully capture the complexities of ship performance. One major limitation is that hydrodynamic resistance does not scale proportionally, particularly in the case of wave-making resistance, which depends on the interaction between hull form and fluid flow. As ship size increases, the Reynolds number changes, influencing the boundary layer and frictional resistance in ways that geometric scaling alone cannot account for [53]. Stability and seakeeping behaviour are affected since a scaled-up ship experiences different wave-induced loads and motion frequencies, as the natural ocean waves do not scale with geometry, potentially leading to undesirable dynamic responses [54].

The ship's required power depends on its resistance and speed, as shown in Equation 3.3, and can be estimated using the Admiralty equation (Equation 3.4) [18]. However, this approximation is only valid in the displacement speed regime; at the higher speed range of OPVs, where semi-displacement effects dominate, the Admiralty relation breaks down. These equations nevertheless highlight the non-linear

nature of propulsion performance, particularly its sensitivity to changes in displacement and speed. The assumption that a scaled vessel will achieve the same efficiency as its original counterpart often leads to suboptimal fuel consumption and power requirements [31].

down

$$P = R_T \cdot V_s \tag{3.3}$$

$$P = \frac{\Delta^{2/3} \cdot V_S^3}{C} \tag{3.4}$$

In practical applications, ship designers often supplement geometric scaling with parametric adjustments to refine hull proportions, optimise weight distribution, and enhance structural and hydrodynamic efficiency. While geometric scaling remains a valuable tool in early-stage ship design, it is rarely used in isolation when developing a fully optimised vessel.[5, 31].

3.2.2. Parametric Scaling

Parametric scaling is a more advanced method that refines hull form characteristics based on operational and performance-driven constraints. Unlike geometric scaling, which applies uniform adjustments to all dimensions, parametric scaling selectively modifies key design variables such as the length-to-beam ratio, block coefficient, or flare angle to optimise specific aspects of performance [24, 31]. This method allows ship designers to fine-tune critical parameters while maintaining overall design. By adjusting hull proportions rather than simply enlarging or shrinking the entire vessel, parametric scaling can improve efficiency, stability, and seakeeping while meeting mission-specific operational needs [5, 55].

Parametric scaling offers flexibility but comes with challenges. Unlike geometric scaling, it requires engineering expertise to define meaningful parameter relationships and iterative adjustments to balance performance and trade-offs. A major challenge is its reliance on empirical data, as historical ship data and regression models are essential for accurate predictions. The complexity of non-linear interactions in hydrodynamics, stability, and structural loads necessitates high-fidelity simulations like CFD and Finite Element Analysis (FEA), increasing computational costs. Small changes in parameter values can lead to significant performance variations, making optimisation an iterative process. Additionally, while parametric scaling enhances performance, it may introduce complex hull shapes that complicate fabrication and regulatory compliance. To mitigate these issues, parametric scaling is often integrated with MDO and machine learning for automated parameter selection. However, these methods remain computationally demanding and require validation against real-world prototypes [56].

3.2.3. Hybrid Approaches

Hybrid scaling blends geometric and parametric methods, balancing simplicity with targeted performance refinements. It is particularly useful for adapting a parent hull while incorporating mission-driven modifications. Common in naval and commercial ship design, this approach allows a standardised hull to be geometrically scaled while adjusting key parameters like hull coefficients, deckhouse configurations, and

propulsion to meet operational needs [5, 8]. Its advantages include incremental hull modifications while preserving hydrodynamic performance, reduced computational effort compared to full parametric scaling, and easier regulatory compliance. It has been successfully applied in naval platforms to standardise hull frameworks while allowing mission-specific adaptations. However, iterative validation and CFD testing remain necessary to ensure performance improvements [57].

3.3. Parametric Modelling

In contrast to *parametric scaling*, which non-uniformly resizes a hull's dimensions, *parametric modelling* is a technique to define the 3D hull form, where designers can directly alter the ship's geometry by changing a set of predefined control parameters. Parametric hull modelling has emerged as an effective tool for optimising ship design processes. This approach leverages computational methods to generate and modify ship hull forms by varying predefined parameters and constraints, enabling designers to efficiently explore a vast design space and accelerate development cycles [58, 59]. Various methods and software are supporting this approach. This section provides an overview of the main modelling techniques used in parametric ship hull design. In general, these methods can be divided into two categories: Explicit Parametrisation and Implicit Parametrisation.

3.3.1. Types of Parametric Modelling in Ship Design

Explicit Parametrization

Explicit Parametrisation directly defines ship geometry using control points or explicit mathematical definitions. Splines represent a specific category of explicit parametrisation utilising piecewise polynomial functions, most commonly Bézier curves, B-Splines, T-Splines, F-Splines, or NURBS [54, 60, 61, 62].

- B-Spline curves are commonly used in ship design due to their flexibility and computational efficiency. They offer local control over the hull shape through control points and knot vectors, allowing designers to make targeted modifications without affecting the entire curve. However, they lack built-in fairness constraints to ensure smooth curvature and surface continuity. Pérez-Arribas [54], demonstrates the effectiveness of using B-splines for defining key geometric features in ship hulls.
- Non-Uniform Rational B-Splines (NURBS) extend B-Splines by incorporating weights, allowing for the representation of conic sections and more complex surfaces. Weighted control points enable the precise shaping of surfaces like circular arcs and ellipses. Transformations such as translation, scaling, and rotation do not affect fundamental shape properties. Hui Zhou et al. [63] highlight the effectiveness of NURBS-based parametric design in accurately defining and optimising ship hull forms, emphasising its ability to effectively represent complex geometrical shapes and facilitating efficient modifications for hydrodynamic optimisation.
- T-Splines generalise NURBS by introducing T-junctions, which allow local refinement without affecting the entire mesh. This reduces the number of control points and supports the efficient modelling of

complex areas such as bows, sterns, and midship transitions. Their compact and flexible control structure makes them well-suited for precise and efficient hull form optimisation [61].

- F-Splines are specialised curves designed to ensure fairness by minimising curvature irregularities and avoiding oscillations. Unlike conventional splines, they use geometric constraints such as curvature distribution and enclosed area rather than only control points. Mainly used in tools like CAESES, F-Splines enable smooth and hydrodynamically efficient hull lines with minimal manual tuning [61, 62].
- Bézier curves, provide an intuitive mathematical description beneficial for hull form manipulation. Khan et al. [60], employed cubic Bézier curves effectively for yacht hull design, utilizing them to create Coons patches, which ensure geometric continuity and maintain hull fairness during parametric modifications

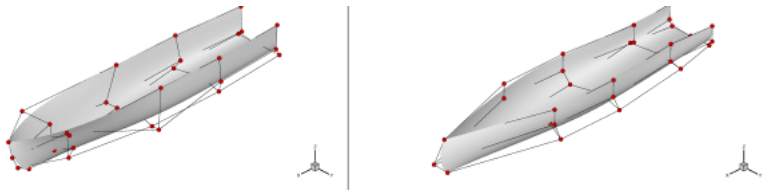

Figure 3.6: Representation of the hull surface adopted in the effective power optimisation problem by means of a single NURBS [24]

Implicit Parametrization

Implicit Parametrisation indirectly defines ship geometry through constraints or deformation frameworks rather than through direct control point manipulation. These methods are particularly effective for complex optimisation tasks where geometric and physical constraints, such as displacement, hydrostatics, or smoothness, must be preserved. Common implicit methods in parametric modelling include Free-Form Deformation (FFD), Lackenby Method, and Modal Deformation.

- Free-Form Deformation (FFD) is a geometric deformation technique introduced by Sederberg and Parry (1986), widely used in ship design to optimize hull forms for hydrodynamic performance. It acts as a deformation layer applied on top of explicitly defined geometry, such as NURBS surfaces, allowing targeted, constraint-friendly shape modifications without altering the underlying topology. FFD embeds the hull within a 3D lattice of control points, enabling smooth local and global deformations. This technique is particularly useful for refining complex features like bulbous bows and sterns. It is highly effective in MOO tasks involving resistance, stability, and seakeeping [64]. Dejhalla et al. [65] integrated FFD with genetic algorithms and hydrodynamic solvers based on Dawson's method, demonstrating significant resistance reduction. An example is illustrated in Figure 3.7.

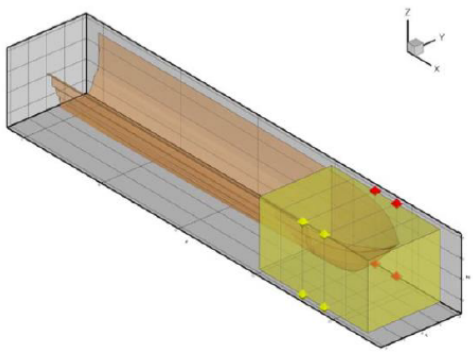

Figure 3.7: Illustration of Free-Form Deformation (FFD) applied to hull form optimisation[64]

- Lackenby Method is a classical hull transformation technique used to adjust ship geometry by systematically shifting transverse sections along the longitudinal axis. Maartens, in his MSc thesis [66], presents the Lackenby method as a systematic way to adjust hull geometry by shifting frames longitudinally while keeping the sectional shape and area unchanged. This method enables modification of key hydrodynamic parameters such as the prismatic coefficient, LCB, and overall hull length. An extension of this technique is the Shifting Method, which generalises the Lackenby approach by allowing 3D transformations of point data—not just longitudinal shifts, but also transverse (Y) and vertical (Z) displacements. This increased geometric flexibility enables a wider exploration of hull design variations while still preserving the essence of the parent hull geometry [66].
- Spline Interpolation with Constraints uses embedded fairness or geometric constraints (e.g., fixed volume or slope continuity), which make the adjustment process implicit rather than explicitly defined by control points. These constraint-driven spline methods are typically integrated into advanced CAD platforms such as CAESES [53], where they enable fairness-preserving manipulation of NURBS and F-splines to support hydrodynamic optimisation.

3.4. Conclusion

This chapter reviewed ship design and scaling methodologies, addressing Sub-question 2:

"*How do contemporary ship-design and scaling methodologies—including geometric, parametric and hybrid approaches—capture the non-linear interactions between key hull parameters (length, beam, draft, block coefficient) and performance indicators (resistance, stability, seakeeping, propulsion efficiency), and thereby support optimisation in the early stages of design?*".

Contemporary ship-design methodologies increasingly emphasise early-stage optimisation frameworks to balance performance, cost, and mission capability. Traditional geometric scaling approaches rely on proportional relationships derived from parent hulls but cannot capture the complex non-linear effects of dimensional changes on key performance indicators. Parametric scaling allows selective adjustment of individual parameters, thereby improving alignment of the hull form with specific performance goals, though still requiring significant designer judgement and iteration. Hybrid approaches attempt to combine

the benefits of geometric and parametric methods, but they remain dependent on designer expertise to interpret the complex, non-linear interactions between parameters. This highlights the need for integrated visual decision-support tools, such as design space mappings and sensitivity plots, that can help designers systematically understand trade-offs, explore the design space efficiently, and make informed decisions during the early design stages.

Advanced parametric modelling techniques enhance design flexibility by enabling direct manipulation of hull geometry under fairness and constraint control. When coupled with structured exploration strategies, these methods allow systematic investigation of large, complex design spaces and the non-linear interactions between hull parameters and performance metrics. This capability provides a robust foundation for integrating MOO methods into early-stage design workflows.

Despite these advances, most scaling approaches in the literature still do not embed direct performance assessment into the design loop. Geometric methods, in particular, rely on proportional similarity and implicitly assume comparable performance across scales, neglecting the non-linear effects of dimensional changes. Parametric and hybrid approaches offer more flexibility, but they too often base scaling on assumed similarity rather than systematic evaluation of resistance, stability, and seakeeping. As a result, current methodologies fall short of providing an integrated, mission-driven framework for OPVs, where multi-mission demands require explicit performance trade-off analysis.

While parametric and hybrid scaling methods advance the capabilities of early-stage hull design, their integration within a systematic, mission-oriented MOO framework remains limited. This gap provides both the motivation and foundation for the next chapter, which builds upon the insights from Chapters 2 and 3 to outline the requirements and structure of a decision-making framework for OPV scaling that explicitly incorporates MOO methods and performance trade-offs from the earliest stages of design.

4

Multi-Objective Optimisation in Ship Design

This chapter reviews the optimization Methodology. By evaluating the strengths and limitations of these approaches, the chapter addresses research question 3: "*What is the current state-of-the-art in design optimisation frameworks for early-stage ship design, and based on this, what are the requirements for a Multi-Objective Optimisation (MOO)-based decision-making framework suitable for OPV scaling?*".

Together with Chapters 2 and 3, this chapter defines the requirements for the new framework and establishes the methodological foundation for the design framework developed in Chapter 5.

4.1. Formulation of MOO

An MOO solves an indeterminate problem by minimising or maximising a set of objective functions. It typically consists of three main components: constraints, variables, and objective functions. Equation 4.1 presents the general mathematical formulation of an MOO problem [18].

$$\begin{aligned} \min_{\mathbf{x}\in\mathcal{X}} \quad & F(\mathbf{x}) = \{f_1(\mathbf{x}), f_2(\mathbf{x}), ..., f_n(\mathbf{x})\} \\ \text{subject to} \quad & g_i(\mathbf{x}) \leq 0, \quad i = 1, ..., m \\ & h_j(\mathbf{x}) = 0, \quad j = 1, ..., p \end{aligned} \tag{4.1}$$

Here, $F(\mathbf{x})$ represents a vector of n objective functions to be minimised. The design vector $\mathbf{x} \in \mathbb{R}^d$ belongs to the feasible design space $\mathcal{X} \subseteq \mathbb{R}^d$, which is defined by m inequality constraints $g_i(\mathbf{x}) \leq 0$ and p equality constraints $h_j(\mathbf{x}) = 0$.

The aim of MOO is to find solutions that represent the best possible trade-offs between conflicting objectives. Unlike single-objective optimisation, MOO typically results in a set of optimal solutions rather

than a single one and are known as a Pareto-optimal solution.

Pareto Optimality Concepts

A solution is considered Pareto optimal if no other solution exists that can improve one objective without degrading at least one other. The collection of such non-dominated solutions forms the Pareto front. The Pareto front helps decision-makers explore trade-offs between conflicting design goals and identify balanced solutions suitable for further development. An example of such a Pareto front is shown in figure 4.1, Bronkhorst [19], showed a Pareto exploring trade-offs between the ORI, R_T, and LWT. In this example, the base vessel is not Pareto optimal; it is dominated by other feasible solutions that offer improvements in one or more objectives.

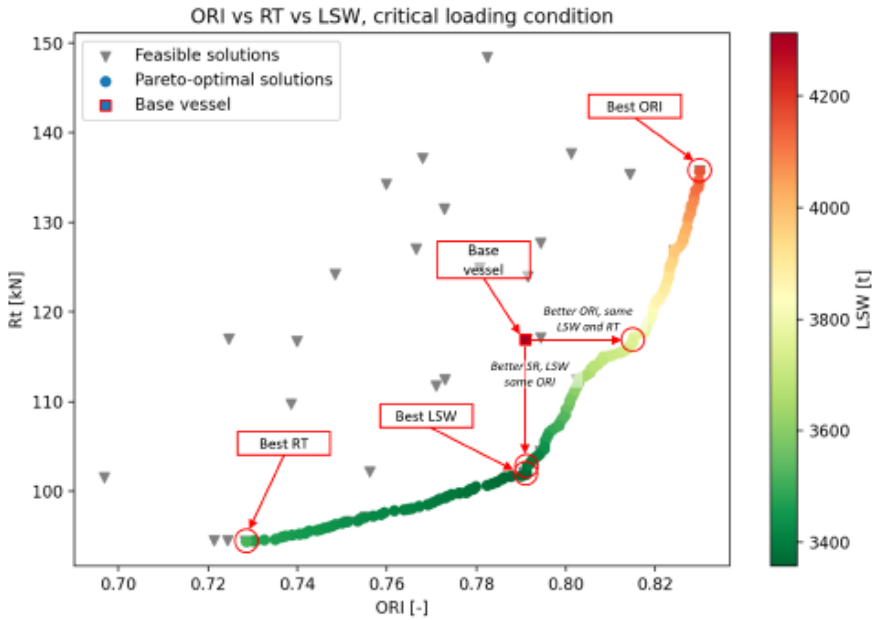

Figure 4.1: Example of Pareto front showing the trade-offs between ORI, R_T), and LWT for feasible OSV designs [19].

Hypervolume as a Pareto Front Quality Metric

The hypervolume (HV) [9] is method used to quantitatively assess Pareto front quality. It measures the n-dimensional volume dominated by the non-dominated solutions, bounded by a reference point, and captures the convergence and diversity of the Pareto front. A higher HV indicates a better Pareto front. The HV can be used to compare different optimisation algorithms and solution sets, with higher values signifying better performance [9].

4.2. State-of-the-Art Review On MOO

Recent advancements in ship design optimisation integrate evolutionary algorithms, surrogate modelling, and response surface models to refine the Pareto front.

Papanikolaou [67], utilise genetic algorithms within a multi-objective optimisation framework using

NAPA and Multi-Objective Genetic Optimisation (MOGA) for holistic ship design, focusing on hull form optimisation of high-speed vessels with respect to powering and wash.

Biliotti et al. [59], uses automated parametric modelling in CAESES and a multi-objective optimization environment in *modeFRONTIER*™ (a commercial multi-objective optimisation platform developed by ES-TECO). Using the Sobol sequence to populate the design space. MOGA is applied to optimise multiple objectives, including resistance at two speeds, the Seakeeping Operability Index, and the Motion Sickness Incidence (MSI).

Winyall et al. [8] integrate parametric 3D hull-form modelling with ship design synthesis using a MOGO framework. Initial sampling is performed using both full-factorial and Latin Hypercube Sampling (LHS) DoE, which is used to build Response Surface Models (RSMs) for resistance and seakeeping. These RSMs enable efficient NSGA-II (Non-dominated Sorting Genetic Algorithm), style optimisation and demonstrate the coupling of geometry-level control with system-level performance evaluation.

Peri [24], investigates three sequential methods to enrich the Pareto front in multi-objective optimization: Local Resampling, Interpolation-Based Resampling, and the Normal Boundary Intersection (NBI) method. The process begins with Sobol sampling for the DoE to obtain an initial approximation of the Pareto front. These techniques are applied iteratively to enhance the resolution and distribution of solutions along the front. For comparison, NSGA-II and Multi-Objective Particle Swarm Optimization (MOPSO) algorithms are also implemented. The study shows that the combined NBI-based approach yields a denser and more uniform Pareto front than traditional methods.

Yurdakul et al. [7], Yurdakul et al. [7] propose a Pareto-based decision-making approach to select improved ship main dimensions at an early design stage. They generate candidate designs using Sobol quasi-random sampling in MATLAB® and analyse performance trade-offs, such as effective power and seakeeping, through a combination of low-fidelity algorithm simulations. The method aims to identify a technological barrier (Pareto frontier), offering better initial conditions for subsequent optimisation.

Ljulj et al. [3, 11], develop a multi-attribute design synthesis framework for Hybrid OPVs, primarily utilising NSGA-II. Their approach integrates the adaptive Monte-Carlo method and employs an OMOE to refine trade-off analysis, enabling system-level evaluation of early-stage configurations beyond parametric modelling.

De Gaaij explored the use of parametric optimisation during the early-stage concept exploration of naval support vessels, using CAESES as a geometry generation and control platform. The optimisation process uses DAKOTA's global optimisation module based on Genetic Algorithms (GA) and is applied to RSMs that approximate resistance and seakeeping objectives. The initial design space is explored using LHS to generate training data for the RSMs, which enables efficient optimisation within the concept design phase.

Bronkhorst et al. [19], study includes the optimisation of Offshore Service Vessels (OSV) using *NAPA*® (a commercial naval architecture software platform developed by NAPA Ltd.) and the SAMO-COBRA

algorithm, developed by De Winter [9]. The method accounts for multiple objectives and constraints, integrating the Operability Reliability Index (ORI) to reflect varying mission profiles.

De Winter [9] introduces a constraint-handling method for MOO in ship design using SAMO-COBRA, which combines constraint dominance with evolutionary algorithms and RBF surrogates. The IOC-SAMO-COBRA extension further reduces costly evaluations by using online constraint relaxation and inexact evaluations, making it well-suited for early-stage design under complex constraints.

4.3. Design of Experiments (DoE)

DoE plays a foundational role in multi-objective ship design optimisation by enabling a systematic and efficient sampling of the design space. A well-designed DoE ensures sufficient diversity and coverage, which is essential for thoroughly exploring the design space and understanding trade-offs between conflicting objectives. Table 4.1 summarises the advantages and disadvantages of three commonly used sampling schemes: Random Sampling, LHS, and Sobol Sequences [68]. The effective use of DoE requires several preconditions:

- clearly defined design variables and ranges,
- feasibility constraints to ensure only meaningful candidates are generated,
- a sufficient sample size to cover the design space while remaining computationally tractable,
- an appropriate distribution strategy (uniform, stratified, or low-discrepancy) to balance exploration and coverage.

Meeting these conditions ensures that the DoE provides representative data for subsequent surrogate modelling and optimisation

Table 4.1: Advantages and disadvantages of three sampling schemes [68]

Sampling Scheme	Advantages	Disadvantages
Random Sampling	- Easy to implement - Computationally inexpensive	- Can be inefficient (requires many samples)
Latin Hypercube Sampling (LHS)	- Covers space more uniformly than random sampling - Better for numerical integration	- Difficult to add samples after the fact - Higher computational cost than Random or Sobol - May not suit non-uniform multivariate distributions
Sobol Sequences	- Reproducible (deterministic) - Better uniformity than Random or LHS - Smallest error for computing integrals	- May not maintain theoretical advantages for non-uniform multivariate distributions

4.4. Optimization Algorithm

The choice of optimisation algorithm depends on computational efficiency, convergence behaviour, and compatibility with ship design constraints. The literature highlights two main families: evolutionary algo-

rithms and surrogate-assisted optimisation.

4.4.1. Global Optimization

Global Optimisation (GO) refers to the use of MOGA to solve complex design problems involving trade-offs between conflicting objectives. In CAESES, MOGA is implemented via the DAKOTA framework [69],

The algorithm is governed by three key parameters: total population size, initial population size, and the number of generations. It begins with an initial population sampled using methods such as Sobol sequences or LHS, with each design candidate evaluated against the defined objectives. Based on these evaluations, fitness functions are used to distinguish better from worse solutions in multi-objective optimisation. MOGA applies a dominance-based ranking using a *domination count* strategy, where a solution is considered *non-dominated* if no other solution performs better across all objectives. Lower domination counts indicate higher fitness. This approach preserves trade-offs without scalarizing multiple objectives [69].

To maintain diversity and prevent premature convergence, MOGA applies a *crowding distance* metric, which favours individuals in less populated regions of the objective space (Figure 4.2a). Selection is carried out using a *below-limit selector*, which retains designs with domination counts below a threshold. The next generation is created by combining elite solutions with offspring generated through crossover and mutation. Non-selected individuals are discarded. This evolutionary process repeats until a maximum number of generations is reached or convergence is achieved—typically when the Pareto front stabilises or diversity changes minimally (Figure 4.2).

Compared to NSGA-II, MOGA in DAKOTA is more flexible: populations can be extended, and additional generations can be introduced without restarting. This makes it particularly effective for iterative, user-driven workflows common in early-stage ship design.

4.4.2. Surrogate-Based Global Optimisation (SBGO)

SBGO builds an approximate model, called a surrogate, to predict objective values across the design space. Instead of evaluating all candidates using high-fidelity simulations, SBGO evaluates a small number of them to approximate the design space efficiently. In CAESES, SBGO is implemented via the DAKOTA framework [69].

SBGO is based on GO using an MOGA but adds a surrogate model to significantly reduce the number of expensive evaluations needed. Like GO, SBGO begins with an initial sampling process to populate the design space with candidate solutions, though typically using a smaller sample size.

These initial candidates are evaluated using high-fidelity tools (e.g., CFD or motion analysis), and the resulting input-output data is used to train a surrogate model, commonly based on Kriging (Gaussian Process Regression). Kriging models the system response as a stochastic process, providing both mean predictions and uncertainty estimates across the design space [6, 37].

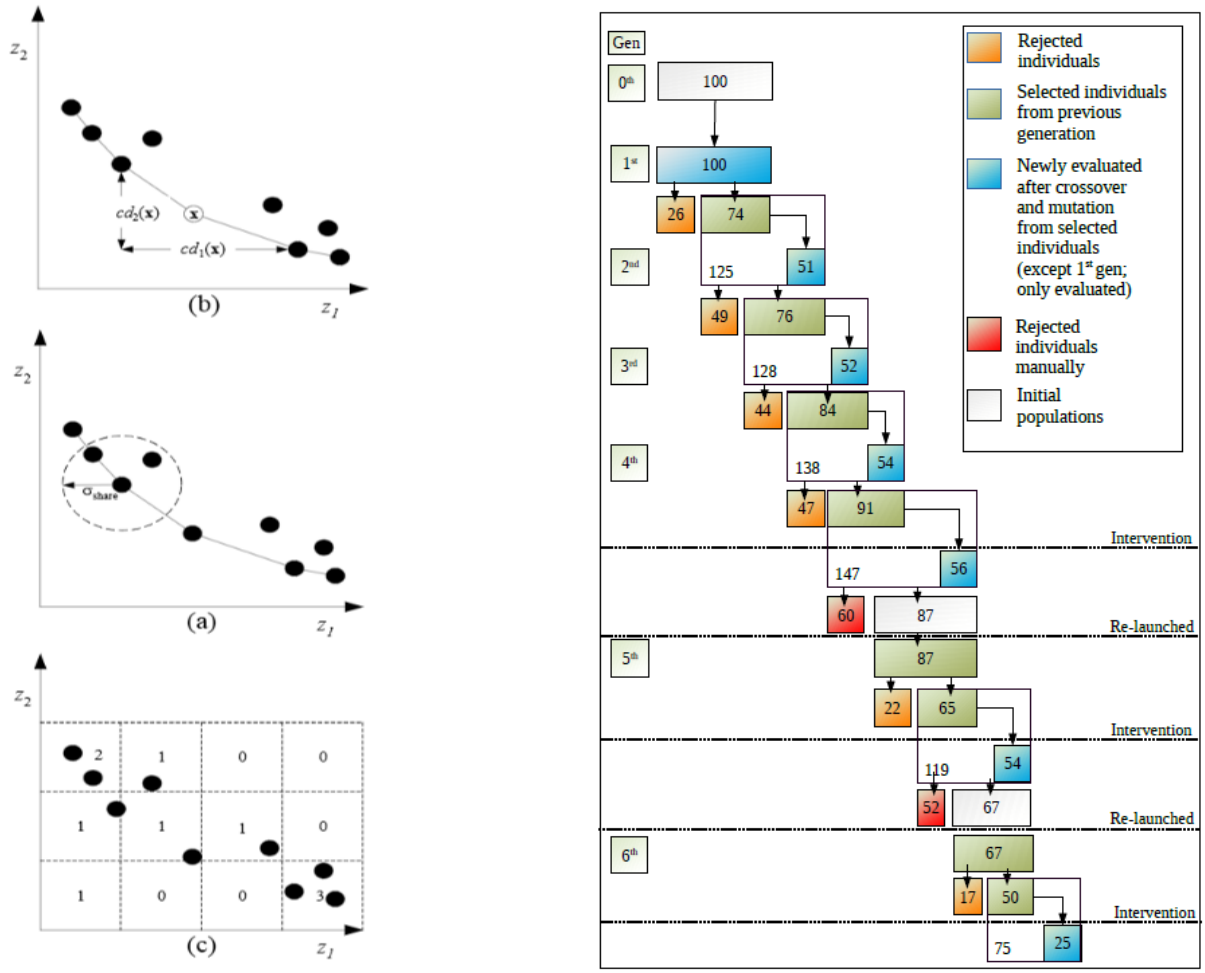

(a) Diversity methods used in MOGA [70].

(b) Generational process of MOGA in CAESES using DAKOTA.

Figure 4.2: Genetic algorithm flowchart, with the number of evaluations (designs) rejected, selected, and evaluated in each of the generations [71].

Once trained, the optimiser explores the surrogate instead of the full model to generate new candidate designs. Promising solutions are re-evaluated with high-fidelity simulations to improve the surrogate's accuracy. This loop—optimise, evaluate, update—continues iteratively until convergence is achieved.

A Gaussian Process (Kriging)

Kriging is a statistical modelling method that treats the output of a design evaluation as a realisation of a random process. It provides both a predicted value and an uncertainty estimate for new design points [72].

Kriging relies on a correlation matrix R, which quantifies how similar the outputs of evaluated design points are, based on their distance in the input space (e.g., length, beam, draft). If two points are close together, their outputs are assumed to be highly correlated, so $R_{ij} \approx 1$. If they are far apart, the correlation diminishes, and $R_{ij} \approx 0$ The structure of R is determined by a kernel function (e.g., Gaussian), which governs how quickly correlation decays with distance. This matrix is essential for interpolating between known evaluations and forms the basis of Kriging's predictive power. The Kriging prediction at a new point

x^* is given by:

$$\hat{f}(x^*) = \mu + r(x^*)^T R^{-1}(y - \mu \mathbf{1})$$

$$\text{Var}[f(x^*)] = \sigma^2 \left(1 - r(x^*)^T R^{-1} r(x^*)\right)$$

where μ is the mean of the process, R is the correlation matrix between training points, $r(x^*)$ is the correlation vector between x^* and the training points, and y is the vector of observed outputs.

4.4.3. Algorithm Selection

Comparing the three algorithms (excluding MOSA, which is not suited for large-scale exploration): NSGA-II defines the number of evaluations by its generations and population size. GO is controlled by a fixed evaluation budget. SBGO begins with an initial sample set and iteratively refines a surrogate model by evaluating only the most promising candidates, improving efficiency. For GO, this is limited by a user-defined maximum. SBGO starts with a small number of high-fidelity evaluations (initial samples), builds a surrogate model, and iteratively refines it by evaluating only the most promising candidates, greatly improving efficiency.

Yustina and Saptawijaya [72] recommend a LHS DoE with at least $11 \cdot (n - 1)$ samples, where n is the number of design variables. For the six-variable, $n = 6$, this translates to a minimum of 55 samples. They used up to 150 initial samples with 200 total evaluations, applying both NSGA-II and MOEA/D with Kriging, BPNN-PSO (Back Propagation Neural Network – Particle Swarm Optimisation), and MLP (Multilayer Perceptron) surrogate models. Kriging, while less accurate, produced the highest hypervolume and fastest computation time. Winter [9] advised a DoE size of $\lceil e \cdot p \rceil$ where p is the number of parallel evaluations(e.g., 17 for $p = 6$) and recommended staying below 300 evaluations. De Gaaij [37] used 100 initial samples and 33 iterations of 12 evaluations, totalling 396. SBGO outperformed NSGA-II and GO in both speed (4.5 hours) and Pareto quality. Bronkhorst [19] used 300 evaluations in 3.5 hours with SAMO-Cobra, incorporating seakeeping analysis. A convergence study is recommended to confirm Pareto front accuracy. De Gaaij extended his SBGO run to 600 iterations and observed marginal improvements beyond 400, identifying this as a practical limit.

Thus, SBGO is particularly suited for concept design phases, where fast yet informed decisions are needed despite limited data and budget.

4.5. Required Framework

Chapter 2 defines OPVs, their mission profiles, and the key design drivers that influence their development. Designing effective OPVs requires balancing trade-offs between endurance, range, resistance, and cost, while ensuring required seakeeping and stability. Chapter 3 explores core ship design principles, including the traditional design spiral, geometric and parametric scaling approaches, and parametric modelling. It concludes that hull form parameters have a significant impact on performance metrics such as resistance,

stability, and seakeeping. Chapter 4 introduces MOO techniques and presents evaluation methods aligned with key design drivers.

These chapters establish the need for a more comprehensive and performance-driven approach to early-stage OPV design. Rather than relying solely on parent hull scaling, this thesis proposes an MOO framework that incorporates mission-specific performance requirements directly into the design process. The aim is to develop a decision-making framework that supports informed trade-offs and enables the generation of optimised hull forms tailored to operational demands, moving beyond the limitations of simple geometric scaling.

To achieve this, the proposed framework must meet the following requirements:

- **Integration of mission-specific performance requirements** Directly link mission demands to hull geometry and design constraints.
- **Effective handling of non-linearities** Account for non-linear relationships between design variables and performance metrics.
- **MOO capability** Incorporate MOO techniques to manage conflicting objectives and provide a Pareto-optimal solution set.
- **Early-Stage design focus** Support early design decision-making while ensuring cost-effectiveness.
- **Consideration of key design drivers** Integrate resistance, stability, seakeeping, endurance, range, and TLCC into the optimisation process.

4.5.1. Resulting Framework

Based on the previous analysis, the resulting framework includes clearly defined objectives, constraints, input parameters, design variables, and evaluation methods. The framework's modularity ensures adaptability, allowing it to be easily modified or expanded by adding or removing design variables, objectives, or constraints. Table 4.2 summarises the core elements, while Figure 4.3 illustrates the global workflow. Design inputs define environmental and operational constraints and provide baseline data for evaluation. The optimisation algorithm steers a set of design variables to satisfy performance objectives under specified constraints. Each design iteration is evaluated using performance metrics until a Pareto front of optimal solutions is achieved.

Table 4.2: Summary of Required Design Framework

Objective	Constraint	Input	Variables	Evaluation Method
Maximise DWT	Δ	Environmental conditions (SS)	Length	Empirical weight estimation
Minimize LWT	L/B	Motion sensitive locations	Beam	H&M resistance method
Minimize resistance	B/T		Draft	GZ curve analysis
Maximise stability	GM/B		C_B	RAO-based seakeeping indices
Maximise seakeeping			Deadrise angle	
			Stem rake	

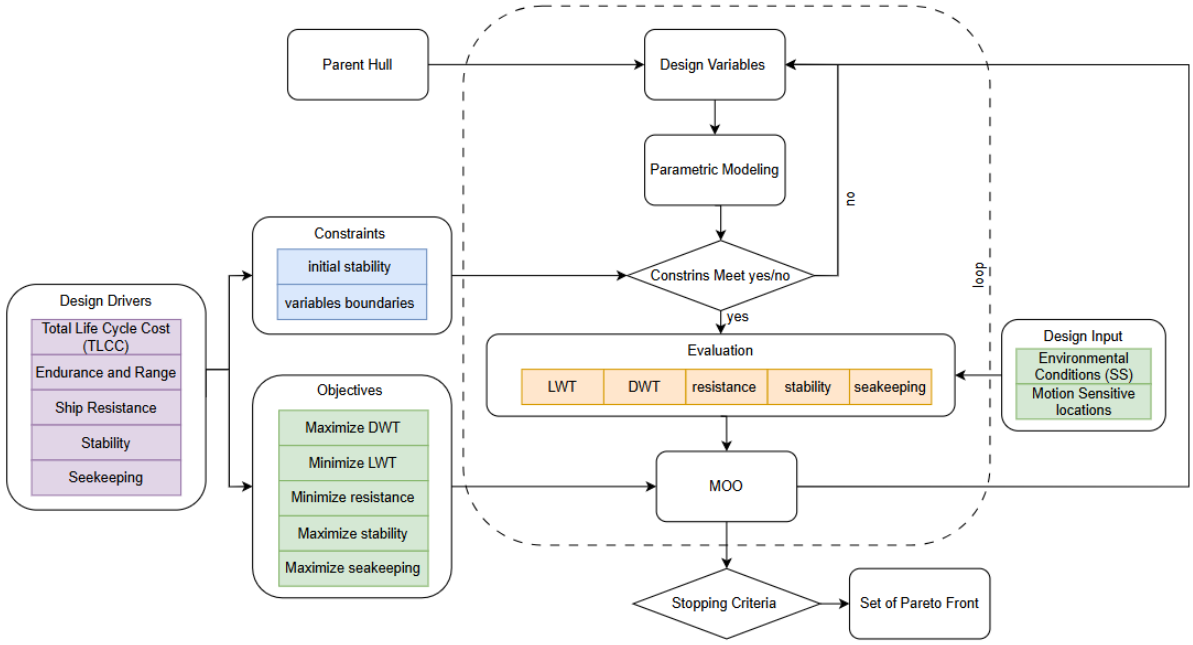

Figure 4.3: Framework flow chart based on design drivers

4.6. Conclusion

This chapter reviewed contemporary optimisation techniques and connected evaluation methods to key design drivers, thereby addressing Sub-question 3:

"*What is the current state-of-the-art in design optimisation frameworks for early-stage ship design, and based on this, what are the requirements for a Multi-Objective Optimisation (MOO)-based decision-making framework suitable for OPV scaling?*"

Current state-of-the-art frameworks in early-stage ship design are increasingly moving beyond traditional, sequential, and manual approaches. By integrating 3D parametric modelling environments with evolutionary algorithms such as GA and SBGO, these frameworks enable systematic exploration of large, complex design spaces. The use of LHS ensures efficient initial design space exploration, while MOO techniques, particularly Pareto-front-based methods, allow balancing conflicting objectives such as resistance, seakeeping, stability, and cost from the earliest design phases.

Based on this review, the requirements for an MOO-based decision-making framework suitable for OPV scaling have been identified. The framework must:

- Integration of mission-specific performance requirements: link mission demands directly to hull geometry and design constraints. This is achieved by systematically evaluating resistance, stability, and seakeeping under mission-driven constraints such as minimum range and roll period limits.
- Consideration of key design drivers: integrate resistance, stability, seakeeping, endurance, range, and TLCC into the optimisation process. These metrics are embedded directly into the framework's

evaluation loop to ensure mission-driven performance assessment.

- Effective handling of non-linearities: capture non-linear relationships between design variables and performance metrics. This is achieved by training surrogate models on systematically sampled design points (via DoE), enabling the optimisation algorithm to resolve complex interactions. The resulting trade-offs are then visualised through Pareto frontiers.
- MOO capability: incorporate optimisation techniques to balance conflicting objectives and generate Pareto-optimal solution sets. The combination of DoE and surrogate-based evolutionary algorithms delivers this capability, exposing trade-offs between conflicting objectives. These trade-offs are then visualised through Pareto frontiers to support informed early-stage decision-making.
- Early-stage design focus: support rapid and cost-effective decision-making under limited information. This is enabled by parametric modelling of the parent hull, which allows the rapid generation of scalable design variants and straightforward parameter variation.

Among available tools, CAESES was identified as a suitable parametric modelling platform, capable of integrating geometry generation, hydrostatics, and performance evaluation workflows. Coupled with LHS-based DoE and Kriging surrogate models within an SBGO approach, the framework can efficiently handle the computational burden of seakeeping assessments, which remain a critical yet time-consuming design driver in OPV design.

This chapter therefore, established the critical requirements for an integrated, mission-driven MOO framework tailored to OPV scaling. By systematically connecting mission performance objectives, key design drivers, and hull form parameters within a unified and computationally efficient workflow, the proposed framework aims to enhance decision-making in the early design phase of OPVs. The subsequent chapter presents the research plan, detailing the methodology, workflow structure, and validation steps for implementing and testing the framework.

5

Design Framework for OPV - Methodology

Based on the foundations laid in Chapters 1–4, a research methodology is formulated to address the framework requirements defined in Section 4.5. This chapter presents the methodology of the proposed framework and is structured into three core modules: parametric modelling, performance evaluation, and MOO. Together, these modules support the development of scalable hull-form design methods for OPVs. A schematic overview of the complete framework is shown in Figure 5.1.

The thesis employs CAESES, both as a parametric CAD platform and as the optimisation engine and design manager. Maxsurf® Motion is integrated for seakeeping and motion analysis.

By detailing its components and setup, this chapter addresses Sub–question 4: *"What components are required for the proposed framework, and how can the setup be structured to support early-stage OPV design?"*.

5.1. CAESES

CAESES is a parametric design and optimisation platform, originally developed in the maritime field but now used across multiple industries. In this thesis, it served as the central environment for modelling, design-space exploration, and optimisation. Its functionality enabled the rapid generation of hull variants, DoE sampling, surrogate modelling (Kriging), and multi-objective evolutionary optimisation. In addition, CAESES was employed to automate workflows via internal feature definitions and external scripting, ensuring smooth integration with evaluation tools. The dedicated maritime module was particularly useful, providing hydrostatics and stability calculations directly within the design loop, thereby supporting early-stage performance assessment.

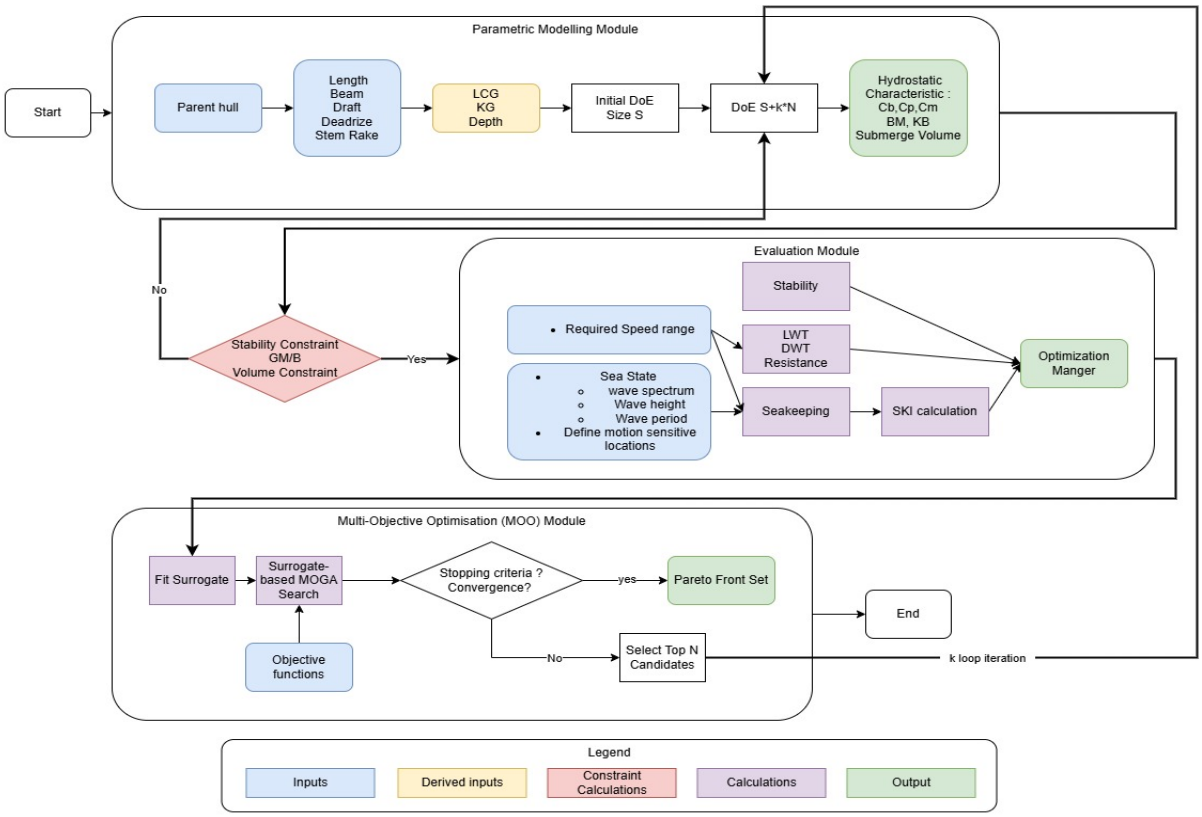

Figure 5.1: Overview of the proposed MOO-based framework for early-stage OPV design.

5.2. Baseline OPV Designs (“Parent Hull”)

Many OPV designs employ an initial baseline, or “parent hull”, as a reference for subsequent modifications and scaling [8, 11]. This approach ensures that core capabilities are preserved while adapting the vessel to evolving mission requirements [55]. However, direct geometric scaling of a parent hull is not always optimal. Andrews et al. [5] caution that relying solely on baseline scaling, without considering mission-specific functional requirements, may constrain performance. Similarly, parametric adjustments applied without operational context can also lead to suboptimal outcomes. These observations reinforce the need for a multi-criteria scaling approach that integrates mission demands with hydrodynamic, stability, and seakeeping considerations.

For this thesis, an Israel Shipyards Ltd. (ISL) OPV design has been selected as the parent hull for optimisation. The design is based on the MSc thesis work of Nir Almany [73] and was subsequently constructed by ISL. [10]. The vessel is intended for patrol duties, maritime safety enforcement, protection of exclusive economic zones (EEZs), and offshore search and rescue operations.

The vessel’s presented in figure 5.2 principal dimensions are presented in Table 5.1. Its hull form features a raked stem and transom stern, with a round-bilge midbody incorporating a chine from the transom to frame 10 ($\sim$10 m from the aft perpendicular, about 22% of L_{WL}). Additional appendages include a skeg and box keel. The vessel is fitted with two rudders, two propellers, a bow thruster, stern ramp, two

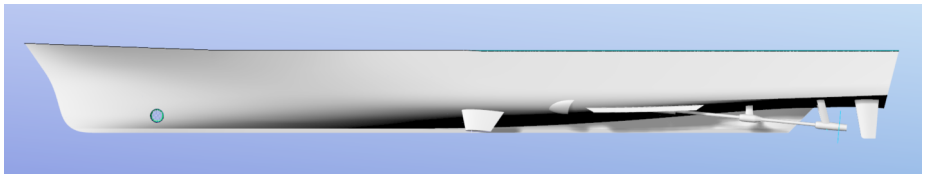

Figure 5.2: Render of Israel Shipyards Ltd. (ISL) OPV 45 hull design used

fin stabilisers, and two bilge keels. For simplicity and computational efficiency, these appendages were excluded from the hydrodynamic modelling in this study. This simplification results in a lower predicted resistance due to the absence of appendage drag and reduced wetted surface area. The influence on hydrostatics will be minor, but in seakeeping and stability analysis the omission of bilge keels and stabilisers leads to an underestimation of roll damping.

Table 5.1: Principal particulars of the ISL OPV 45, selected as the parent hull.

Main particulars	Value
Length Overall (L_{OA})	45.7 m
Beam	8.6 m
Draft	2.3 m
Displacement	330 t
Maximum Speed	24 kn

5.3. Parametric Modelling

5.3.1. Geometry Modelling

To implement parametric modelling in CAESES, a set of topological features was defined to balance fidelity to the parent hull with sufficient design freedom. The hull was represented using principal reference lines: the design waterline (WL), main deck (MD) line, centreline (CL), chine line, and a series of transverse frames. Additional curves were introduced to represent appendages such as the skeg and box keel.

The modelling process began with exporting offset points from the ISL design model in Rhino. These points were organised into an Excel offset table and redefined as functions of five design variables: L_{OA}, L/B , B/T, deadrise angle, and rake angle. The points were then imported into CAESES, where they were used to generate the hull curves.

Curves were constructed using a combination of F-splines, C-splines, multi-segment splines, and interpolation curves. This provided flexibility in controlling tangents at the start and end of each spline, as well as the number and placement of interpolation points, rather than relying solely on external control points. This ensured hull fairness and smoothness while preserving the geometric fidelity of the original hull lines.

- F-splines: Applied for frames in the aft section where a chine is present. These frames were constructed using two splines joined at the WL. F-splines do not require intermediate interpolation

points, producing smooth curves with controlled end tangents while capturing the chine geometry.

- Multi-segment splines: Used for frames without a chine, with the intermediate point located at the WL. Each segment incorporated one interpolation point, enabling localised geometric control while maintaining overall fairness.
- Interpolation splines: Applied for the WL and MD lines. These splines pass exactly through the extracted offset points, ensuring strict preservation of the original geometry along these critical references. The interpolation points correspond to the intersections of frames with the WL and MD.
- C-splines: Applied for the centreline curve (CLC). These splines allow multiple interpolation points along a line, supporting accurate reconstruction of complex local features while maintaining curvature continuity.

The principal sections used for reconstruction included frames at stations -1.8, 0, 2.6, 10, 15, 20, 25, 30, 35, 37, and 40. Surfaces were created by lofting through these generated curves. Lofting is a surface-generation method that connects a sequence of transverse and longitudinal curves to form a continuous 3D surface. In this model, the frames acted as the primary surface generators, while the WL, MD, and CL curves were used as rails to guide the loft. This ensured that the surface smoothly interpolated between frames while maintaining alignment with the longitudinal reference lines, thereby preserving both fairness and geometric fidelity.

To reduce complexity and computational cost, certain simplifications were applied. The main deck depth was assumed constant along the vessel (i.e., no sheer or camber), and detailed local features were omitted from the model.

The resulting parametric hull model is illustrated in Figures 5.3–5.5, showing both the reference curves (frames, WL, MD, CL) and the lofted surfaces.

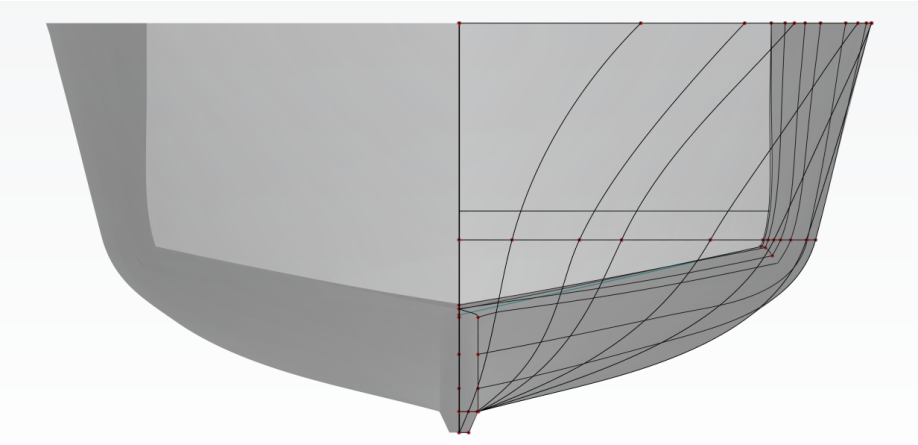

Figure 5.3: Reconstructed hull fore view, showing WL, MD, and frames

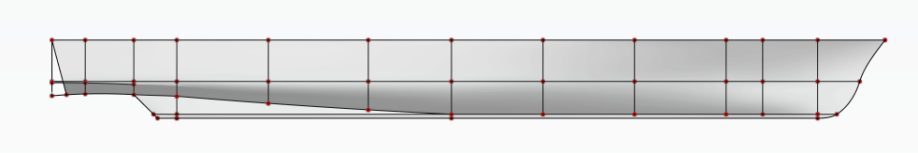

Figure 5.4: Reconstructed hull side view, showing WL, MD, and frames

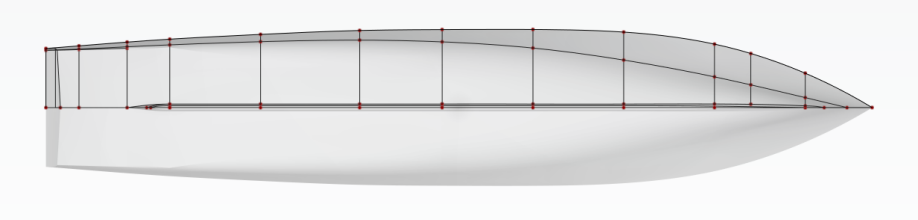

Figure 5.5: Reconstructed hull top view, showing WL, MD, and frames

5.3.2. Design Variables

The selection of design variables is based on the literature review presented in Section 2.4.1, focusing on parameters with the greatest influence on KPI relevant to OPVs. Increasing the number of variables enhances geometric freedom and enables the exploration of more novel designs. However, it also enlarges the design space and significantly increases computational time.

The selected design variables for the parametric geometry and their boundaries are presented in table 5.2

Table 5.2: Design variables and ranges used for the parametric optimisation study.

Design Variable	Lower limit	Upper limit
Length Overall (L_{OA}) [m]	40	90
Length-to-Beam Ratio (L/B)	4	7
Beam-to-Draft Ratio (B/T)	3	5
Stem Rake Angle [deg]	$0°$	$20°$
Deadrise Angle [deg]	$0°$	$15°$

5.3.3. Constraints

As mentioned in the design variables section, the ratios L/B and B/T were applied instead of directly using beam or draft as independent design variables. This formulation indirectly constrains the feasible design space by ensuring proportional scaling relationships between the principal dimensions.

To guarantee sufficient initial stability, a constraint on the normalised metacentric height was imposed:

$$0.05 \leq \frac{GM}{B} \leq 0.25$$

The lower bound ensures a minimum level of transverse stability, while the upper bound was deliberately relaxed to 0.25 in order to avoid over-constraining the design space. It is acknowledged, however, that

allowing higher GM/B values may result in overly stiff designs, which can lead to increased accelerations and reduced seakeeping comfort. This aspect was explicitly checked during the motion evaluation stage to ensure that feasible designs did not exhibit unacceptable dynamic behaviour. This is in contrast to the stricter upper limit of 0.15 recommended by Ljulj et al. [11]. The constraint was applied during the DoE generation stage to filter out designs with unrealistic transverse stability.

The metacentric height was estimated using Equation 5.1, where KB and BM were derived from CAESES hydrostatics, and KG was estimated from the parent hull using Equation 5.2. This assumption is based on a similar internal arrangement and weight distribution. The empirical coefficient C was taken as 0.7, following Gualeni [34], and reflects the ratio observed in the parent hull.

It should be noted that KG is inherently a function of displacement weight, which in turn depends on mission profile, owner requirements, and onboard equipment. In early-stage design, such information is typically unavailable. In practice, rules of thumb are often applied to approximate KG based on ship type and size (e.g., regression-based estimates from reference vessels). Therefore, the present formulation should be regarded as an indicative target for KG, or as a selection tool to identify designs that are most likely to be feasible and best suited for subsequent refinement. Equation 5.1 represents the metacentric height for initial stability, valid for small heel angles and hulls with near-vertical sides.

$$GM = KB + BM - KG \tag{5.1}$$

$$KG = C \cdot D \tag{5.2}$$

To ensure that all candidates did not exhibit an excessively “stiff” response, an additional post-processing constraint was applied during results analysis, requiring the natural roll period to be greater than 6 [s]. This criterion is expressed through the following formulation of the natural roll period:

$$T_\phi = 2\pi \sqrt{\frac{k_{xx}^2}{g \cdot GM}} \tag{5.3}$$

where:

- T_ϕ = natural roll period [s],
- k_{xx} = transverse radius of gyration [m],
- g = gravitational acceleration [m/s^2],
- GM = metacentric height [m].

Finally, a no-trim condition was imposed by setting the longitudinal centre of gravity equal to the longitudinal centre of buoyancy ($LCG = LCB$).

5.4. Evaluation Methods

5.4.1. Hydrostatics

Using the CAESES maritime module, the hydrostatic particulars of the parent hull were extracted. These values provide the fundamental geometric and stability characteristics of the vessel and serve as the basis for all subsequent performance calculations, including LWT, resistance, stability, and seakeeping assessments.

Name	Value		Name	Value	
∇	323.654 m³	f(x)	A_{max}	11.498 m²	f(x)
T_F	2.333 m	f(x)	S	360.525 m²	f(x)
T_A	2.333 m	f(x)	C_B	0.381	f(x)
L_{OA}	45.5 m	f(x)	C_P	0.684	f(x)
L_{PP}	42.408 m	f(x)	C_M	0.557	f(x)
L_{WL}	43.698 m	f(x)	C_{WP}	0.71	f(x)
B_{WL}	7.573 m	f(x)	I_T	984.011 m⁴	f(x)
x_{AP}	0 m	f(x)	$\overline{BM}$	3.04 m	f(x)
x_{MF}	21.204 m	f(x)	$\overline{KB}$	1.586 m	f(x)
x_{max}	19.975 m	f(x)	L_{CB}	19.055 m	f(x)
x_{FP}	42.408 m	f(x)	L_{CF}	17.169 m	f(x)
A_W	258.786 m²	f(x)	$\overline{KM}$	4.626 m	f(x)
A_M	11.162 m²	f(x)			

Figure 5.6: Hydrostatic particulars of the parent hull as calculated in CAESES.

LWT Estimation

Roh and Lee [18] propose estimating LWT by decomposing it into three primary components, as shown in Equation 5.4, where W_s is the structural weight, W_o is the outfitting weight, and W_m is the machinery weight.

$$LWT = W_s + W_o + W_m \tag{5.4}$$

Each component is further expressed as a function of the vessel's principal dimensions and design parameters, as shown in Equation 5.5. The coefficients C_S (structural), C_O (outfitting), and C_{power} (machinery) are determined from the parent vessel's weight book and are summarised in Table 5.3.

$$LWT = C_S \cdot L^{1.6} \cdot (B + D) + C_O \cdot L \cdot B + C_{\text{power}} \cdot (\rho \cdot L \cdot B \cdot T \cdot C_B \cdot (1 + \alpha))^{2/3} \cdot V_S^3 \tag{5.5}$$

This formulation provides a scalable foundation for estimating lightship weight in early-stage design and enables CAPEX-related trade-offs to be incorporated into the optimisation process. Its robustness, however, remains limited by the fact that the coefficients were derived from a single parent vessel with a

specific arrangement. In practice, different mission requirements, equipment fits, or owner specifications would lead to different weight distributions and coefficients. A more reliable and scalable application would therefore require validation against additional OPVs and the derivation of a bandwidth of coefficients, ideally through regression across multiple weight books. Since only one detailed dataset was available in this study, the method is applied strictly as an early-stage approximation to capture relative trends and support trade-off analysis, rather than as a definitive predictor of lightship weight.

Table 5.3: Coefficients for lightship weight estimation based on parent hull.

	C_S	C_O	C_{power}	α
value	23.87	197.31	0.0059	0.1
units	$\text{Ton}/\text{m}^{2.6}$	Ton/m^2	$\text{Ton}^{1/3}\,\text{s}^3/\text{m}^3$	–

DWT Estimation

DWT is defined as the vessel's carrying capacity, representing the total weight of cargo, fuel, water, provisions, crew, and passengers that the ship can safely carry. Section 2.2.2 defines DWT as a key indicator of endurance and range performance. For OPVs, DWT primarily consists of consumables such as fuel and freshwater, both of which directly influence the vessel's operational range [20]. The relationship between DWT and range is given in Equation 5.8.

DWT is defined as the difference between the vessel's total displacement (Δ) and its LWT, as shown in Equation 5.6. For OPVs, DWT represents the available weight capacity for fuel and mission-related stores, and thus acts as a direct proxy for endurance and range.

Total displacement is obtained from Archimedes' law, where the submerged volume (∇) is extracted from the model hydrostatics and multiplied by the seawater density (ρ), as expressed in Equation 5.7.

$$DWT \;=\; \Delta - LWT \tag{5.6}$$

$$\Delta = \rho \cdot \nabla \quad \text{where:} \quad \rho = 1.025[\text{Ton/m}^3] \tag{5.7}$$

A feasible design cannot have $DWT < 0$, as this would imply that the vessel does not float. Similarly, $DWT = 0$ is not realistic, since this would indicate no reserve capacity for fuel or other consumables. Therefore, a feasibility constraint must be applied to ensure realistic designs.

For OPVs, the fuel fraction is typically between 60–70% of the DWT. By combining this with the specific fuel consumption (SFC), propulsion efficiency, and the estimated resistance, the vessel's range can be calculated using Equation 5.8. In this study, a minimum operational range of 1500 nm was imposed as a constraint and evaluated during the results analysis. The range was computed using Equation 5.8, assuming 68% of the DWT allocated to fuel, a propulsion efficiency of 65%, and an SFC of 0.180 [kg/kWh]. These assumptions are consistent with common practice for medium-speed marine diesel engines, where

fuel fractions of 60–70%, propulsion efficiencies of 0.60–0.70, and SFC values of 175–185 [g/kWh] are typically reported [74]

$$\text{Range}_{\text{new}} = \frac{DWT_{\text{new}} \cdot f_{\text{fuel}} \cdot \eta_{\text{prop}}}{\text{SFC} \cdot R_{T,\text{new}}} \tag{5.8}$$

5.4.2. Resistance

The H&M method was employed for resistance prediction in this thesis. This approach is one of the most widely used in early-stage naval design and is particularly common in MOO studies for OPVs and related platforms [3, 8, 19, 37, 75]. Although originally developed for displacement merchant vessels, it has been shown to provide reliable predictions for round-bilge, semi-displacement hulls up to a Froude number of $Fn = 0.5$. At higher Froude numbers, accuracy decreases due to the increasing dominance of wave-making resistance.

In this study, a single evaluation speed of $V_S = 18$ knots was adopted. This choice reflects the typical patrol speed of OPVs, at which they spend the majority of their operational time, and therefore ensures that the optimisation results are relevant to their most common use case rather than to rarely used sprint speeds. After selecting this representative speed, an analysis confirmed that across the full length range under investigation the resulting Froude number remains below 0.5, keeping the H&M method within its validated applicability limits. While this ensures consistency across variants in the present comparative study, it is acknowledged that higher-fidelity resistance and powering methods, better tailored to OPVs, would be required for detailed design or for optimisation at higher speeds. As such, the method provides reliable relative trends, but does not capture the full spectrum of OPV operating speeds. More dedicated power prediction approaches could be employed in future studies to extend the analysis, particularly toward higher-speed regimes or alternative propulsion concepts (e.g., waterjets).

In comparative parametric hull studies, the influence of appendages can be simplified. In this thesis, only the skeg was modelled and included in the resistance estimation, as it is expected to contribute the dominant appendage-related effects. Other appendages (rudders, bilge keels, stabilisers, etc.) were omitted, since their relative impact is expected to remain comparable across all variants and thus cancels out in the optimisation. This simplification, however, also limits the scope for exploring design improvements linked to appendage selection or integration. The implementation of the H&M method used in this study is provided in Appendix C

5.4.3. Stability Assessment GZ Curve Evaluation

Stability is a fundamental design driver for OPVs, ensuring safe operability across a wide range of missions and environmental conditions. In this study, stability is incorporated through two complementary approaches: constraint-based filtration and righting arm (GZ) curve evaluation.

Static intact stability is evaluated by generating the GZ curve using the CAESES maritime module. The IMO 2008 IS Code, Part A, Chapter 2 [76], specifies minimum requirements for stability, including righting

arm values, the area under the GZ curve, the range of positive stability, and the initial metacentric height. Although these standards were originally developed for merchant vessels, they are widely applied to naval ships such as OPVs [31]. Table 5.4 summarises the relevant IMO criteria, together with the optimisation targets used in this study.

Table 5.4: Stability optimisation criteria for OPVs.

Stability Parameter	IMO Criteria	Optimisation Target	Description	Reference
Area under GZ curve ($0°$–$30°$)	≥ 0.055 m·rad	Maximise	Proxy for initial stability and resistance to heeling	IMO 2.2.1a
Area under GZ curve ($0°$–$40°$)	≥ 0.09 m·rad	Maximise	Resistance to large heel or capsize; survivability	IMO 2.2.1b
Area under GZ curve ($30°$–$40°$)	≥ 0.03 m·rad	Maximise	Stability reserve near critical angles; recovery margin	IMO 2.2.1c
GZ at $\phi \geq 30°$	≥ 0.20 m	Maximise	Stability margin at large heel	IMO 2.2.2
Angle at Max GZ	$\geq 25°$	$25°$–$35°$	Indicates maximum restoring capability	IMO 2.2.3
Initial GM	≥ 0.15 m	Maximise (within bounds)	Transverse stiffness; sensitive to weight distribution	IMO 2.2.4
Range of Positive Stability	$\geq 60°$	Maximise	Heel range with restoring ability; broader range = survivability	IMO (general)

Dynamic stability, i.e. the vessel's response to time-varying forces such as wind gusts, waves, or abrupt manoeuvres, is acknowledged but not explicitly modelled in this early-stage framework, as it requires detailed mass distribution and windage characteristics. Instead, static GZ-based criteria are adopted as proxies for overall robustness.

Stability Index (SI)

To integrate intact stability into the MOO framework, this thesis introduces a novel dimensionless SI formulation. The index normalises GZ-based criteria against the IMO thresholds, thereby expressing stability as a continuous optimisation objective rather than a binary pass/fail condition. The SI is defined as:

$$SI = \frac{1}{3}\left(\frac{A_{0-30}}{A_{0-30}^{\text{IMO}}} + \frac{A_{0-40}}{A_{0-40}^{\text{IMO}}} + \frac{A_{30-40}}{A_{30-40}^{\text{IMO}}}\right) \tag{5.9}$$

where A_{0-30}, A_{0-40}, and A_{30-40} are the actual areas under the curve GZ in the respective heel angle are the actual areas under the GZ curve in the respective heel angle ranges, and A^{IMO} denotes the corresponding minimum IMO requirements. An SI value greater than 1 indicates compliance with IMO intact stability criteria, while higher values correspond to larger safety margins.

Only these three area-based IMO criteria were selected, as they are the most representative of the overall righting-energy characteristics of OPVs in the operational heel range, and can be consistently calculated in early-stage design without requiring detailed internal arrangements. Other IMO criteria, such as maximum righting arm or angle of vanishing stability, were excluded to avoid redundancy and because their values are strongly arrangement-dependent, which is not yet defined at this stage. The three selected

ratios were averaged with equal weighting to avoid imposing subjective prioritisation among them and to ensure that the SI remains a neutral, general-purpose index. In future work, the weighting could be adapted to reflect mission-specific stability priorities (e.g., helicopter operations vs. weapons accuracy), but for the present framework a uniform average provides a simple and transparent baseline.

By defining SI in this way, stability is incorporated into the optimisation process as a quantitative and trade-off–oriented objective. This represents a methodological contribution of the thesis, enabling stability to be directly optimised alongside resistance, seakeeping, and other design drivers in the early-stage evaluation of OPV designs.

5.4.4. Seakeeping Evaluation

Seakeeping performance was assessed using Maxsurf® Motions, where a Strip theory (2D linear frequency-domain analysis) is applied. This method analyses the hull as a series of independent transverse sections under the assumption of linear potential flow. It offers good accuracy for conventional hull forms at a relatively low computational cost [30].

A forward speed of 12 knots was selected for the seakeeping analysis, in contrast to the 18 knots used in the resistance evaluation and optimisation. In SS6, higher transit speeds would likely amplify motions and accelerations beyond practical limits, making them unrepresentative of operational practice. The reduced speed of 12 knots therefore, provides a more realistic basis for assessing OPV behaviour in rough conditions.

The hull geometry was exported from CAESES as an IGES file and imported into Maxsurf® Modeler, where it was converted into a `.msd` file with defined hydrostatic reference points (WL, FP, AP). The `.msd` file was then opened in Maxsurf® Motions, where the following environmental conditions, mass properties, and monitoring points were defined:

- **Sea state:** JONSWAP spectrum, SS6, with significant wave height $H_s = 5$ m and peak period $T_p = 9.95$ s.
- Forward speed: $V_s = 12$ kn.
- Headings: $\mu = 0°, 45°, 90°, 135°, 180°$.
- Mass properties: Radii of gyration fixed to parent hull values ($k_{xx} = 33.9\% \cdot B_{OA}$, k_{yy}, $k_{zz} = 22.6\% \cdot L_{OA}$).
- Vertical CG: KG.
- Bridge location: Estimated 4 m above MD.
- Deck wetness location: MD at forward perpendicular (FP).
- Slamming location: Frame 40 at the baseline (BL).

The following response parameters were extracted:

- Roll RMS (at CG).
- Pitch RMS (at CG).
- Absolute vertical acceleration RMS (at bridge).
- Lateral acceleration RMS (at bridge).
- Relative vertical motion at MD, FP (deck wetness).
- Relative vertical motion at Frame 40, BL (slamming).
- Relative vertical velocity at Frame 40, BL (slamming velocity).
- Motion Sickness Incidence (MSI, at bridge).

Deck wetness and slamming probabilities were calculated in post–processing from the extracted spectral moments:

$$P_{\text{wet}}(\%) = \exp\left(-\frac{F^2}{2\,m_{0,\text{bow,rel}}}\right) \times 100 \tag{5.10}$$

$$P_{\text{slam}}(\%) = \exp\left(-\frac{T^2}{2\,m_{0,\text{slam,rel}}} - \frac{V_{cr}^2}{2\,m_{2,\text{slam,rel}}}\right) \times 100, \qquad V_{cr} = 0.093\sqrt{g\,L_{OA}} \tag{5.11}$$

where F is freeboard, T is draft, $g = 9.81$ m/s^2, and L_{OA} is the overall length.

5.4.5. Criteria

The motion statistics were compared against selected seakeeping criteria adapted from NORDFORSK (1987), Tello et al. [77], and USCGC standards. Table 5.5 summarises the applied thresholds.

Table 5.5: Seakeeping optimisation criteria for OPVs.

Motion Parameter	Limit	Location	Description	Reference
Roll angle (RMS)	$\leq 6^\circ$	CG	Crew performance, safety on deck	Tello et al. (2011)
Pitch angle (RMS)	$\leq 3^\circ$	CG	Equipment/sensor operability	Tello et al. (2011)
Vertical acceleration	$\leq 0.2g$	Bridge	Comfort, motion sickness	NORDFORSK (1987)
Lateral acceleration	$\leq 0.2g$	Bridge	Balance control	Tello et al. (2011)
Slamming frequency	≤ 0.03	Fr. 40 BL	Structural loads, safety	NORDFORSK (1987)
Deck wetness probability	≤ 0.05	FP deck	RHIB/helicopter ops, safety	NORDFORSK (1987)
Motion sickness incidence (MSI)	≤ 40% (120 min)	Bridge	Endurance, productivity	USCGC

5.4.6. Seakeeping Index

To integrate seakeeping into the multi-criteria optimisation loop, a dimensionless SKI was defined. For each heading μ, the SKI is calculated as:

$$SKI_\mu = 1 - \frac{1}{n}\sum_{i=1}^{n}\frac{x_i}{x_{i,\text{max}}} \qquad 0 \leq SKI_\mu \leq 1 \tag{5.12}$$

where x_i is the measured motion response, $x_{i,\text{max}}$ is its associated threshold from Table 5.5, and n is the number of seakeeping criteria considered. An SKI_μ value of 1 indicates full compliance (all responses below thresholds), while values approaching 0 indicate poor performance.

The combined seakeeping index for SS6 is obtained by averaging over the five headings:

$$SKI_{\text{SS6}} = \frac{1}{5} \sum_{\mu \in \{0,45,90,135,180\}} SKI_\mu \tag{5.13}$$

This formulation provides a single, dimensionless measure of seakeeping performance that accounts for both heading sensitivity and compliance with operational limits. The SKI_{SS6} can be directly compared with resistance and stability indices within the optimisation framework, facilitating trade-off analysis between hydrodynamic efficiency, stability, and operability. The full implementation of SKI used in this study is provided in Appendix D

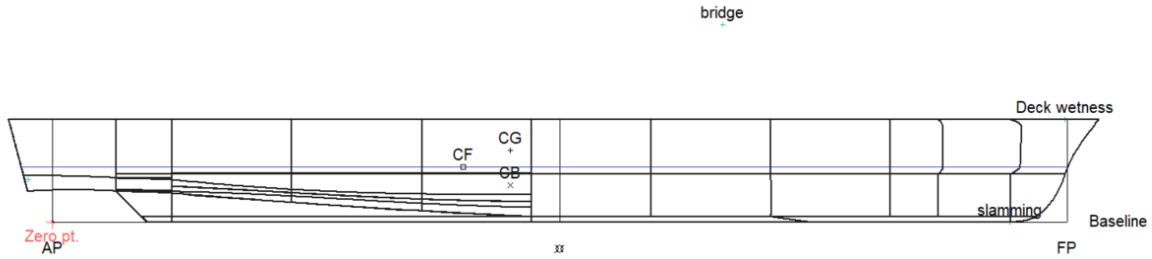

Figure 5.7: Model view from Maxsurf® Motions showing reference locations for motion analysis

5.5. Multi-Objective Optimization

5.5.1. Micro-Batch Evaluation Strategy

Because no direct software connection exists between CAESES and Maxsurf®, a live evaluation loop was not feasible. To address this limitation, a *micro-batch evaluation strategy* was adopted. In this approach, CAESES generated small groups of candidate designs (10–20 per iteration), which were then exported and evaluated offline in Maxsurf® Motions. The resulting seakeeping responses were post-processed to compute the SKI and subsequently re-imported into CAESES, updating the optimisation database.

Each SBGO iteration proposed a new batch of designs based on the current surrogate model. These candidates were exported, analysed in Maxsurf®, and their results fed back into the DAKOTA framework, thereby expanding the results archive and refining the surrogate. This strategy preserved the iterative learning cycle of the surrogate model, while making the evaluation process practical through offline integration.

The search began with batches of 10 candidates per iteration to ensure frequent retraining of the surrogate and stable improvement in the early exploratory phase. Once the surrogate demonstrated

improved accuracy and the search converged toward the Pareto front, the batch size was increased to 15 candidates per iteration. This adjustment improved local trade-off surface coverage and accelerated convergence while preserving diversity across the front.

5.5.2. Initial Sampling and Motivation

The optimisation was initialised with a LHS of 100 design points, spanning the ranges of the selected design variables (Table 5.2). This initial sample ensured broad coverage of the design space and provided a robust starting dataset for training the surrogate model.

5.5.3. Surrogate-Based Global Optimisation (SBGO)

The optimisation framework employed a SBGO strategy, implemented in DAKOTA and embedded within CAESES. The algorithm combined DAKOTA's Multi-Objective Genetic Algorithm (MOGA, based on the JEGA framework) with a Kriging (Gaussian Process) surrogate model. The surrogate was used to predict promising candidate solutions at each iteration, thereby reducing the number of expensive evaluations in Maxsurf®.

After each iteration, the quality of the Pareto front was monitored using the hypervolume metric, which served as a measure of convergence and front diversity. This setup enabled efficient exploration of the multi-objective design space, while keeping computational costs manageable and maintaining the fidelity required for seakeeping evaluation.

5.5.4. Normalization of Objectives and Variables

In early optimisation runs, neither the objectives nor the design variables were scaled. This introduced bias into the multi-objective ranking, as metrics with larger numerical ranges exerted disproportionate influence. To eliminate this effect, both design variables and objectives were normalised.

Objective normalisation: A "worst + 10%" scaling scheme was adopted. For each objective f_i, the normalised value f_i^* was calculated as:

$$f_i^* = \frac{f_i}{1.1 \cdot f_{i,\text{worst}}}, \qquad 0 \leq f_i^* \leq 1 \tag{5.14}$$

where $f_{i,\text{worst}}$ is the worst observed value in the initial LHS sample. The factor of 1.1 inflates the denominator by 10% to avoid boundary locking.

Variable normalisation: Design variables x_j were normalised relative to their lower and upper bounds as:

$$x_j^* = \frac{x_j - x_{j,\text{min}}}{(x_{j,\text{max}} - x_{j,\text{min}})}, \qquad 0 \leq x_j^* \leq 1 \tag{5.15}$$

where $x_{j,\text{min}}$ and $x_{j,\text{max}}$ are the lower and upper limits of the variable range, respectively. This ensured that all variables contributed equally in distance-based metrics such as niching and orthogonal distance thresholds.

Together, these normalisation schemes were introduced with the aim of stabilising the SBGO search, reducing numerical dominance bias, and improving the comparability of objectives and variables on the Pareto front. The actual effect of this choice is evaluated in Chapter 7, where hypervolume convergence histories are presented.

5.6. Conclusion of Methodology

This chapter has presented the methodology developed to integrate scaling and mission-oriented MOO into an early-stage OPV design framework. The process was structured into three main modules: parametric modelling, performance evaluation, and optimisation.

First, a parametric hull model was constructed in CAESES, based on the ISL OPV parent hull, using selected design variables and constraints to balance geometric fidelity with design flexibility. Hydrostatics, resistance, stability, and seakeeping evaluations were then defined using a combination of low- and mid-fidelity methods, including the H&M resistance model, IMO intact stability criteria, and strip-theory-based seakeeping analysis in Maxsurf®. Indices such as the SI and SKI were introduced to condense multi-criteria performance into continuous, dimensionless measures suitable for optimisation.

Finally, a surrogate-assisted optimisation framework was implemented in CAESES/DAKOTA, featuring Latin Hypercube initial sampling, a micro-batch evaluation strategy to enable offline integration with Maxsurf®, and objective/variable normalisation to eliminate ranking bias. Objective refinement led to a reduced but balanced set of four objectives—LWT, resistance, SI, and SKI—enabling robust exploration of the design space while enforcing feasibility through range-based DWT constraints.

Together, these modules form a scalable and computationally efficient methodology for early-stage OPV design. The framework supports rapid trade-off analysis across hydrodynamic efficiency, stability, and seakeeping performance. providing a robust foundation for the verification and validation activities that follow in the next chapter. In doing so, this chapter has addressed Sub–question 4: *"What components are required for the proposed framework, and how can the setup be structured to support early-stage OPV design?"*.

6

Validation Study

This chapter validates the proposed modelling framework. Validation is performed by comparing predictions of the reconstructed parametric parent hull against external datasets provided by ISL. These datasets include towing–tank measurements, CFD studies, and intact–stability documentation.

Since the as–built geometry of the ISL vessel is confidential, to respect confidentiality and to reconcile minor differences in loading conditions and reference frames, results are reported either as *normalised quantities* or as *percentage deviations* with respect to the CAESES baseline.

Scope of checks. The validation focuses on the following aspects:

- Hydrostatics: accuracy of displacement, centres, and hydrostatic coefficients;
- Stability: accuracy of GM, GZ metrics, KM, KB, and BM;
- Resistance/powering: comparison of model–scale and trial–scale predictions;
- LWT: consistency with weight documentation and regression methods;
- Seakeeping: accuracy of RAOs, accelerations, and SKI under matched sea states and headings.

The final section synthesises the findings of these validation checks and addresses research sub–question 5: *"How can the effectiveness of an integrated scaling and mission-oriented MOO framework be validated to ensure robust and reliable early-stage OPV design decisions?"*

6.1. Parent–hull accuracy

6.1.1. Hydrostatics Validation

The hydrostatic particulars of the *existing vessel* were compared with those of the reconstructed parametric model in CAESES to establish a baseline for validation. Data were assembled from four independent sources: (i) the CAESES model, (ii) the intact stability booklet, (iii) the resistance test report, and (iv)

the seakeeping assessment. Each of these references was produced at different times by different organisations and often under slightly different loading conditions or reference conventions.

For consistency, the CAESES model is taken as the numerical baseline. Percentage deviations reported for the external sources are therefore expressed relative to this baseline. Table 6.1 presents side-by-side values for all four sources, together with the corresponding deviations.

Table 6.1: Cross-check of principal particulars and hydrostatic coefficients for the parent hull. Percentages indicate deviation from the CAESES model baseline.

Particular	Symbol	Unit	CAESES model	Intact stability	CFD	Towing tank	Seakeeping assessment
Displacement	∇	m^3	324	$+1\%$			-1%
Displacement	Δ	t	331	$+1\%$	-7%	-4%	-1%
Length overall	L_{OA}	m	45.5	$+1\%$			
Length between perpendiculars	L_{PP}	m	42.4		0%	0%	
Length waterline	L_{WL}	m	43.7	$+4\%$		0%	0%
Beam overall	B_{OA}	m	8.6	0%		$+4\%$	
Beam waterline	B_{WL}	m	7.57	0%	$+4\%$	0%	0%
Draft	T	m	2.3	$+1\%$	-2%	0%	0%
Wetted surface area	S	m^2	360.5	$+20\%$		$+1\%$	
Block coefficient	C_B	–	0.381	$+4\%$	$+12\%$	$+15\%$	$+10\%$
Prismatic coefficient	C_P	–	0.683	-8%	-2%		
Midship coefficient	C_M	–	0.557	$+13\%$	$+15\%$		
Waterplane coefficient	C_{WP}	–	0.710	$+3\%$	$+14\%$		$+11\%$
Metacentric radius	BM	m	3.083				$+3\%$
keel to centre of buoyancy	KB	m	1.565	$+0\%$	-4%		1%
LCB from AP	LCB	m	19.07	-2%	0%	0%	0%
keel to metacentre	KM	m	4.648	0%	$+2\%$		$+1\%$
vertical centre of gravity	KG	m	3.017	$+19\%$			$+6\%$

It should be noted that the intact stability booklet is based on a fully appended model, whereas the CFD, towing–tank, and seakeeping references are based on the bare hull. This explains, for example, the significant 21% difference in wetted surface area between CAESES and the stability reference. Similarly, a 19% difference in KG arises from the fact that the stability documentation assumes a different displacement and loading condition than the CAESES baseline. Overall, the core hydrostatic quantities $\left(\nabla,\, L_{WL},\, B_{WL},\, T,\, KB,\, BM,\, KM\right)$ agree within a few percent across sources, which is considered adequate for early-stage validation. Larger deviations are observed for the form coefficients (C_B, C_P, C_M, C_{WP}), with differences reaching up to 15%. These discrepancies arise from several interacting factors. First, form coefficients are ratios of volumes and areas (e.g. prismatic coefficient $C_P = \nabla/(A_M \cdot L_{PP})$), which makes them highly sensitive to small local shape differences even when the global dimensions and displacement remain consistent. Second, the reference models are not geometrically

identical: the stability booklet includes appendages (bilge keels, shafts, rudders) while the CFD and towing tank use a bare hull, and CAESES employs a simplified NURBS reconstruction. This leads to systematic shifts in wetted area (S) and waterplane shape, directly affecting C_{WP} and C_B. Finally, the displacement conditions differ: hydrostatics from the intact stability document are based on a specific loading case with a slightly higher displacement, whereas the CAESES baseline assumes a neutral reference condition. Since coefficients are evaluated at the design draft, even a 1–2% change in draft or KG can amplify into 10% differences in coefficients. Taken together, these effects explain why form coefficients differ more strongly than primary hydrostatics, while still remaining within acceptable tolerances for early-stage validation.

6.1.2. Stability: GZ Curve

Intact-stability performance of the parent hull was validated by comparing the CAESES-derived GZ characteristics with the shipyard's reference stability documentation. External results are reported as percentage deviations relative to the CAESES baseline (Table 6.2). The comparison covers the standard IMO-type metrics:

- areas under the GZ curve over 0–30° and 0–40°
- the incremental area over 30–40°
- GZ at 30°
- heel at GZ_{max}
- the initial metacentric height $GM(0)$

The shipyard documentation provides several load-case scenarios. For validation, the case closest to the reconstructed CAESES baseline (denoted here as CAESES LC1, $\Delta \approx 324$ t) was compared with the corresponding shipyard load case. This alignment, however, still produced substantial discrepancies in the stability metrics, with deviations up to -81% in the 30–40° area (column "Shipyard vs LC1"). The main cause is the residual difference in displacement and draft between the two definitions, which strongly affects the GZ curve at large heel.

To remove this mismatch, a second CAESES run (LC2, $\Delta \approx 336$ t) was performed at the same displacement as the selected shipyard case. This adjustment brought the hydrostatics into closer alignment and reduced the deviations considerably. At LC2, the key intact-stability measures (areas up to 30°, GZ at 30°, $GM(0)$, heel at GZ_{max}) differ by only a few percent. The remaining gap is concentrated in the 30–40° area (-22%), which is expected. This incremental area is highly sensitive to KG placement, flare, freeboard immersion, and trim assumptions. In addition, the CAESES parametric model does not include appendages, and the midship coefficient C_M was already shown to differ from the shipyard reference. Both factors increase the righting moment at large heel in the shipyard data, whereas they are absent or simplified in CAESES.

Overall, the CAESES reconstruction reproduces the GZ curve shape and magnitude with good fidelity once displacement is matched. While residual deviations remain at extreme heel, the IMO intact-stability

criteria are satisfied with adequate margin, confirming the validity of the CAESES baseline for subsequent analysis.

Table 6.2: Comparison of key intact-stability metrics between CAESES and the shipyard report (half-load condition).

Metric	CAESES	CAESES	Shipyard (vs. LC1)	Shipyard (vs. LC2)	Criteria
	LC1: 324 Ton	LC2: 336 Ton	[%]	[%]	
Area 0–$30°$	0.2114	0.147	-46%	-1%	0.055
Area 0–$40°$	0.3472	0.238	-57%	-8%	0.09
Area 30–$40°$	0.1358	0.091	-81%	-22%	0.03
GZ at $30°$	0.7880	0.535	-52%	-4%	30
Heel at GZ_{max}	$36.05°$	$31.685°$	-6%	7%	0.2
$GM(0)$	1.6152	1.152	-39%	1%	0.15
Stability index	0.3185	0.224	0.205	0.205	

6.1.3. Resistance Validation (Bare Hull)

Bare–hull total resistance R_T was predicted with the H&M method, using the ITTC'57 friction line and H&M form factor $(1+k)$. For validation, results were compared against (i) ISL towing–tank measurements and (ii) an independent CFD study at three speeds spanning the semi–displacement regime. The H&M implementation used here is provided in Appendix C. Deviations of experimental and CFD results are reported as percentages relative to H&M predictions. The numerical results are summarised in Table 6.3.

All three datasets use the same L_{PP}. However, the CFD geometry differs slightly from the CAESES/H&M model, with a 4% larger B_{WL} and a 2% smaller T. As a result, the wetted surface area and slenderness differ, which in turn influences both frictional and residuary components. Form coefficients (C_B, C_P, C_M, C_{WP}) therefore diverge more noticeably across sources.

In addition, the towing–tank "bare hull" includes small geometric details (e.g., thruster tunnels) that increase wetted surface and disturb the wave field. These effects tend to raise the measured R_T relative to the idealised H&M and CFD geometries.

Despite these systematic but explainable biases, the H&M method is considered adequate for early–stage OPV screening. In particular, at the reference speed of 18 knots used throughout the framework, H&M predictions remain within the expected deviation range for semi–displacement hulls.

Table 6.3: Bare–hull resistance validation: H&M vs. towing–tank and CFD. Percentage deviations are relative to H&M predictions.

Speed	**Fn**	**H&M R_T [kN]**	**Tank test (Δ)**	**CFD (Δ)**
12	0.298	40.59	$+8\%$	-17%
18	0.447	108.00	$+22\%$	$+9\%$
24	0.596	216.80	$+9\%$	-10%

6.1.4. Seakeeping Validation

The motion behaviour of the reconstructed hull was validated by comparing results from the ISL seakeeping assessment with a corresponding analysis conducted in Maxsurf® Motions. For consistency, only bare–hull results were considered. The Maxsurf® simulations were configured to replicate the same conditions reported in the shipyard assessment, with matching draft and zero–trim assumptions.

Three representative sea states were investigated:

- SS3: $H_s = 1.2$ [m], $T_p = 4.9$ [s],
- SS4: $H_s = 2.0$ [m], $T_p = 6.0$ [s],
- SS5: $H_s = 2.8$ [m], $T_p = 7.0$ [s].

These conditions span a progression from moderate to rough seas and provide a basis for assessing the accuracy of the reconstructed model in reproducing the motion responses reported by ISL.

Three aspects of seakeeping performance were examined:

- Roll decay: comparison of the natural roll period and damping characteristics;
- Motions at CG: pitch, heave, and roll motions at the vessel's centre of gravity;
- Basic seakeeping responses: RAOs and RMS values for key motions and accelerations under specified headings and sea states.

This comparative approach provides a check on the ability of the framework to reproduce first–order motion behaviour, ensuring that the simplified strip–theory modelling in Maxsurf® remains consistent with the independent ISL assessment.

Roll Decay

The natural roll behaviour of the reconstructed hull was validated by comparing a roll–decay simulation in Maxsurf® Motions with reference results from the ISL seakeeping assessment. Figure 6.1 shows the time histories of roll motion for three cases:

1. the Maxsurf® model without appendages
2. the ISL reference hull without appendages
3. the ISL reference hull fitted with bilge keels and stabilising fins

Conditions are assumed as zero forward speed (stationary in calm water). The roll–decay simulations were compared for zero forward speed ($V = 0$ kn) in calm water (no waves).

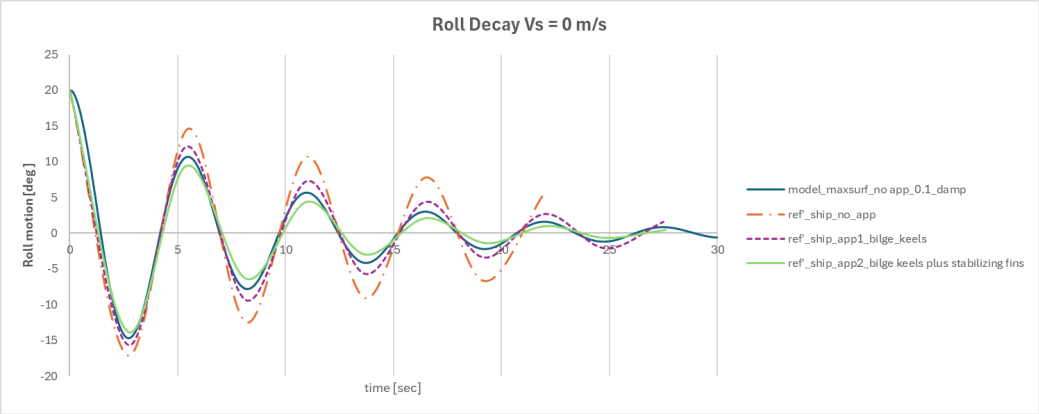

Figure 6.1: Roll decay test: comparison between reconstructed Maxsurf® model and ISL reference data (bare hull and appended configurations).

The comparison demonstrates that the parametric Maxsurf® model reproduces the natural roll period of the bare hull with good accuracy. The Maxsurf® model shows stronger damping compared to the bare–hull reference, which can be attributed to numerical damping settings in Maxsurf® and to scaling effects in the physical model tests. Nevertheless, the alignment of oscillation peaks indicates that the natural roll frequency is captured correctly.

This validation step is important because roll decay directly reflects the natural roll period, which depends on both hydrostatics (GM) and mass distribution (k_{xx}). Accurate reproduction of the natural period therefore confirms that the reconstructed parametric model captures the essential stability properties of the parent hull. The result provides confidence in the model's baseline dynamic behaviour and supports the reliability of subsequent RAO-based seakeeping analyses.

Response Amplitude Operators (RAOs)

The RAOs of the reconstructed hull were compared against reference data from the ISL seakeeping assessment for the three primary rigid–body motions: heave, pitch, and roll. Figures 6.2–6.4 show the RAOs for heading $135°$ at $V_s = 18$ knots.

Overall, the comparison demonstrates that the reconstructed model reproduces the correct natural frequencies and the general shape of the RAO curves. The resonance peaks align closely across all three modes, indicating consistency in hydrostatics and inertia properties. Larger discrepancies are observed in the peak amplitudes, particularly for heave and roll. These can be attributed to differences in damping (as also highlighted by the roll–decay comparison), the strip–theory assumptions in Maxsurf®, scale effects between model and full scale, and geometric differences between the reconstructed hull and the ISL reference, especially in the form coefficients (e.g. C_{WP} and C_M).

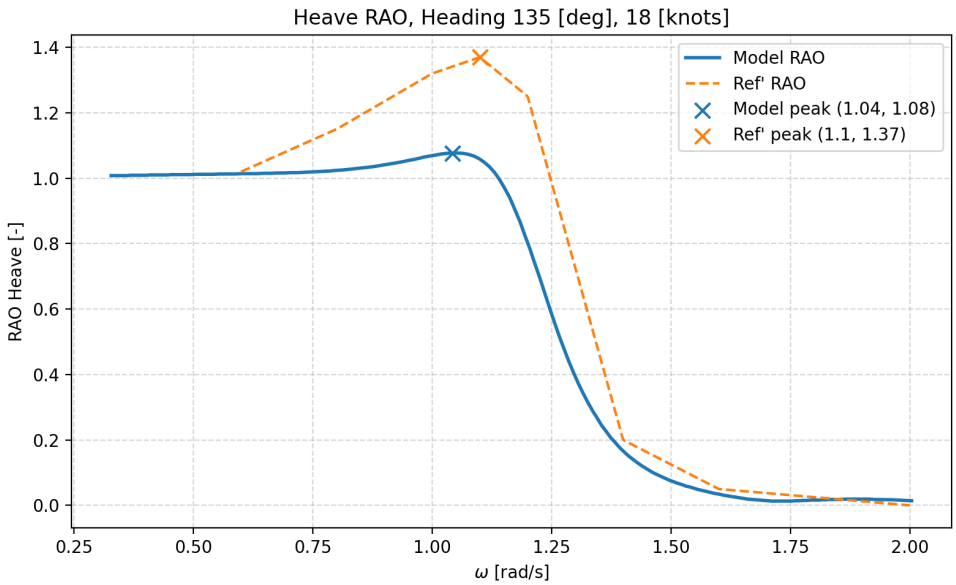

Figure 6.2: Heave RAO comparison between reconstructed Maxsurf® model and ISL reference at 18 knots, heading $135°$.

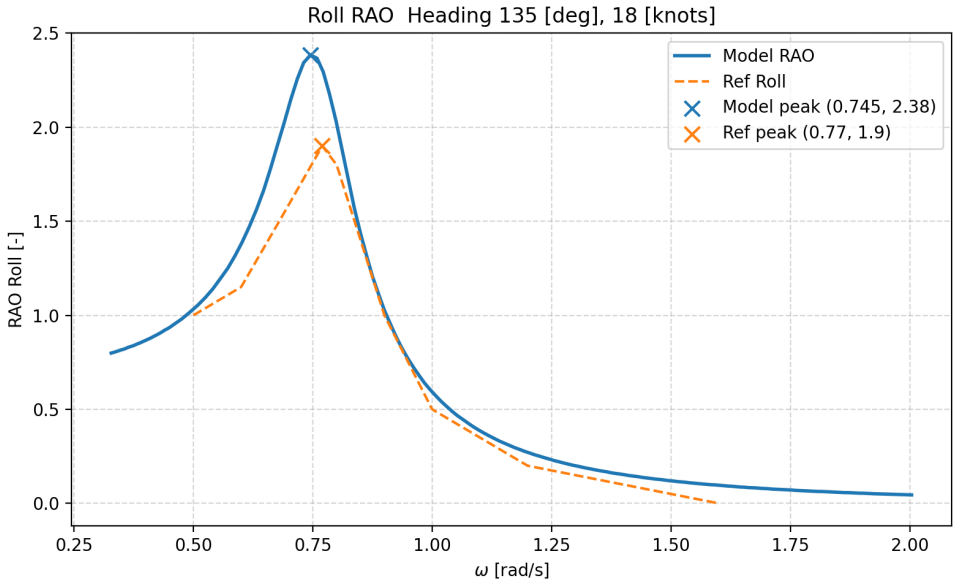

Figure 6.3: Roll RAO comparison between reconstructed Maxsurf® model and ISL reference at 18 knots, heading $135°$.

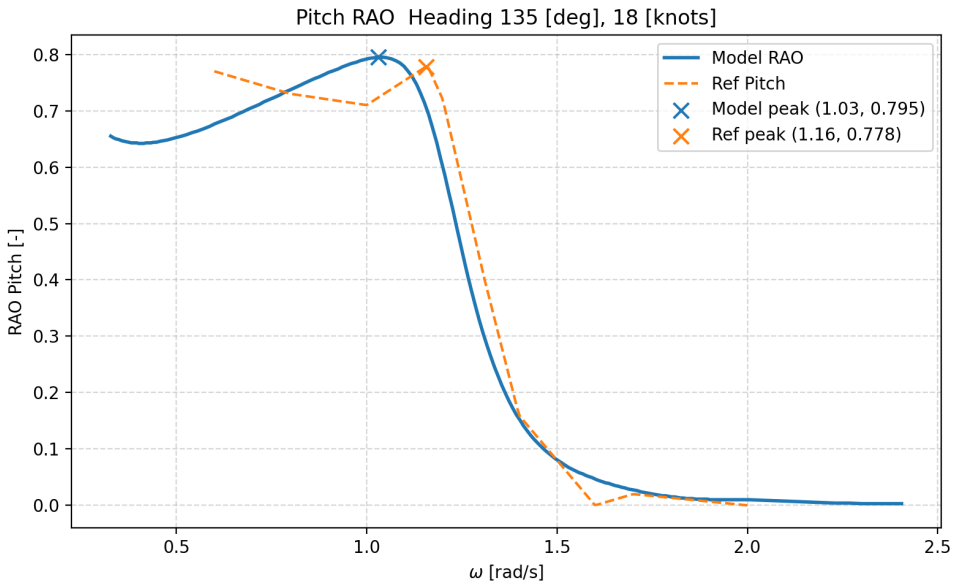

Figure 6.4: Pitch RAO comparison between reconstructed Maxsurf® model and ISL reference at 18 knots, heading $135°$.

The results confirm that the reconstructed parametric model provides an adequate representation of the parent hull's seakeeping behaviour. Despite some deviations in response amplitude, the alignment of resonance peaks across pitch, heave, and roll indicates that the framework captures the essential motion characteristics needed for early–stage optimisation.

Basic Seakeeping Motion Responses

Basic motion responses were validated for heave, roll, and pitch across three representative sea states (SS3, SS4, SS5), seven headings ($0°$–$180°$ in $30°$ increments), and three forward speeds (0, 6, 12 kn). The Maxsurf® Motions analysis was carried out using unidirectional wave spectra, while the ISL reference seakeeping study employed multidirectional spectra. To ensure comparability, the ISL results were mirrored about $180°$ in the polar plots, so that both datasets covered the same $0°$–$180°$ range (with $180°$ corresponding to head seas).

Figures 6.5–6.7 show the polar RAOs for heave, roll, and pitch motions in sea states 3–5.

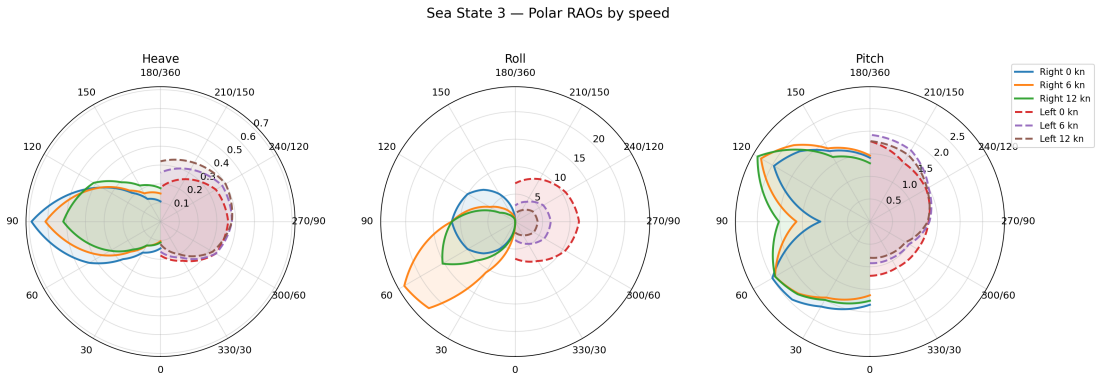

Figure 6.5: Polar RAOs of heave, roll, and pitch in Sea State 3 for multiple headings and speeds.

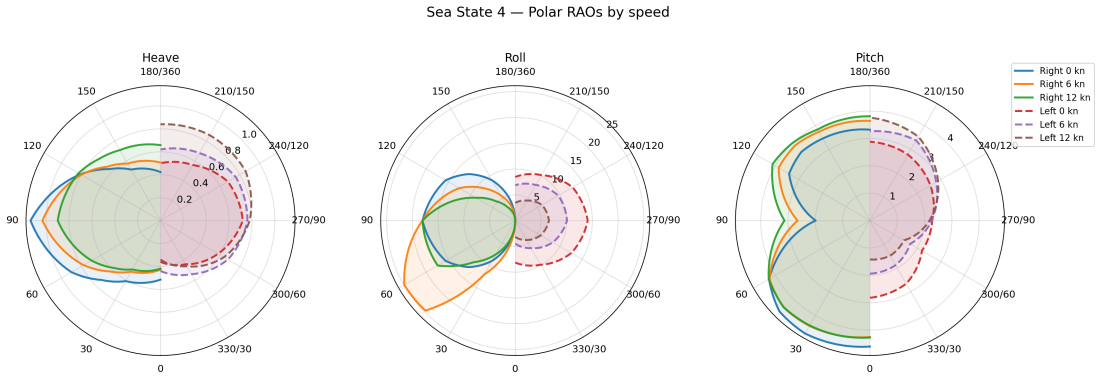

Figure 6.6: Polar RAOs of heave, roll, and pitch in Sea State 4 for multiple headings and speeds.

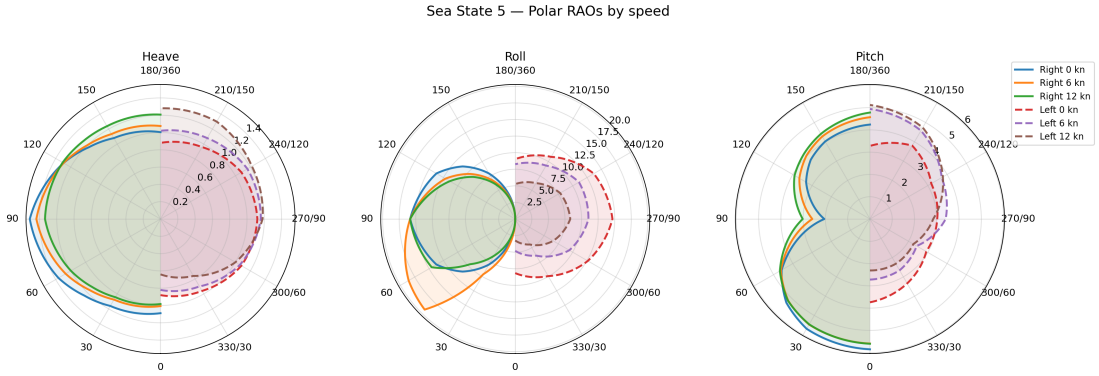

Figure 6.7: Polar RAOs of heave, roll, and pitch in Sea State 5 for multiple headings and speeds.

The polar plots show that the reconstructed model reproduces the directional dependence of motion responses, with maxima occurring in beam and quartering seas as expected. Differences in absolute magnitudes are observed between the two analyses, which can be attributed to the unidirectional spectrum assumption in Maxsurf® compared to the multidirectional treatment in the ISL reference study. In particular, the unidirectional model produces zero roll at $0°$ and $180°$, while the multidirectional analysis captures some residual roll excitation due to cross–wave components. Similarly, pitch responses appear sharper in

the unidirectional case and more moderate in the multidirectional case.

This explains why damping estimates differ between the roll–decay test and the RAO responses: roll decay represents free–decay damping at zero forward speed, whereas RAOs capture the frequency response under spectral excitation at finite speeds and headings. Nevertheless, the relative trends across headings, speeds, and sea states are consistently reproduced, confirming that the framework provides a reliable basis for seakeeping evaluation in early-stage design.

6.2. Validation Conclusion

This chapter has validated the proposed framework against reference data from the ISL parent hull, addressing Sub–question 5: *"How can the effectiveness of an integrated scaling and mission-oriented MOO framework be verified and validated to ensure robust and reliable early-stage OPV design decisions?"*

The validation against hydrostatics, stability, resistance, and seakeeping confirms that the reconstructed parametric model provides an adequate representation of the ISL parent hull for early–stage optimisation purposes. The validation against hydrostatics, stability, resistance, and seakeeping confirms that the reconstructed parametric model provides an adequate representation of the ISL parent hull for early-stage optimisation purposes. Core hydrostatic properties and dynamic behaviour (e.g. the natural roll period) are reliably reproduced, with deviations in form coefficients attributable to geometric simplifications in the reconstruction and differences in loading conditions across sources. Overall, the reconstructed model preserves the governing physical behaviour of the parent hull and provides sufficient fidelity for early-stage optimisation.

In hydrostatics, displacement, centres, and metacentric properties agreed within a few percent, while larger deviations in coefficients (up to 15%) reflect modelling choices rather than fundamental inconsistencies. Stability comparisons show that the model reproduces the overall shape of the GZ curve and satisfies IMO intact-stability criteria, with minor differences again traceable to geometric simplifications.

Resistance predictions with H&M fall within the expected error range for semi-displacement hulls when benchmarked against towing–tank and CFD results. Discrepancies are consistent with the differing fidelity of the methods and with scale effects in the experimental model. While suitable for early-stage optimisation due to its low cost, the H&M method could be complemented by alternative approaches for closer agreement at higher Froude numbers.

For seakeeping, the model reproduces natural frequencies and the qualitative form of RAOs across headings and sea states. Differences in amplitudes reflect the limitations of strip theory and the use of unidirectional spectra in Maxsurf compared to the multidirectional ISL reference, yet overall motion behaviour remains consistent.

In summary, validation confirms that the proposed framework is accurate, reliable, and consistent with naval-architectural principles. It provides sufficient fidelity for early-stage OPV design and comparative scaling studies, while acknowledging that higher-fidelity tools remain essential in later design stages. The

results establish a robust foundation for exploring design scaling and mission-oriented optimisation in the following case study.

7

Test Case

This chapter demonstrates the practical application of the MOO framework developed for scaling OPVs, with a focus on its verification. Whereas validation (Chapter 6) compared reconstructed model predictions against external reference data, verification evaluates whether the framework behaves consistently with established principles and expected naval-architectural physics.

The chapter is organized into three main sections. First, the Convergence Analysis (Section 7.1) examines the evolution of the hypervolume and Pareto front projections, highlighting the constraints and objectives that shaped the set of optimal designs. Second, the Trend Analysis (Section 7.3) confirms that the framework reproduces well-known naval architectural behaviors, such as the influence of hull length, beam, and draft on resistance, stability, and seakeeping. Finally, the Application and Implications (Section 7.4) discusses the significance of these results for real-world OPV design and how the framework can support early-stage design decisions.

The case study is based on the reconstructed S45 OPV from ISL, introduced in Chapter 5. Through this test case, the chapter provides a clear understanding of how the MOO-based approach behaves under realistic conditions and how it can be leveraged to make robust and reliable early-stage design choices for OPVs. In doing so, it directly addresses Research Sub-question 5: *"How can the effectiveness of an integrated scaling and mission-oriented MOO framework be validated to ensure robust and reliable early-stage OPV design decisions?"*

7.1. Pareto optimal and Pareto front

The Pareto front is defined as the set of non-dominated solutions, representing design candidates that are not outperformed by any other candidate across all objectives. In this case study, four objectives were considered: the SKI, SI, R_T, and LWT. To preserve a feasible design space, constraints on the GM/B

ratio, roll period (T_{roll}), and operational range were applied during candidate generation.

$$0.05 \leq GM/B \leq 0.25, \quad 6.0 \leq T_{\text{roll}} \leq 10.0 \text{ [s]}, \quad \text{Range} > 1500 \text{ [nm]}.$$

Literature recommends a GM/B ratio between 0.05 and 0.15. However, the reconstructed parent hull exhibited a GM/B ratio close to 0.20. This elevated value can be attributed to the relatively full waterplane distribution of the parent vessel, which increases the transverse waterplane moment of inertia and consequently raises the initial stability. While this improves static margins, it also shortens the natural T_{roll} and results in dynamically "stiff" behaviour. To accommodate this geometry, the upper limit was extended to 0.25. However, a secondary constraint on T_{roll} was introduced in post-processing to exclude dynamically unrealistic designs.

Figure 7.1 illustrates the relation between GM/B and T_{roll}, with colours indicating the C_{WP}. The plot confirms that high GM/B values systematically correspond to short T_{roll}, particularly in designs with fuller waterplanes. This demonstrates that static criteria such as GM/B are insufficient on their own, and that direct constraints on T_{roll} provide a more robust filter against seakeeping deficiencies.

An additional requirement of a minimum operational range of $1,500$ nm was imposed to ensure mission feasibility. This was calculated using resistance predictions at 18 knots combined with the corresponding DWT estimate. It should be noted that these filters represent an early-stage design scenario using a bare-hull model. In later design stages, when appendages are included, additional damping effects are expected to influence both T_{roll} and GM/B.

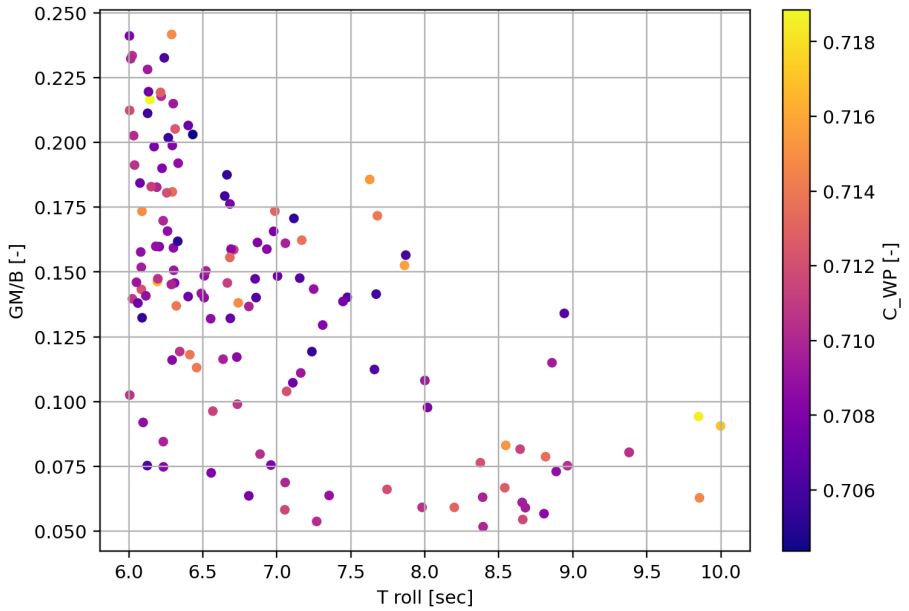

Figure 7.1: Relation between GM/B and T_{roll} coloured by waterplane coefficient (C_{WP}). High GM/B values correspond to unrealistically short T_{roll}s, highlighting the need for dynamic constraints in addition to static stability margins.

For completeness, a supporting figure showing the relation between GM/B and the IMO intact stability requirements is provided in Appendix F (Figure F.1). The results confirm that all designs with $GM/B > 0.05$ satisfy the IMO (2008) criteria. Therefore, maintaining a GM/B ratio above 0.05 remains a valid baseline, as all candidates meeting this constraint also fulfilled IMO stability requirements. However, the additional T_{roll} constraint ensures that the feasible design set is more consistent with realistic seakeeping behaviour.

Table 7.1 presents how these constraints filtered the 465 candidate designs generated by the CAESES optimisation engine. Out of 465 candidates, 422 satisfied the GM/B requirement ($0.05 \leq GM/B \leq 0.25$), 454 fulfilled the range requirement, and 182 met the T_{roll} criterion. When all constraints were combined, 177 designs were classified as feasible. Among these, approximately 32% had a GM/B ratio above 0.15.

Metric	Count	Percent of total [%]
Total candidates	465	100.0
GM/B in (0.05, 0.25)	422	90.8
T_{roll} in [6.0, 10.0] s	182	39.1
Range $>$ 1500 nm	454	97.6
Roll-feasible total	182	39.1
Roll-feasible with GM/B ≤ 0.15	118	25.4
Roll-feasible with GM/B $>$ 0.15	64	13.8
Feasible (all constraints)	177	38.1

Table 7.1: Constraint filtering of candidate designs.

These results indicate that the T_{roll} constraint is a more effective indicator of seakeeping feasibility than the GM/B ratio alone. While 91% of the candidates satisfied the GM/B bounds, only 39% met the T_{roll} requirement. This demonstrates that static stability margins, such as GM/B, are not sufficient to ensure acceptable dynamic behaviour. Directly constraining the T_{roll} filters out over-stiff designs that would otherwise appear feasible, thereby improving the robustness of the feasible design set.

The resulting Pareto-optimal set is shown in Figure 7.2, where SKI, SI, and R_T are plotted in three dimensions, with LWT indicated through colour coding. Because a full four-dimensional Pareto set is difficult to visualise, Figure 7.3 provides a series of 2D projections, each showing trade-offs between two objectives. In these projections, the 2D Pareto frontier is shown in blue, and designs are coloured by a gradient of $0.15 \leq GM/B \leq 0.25$. Both the 4D Pareto-optimal set and the 2D front include only non-dominated candidates. Reference points for the baseline ship and the reconstructed parent hull are also indicated for comparison.

The reconstructed parent hull is not included in the Pareto-optimal set or the feasible solution space because it fails the roll-period constraint, with a computed T_{roll} of only 4.5 [s]. This makes the design dynamically infeasible under the bare-hull assumption. In reality, however, the full vessel is equipped with appendages, stabilisers, rudders, and bilge keels, all of which provide additional damping and would increase the effective T_{roll} into the acceptable range. It is therefore important to emphasise that this analysis

considers a bare hull without appendages. As a result, the parent hull does not appear in the Pareto front projection. This also explains why, in the SI-R_T and LWT-SI subplots, the reconstructed hull lies outside the Pareto front and appears more optimal: it performs well in those two objectives but is excluded due to failing the dynamic feasibility constraint. In the R_T–LWT projection, the Pareto set degenerates to a single non-dominated candidate, so no continuous 2D Pareto line is shown.

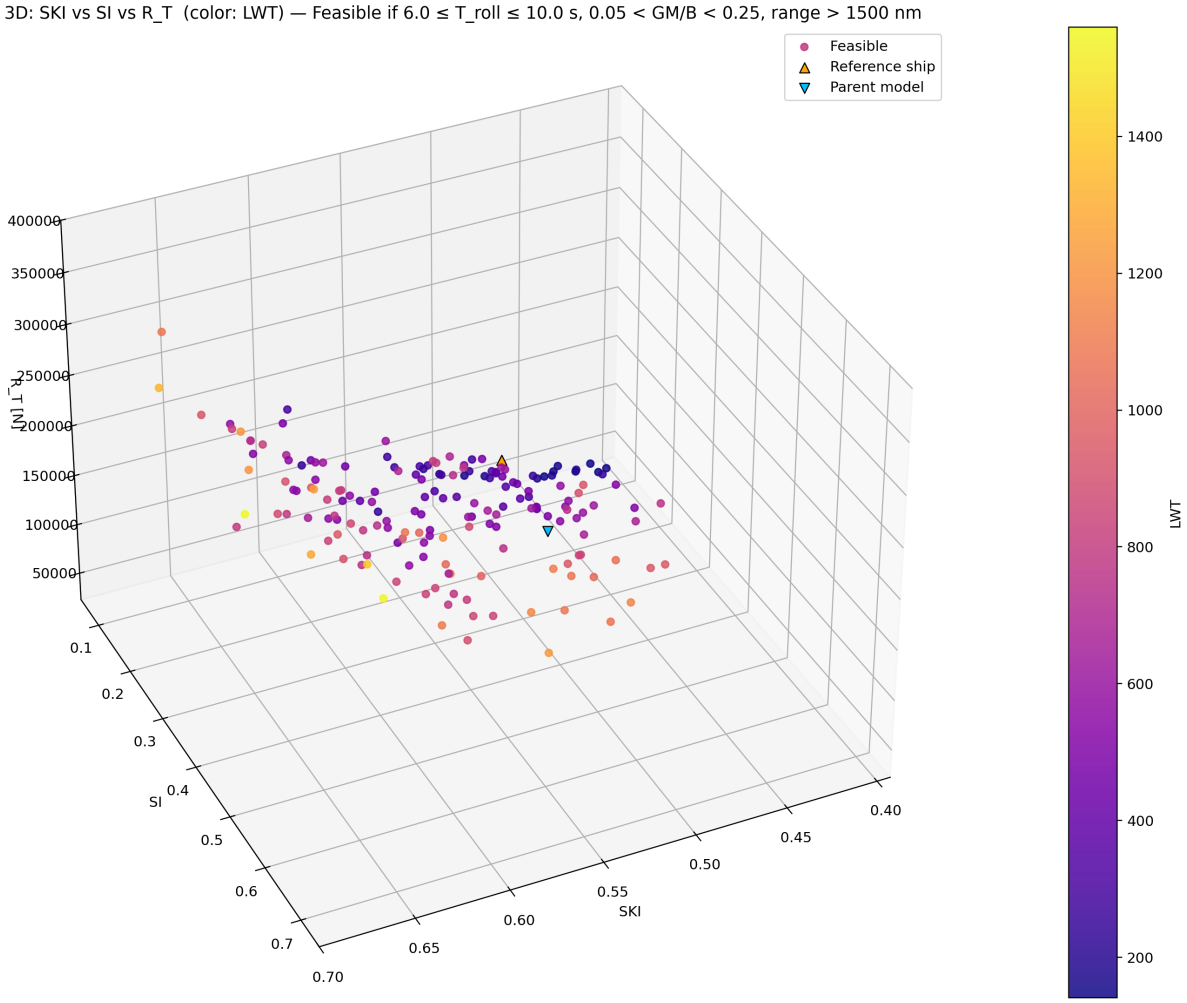

Figure 7.2: Four-dimensional Pareto set visualisation showing R_T, SKI, and SI, with LWT mapped by colour. Only Pareto-optimal candidates are shown.

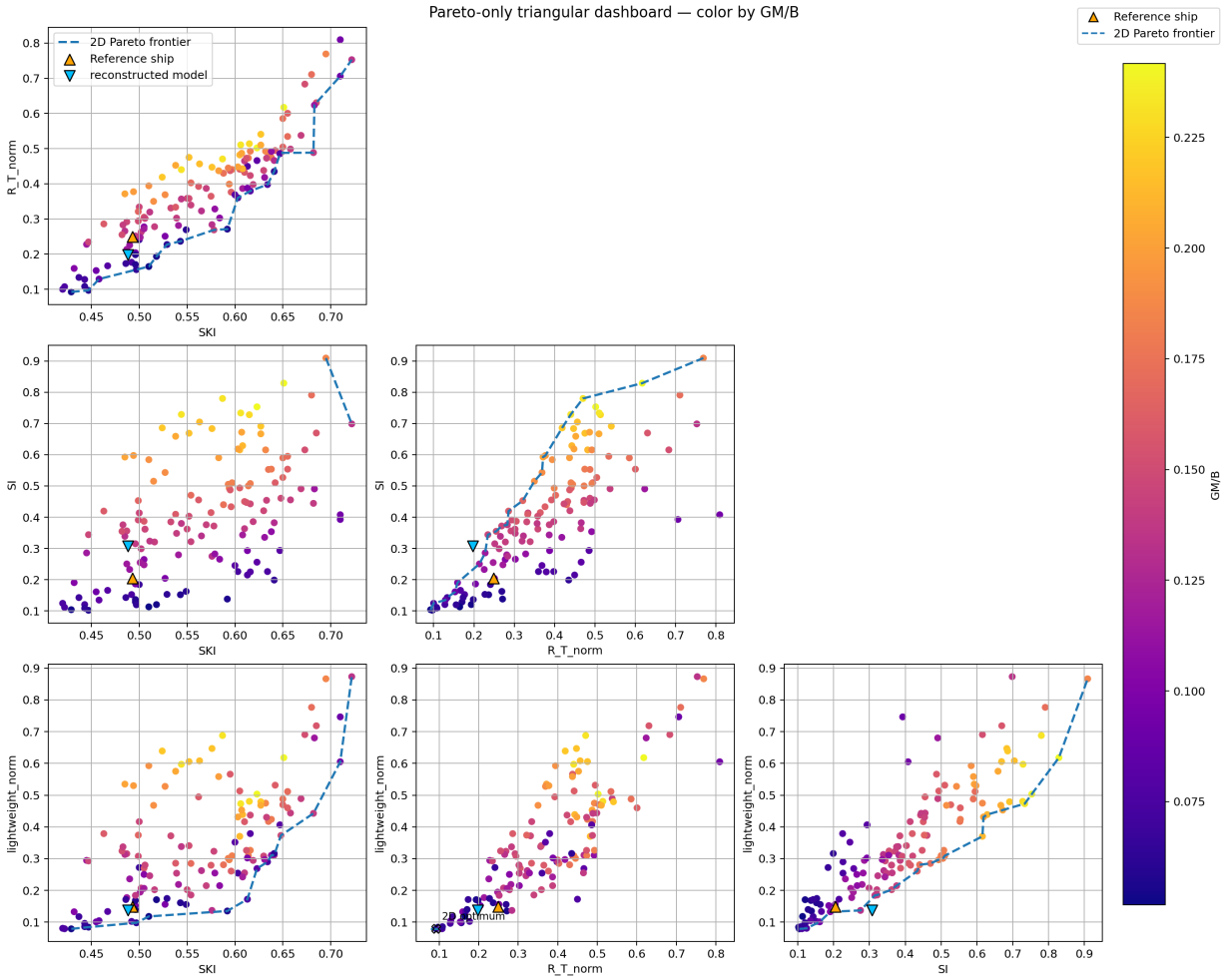

Figure 7.3: Dashboard of 2D projections of the 4D Pareto front, showing the projected 2D Pareto front (blue) and a colour gradient for GM/B. The parent hull and baseline ship are indicated as reference markers. Only Pareto-optimal candidates are shown.

7.2. Convergence and Monitoring Using Hypervolume

The convergence of the MOO process was assessed using the hypervolume (HV) indicator, a widely recognised metric for quantifying both the quality and diversity of Pareto fronts [72]. The HV measures the region of the objective space dominated by the current set of non-dominated solutions, relative to a predefined reference point. Larger HV values reflect a Pareto front that is closer to the ideal point and better distributed across trade-offs. This scalar measure is particularly valuable when more than two objectives are considered, since visual inspection alone becomes insufficient to track convergence [9].

The reference point was established through LHS of 100 initial designs, from which the worst observed performance in each objective was selected and inflated by 10% to prevent boundary lock. This yielded reference values:

- $SKI = 0.3735$
- $R_T = 0.8907$

- $LWT = 0.9605$
- $SI = 0.0290$

The use of LHS ensured a broad initial coverage of the design space, while inflation provided a conservative margin that stabilised the convergence assessment. The HV implementation used here is provided in Appendix E.

HV was calculated exclusively on feasible designs that satisfied all imposed constraints, ensuring that convergence reflected realistic design candidates rather than infeasible outliers. Convergence was considered achieved once HV exhibited a plateau, defined as a relative change below a set threshold over three consecutive iterations. Beyond this point, additional evaluations provided only marginal gains, indicating that the surrogate-assisted optimisation had stabilised on a representative Pareto front.

Figure 7.4 presents the incremental (top) and cumulative (bottom) HV contributions. The incremental plot shows that only a few iterations made substantial improvements, with later designs adding marginal value. The cumulative HV exceeded 99% of its final value after approximately 25 iterations, confirming that the search had adequately explored the trade-off space and that the optimisation process had converged to a stable front. The steady plateau also indicates that the surrogate model provided reliable guidance in locating the true Pareto-optimal region, rather than overfitting to local extremes.

In addition, a noticeable increase in hypervolume occurred after the introduction of normalised variables and objectives, which temporarily renewed the convergence process. This confirms the methodological choice discussed in Chapter 5, where normalisation was introduced to reduce numerical dominance and improve comparability among objectives. The jump in HV illustrates that this step not only stabilised the search but also enabled the discovery of new Pareto-optimal candidates, strengthening both the diversity and robustness of the optimisation outcome.

This outcome confirms that the optimisation framework produced a diverse and converged set of solutions, offering a reliable basis for subsequent trend analysis and decision-making in early-stage OPV design.

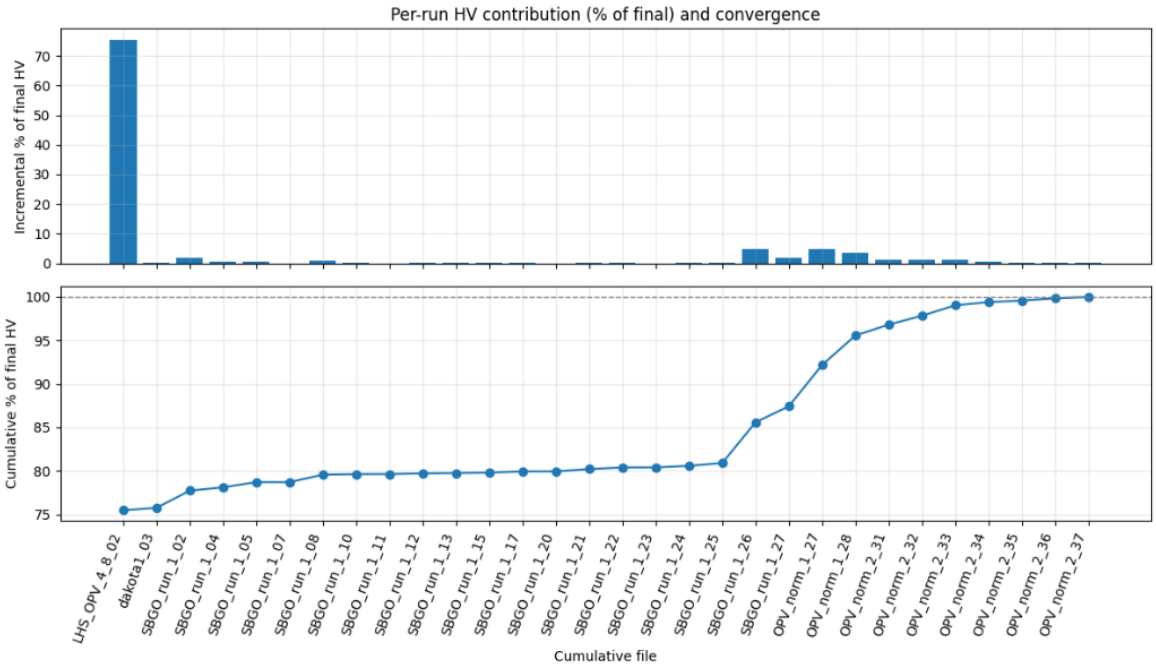

Figure 7.4: Incremental (top) and cumulative (bottom) hypervolume contributions, expressed as a percentage of the final HV, demonstrating convergence of the Pareto front.

7.3. Trend Analysis

The trend analysis evaluates whether the optimisation framework reproduces expected naval-architectural behaviour across the key design variables.

7.3.1. Resistance Trends

Three complementary analyses were conducted to verify that the framework reproduces established resistance scaling laws.

Figure 7.5 presents calm-water resistance R_T against Froude number, evaluated at the design speed of 18 knots ($V_s = 9.26$ m/s). Because speed is fixed, variation in Fn directly reflects the influence of length. The global regression trend ($R^2 = 0.44$) shows that longer hulls (lower Fn) systematically exhibit reduced resistance, consistent with classical Froude scaling, though the correlation appears moderate due to the breadth of the design space.

L/B is represented as a colour gradient, clearly demonstrating the hull slenderness effect. At constant Fn, slender hulls (higher L/B ratios) consistently exhibit lower resistance than fuller hulls (lower L/B ratios). To isolate this slenderness influence, a subset analysis was performed for hulls with similar slenderness ratios ($L/B \in [6.0, 7.0]$), highlighted with circular markers. This subset exhibits a dramatically improved correlation with Fn ($R^2 = 0.93$).

The striking improvement in correlation from $R^2 = 0.44$ for all data to $R^2 = 0.93$ for the controlled subset demonstrates that slenderness variation is the primary source of scatter in the global dataset. This

validates that the framework correctly captures both length effects through Froude scaling and slenderness effects, with both mechanisms being equally critical for accurate resistance prediction in design studies.

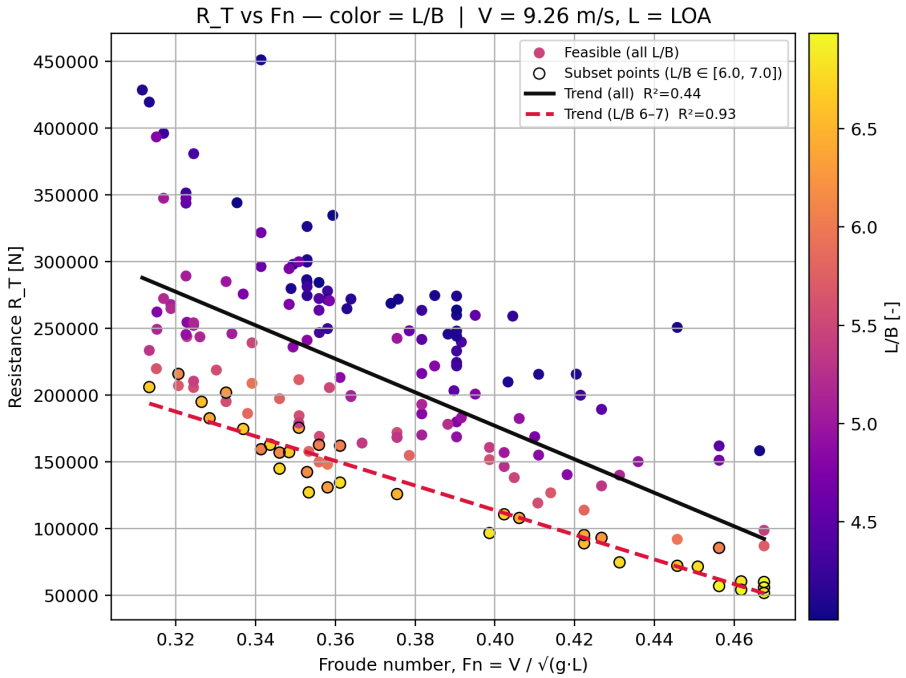

Figure 7.5: Resistance R_T versus Froude number Fn at 18 knots ($V = 9.26$ m/s). Colour indicates L/B. The subset analysis (circled points, $L/B \in [6.0, 7.0]$) demonstrates excellent Froude scaling ($R^2 = 0.93$), compared to the global trend ($R^2 = 0.44$) across the full design space.

Second, the size effects were examined by plotting resistance against L_{OA} (Figure F.2), beam, and draft (Figure 7.6). The results demonstrate strong correlations ($R^2 = 0.89$ for beam, $R^2 = 0.92$ for draft), confirming that increasing principal dimensions leads to higher resistance, primarily due to displacement growth and larger wetted surface area. The colour coding highlights secondary effects of form coefficients, although the independent influence of parameters such as C_B and C_P (Figure F.3) cannot be fully isolated in this dataset, since variations in length and displacement dominate the overall trends.

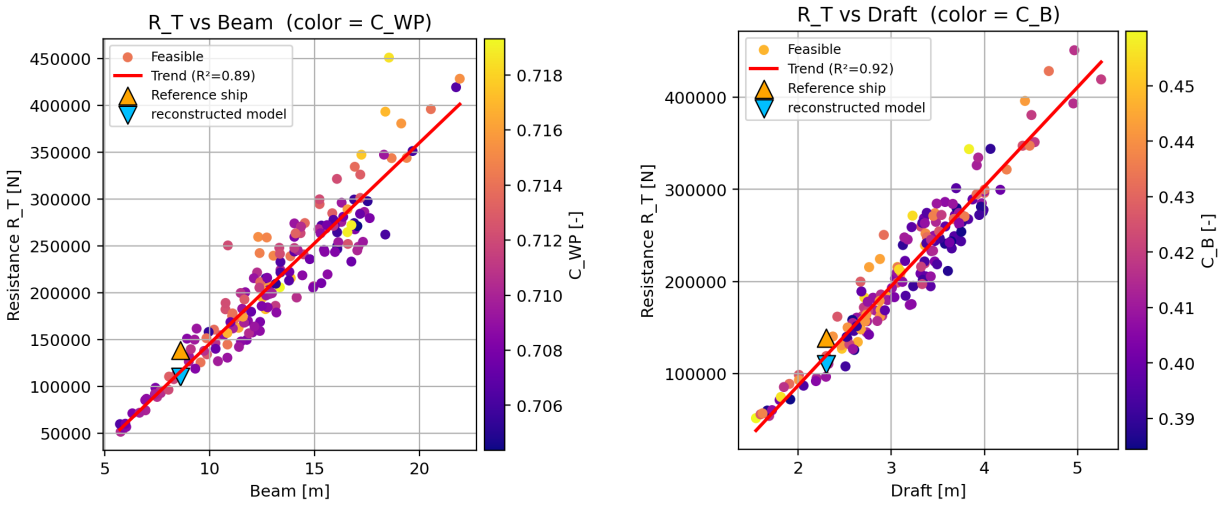

(a) Total resistance R_T vs. Beam (colour: C_{WP})

(b) Total resistance R_T vs. Draft (colour: C_B)

Figure 7.6: Scaling sensitivities of total resistance R_T with respect to beam and draft. Colour encodes either C_{WP} or C_B, highlighting the influence of waterplane and block coefficients.

Finally, the volume effect was assessed by plotting resistance against displacement volume (Figure 7.7). The relationship is strongly nonlinear ($R^2 = 0.83$). A power-law regression,

$$R_T \;=\; 1.84 \times 10^5 \; \nabla^{0.567},$$

captures the observed trend, consistent with viscous scaling (via wetted area growth) together with wave-making contributions at the design speed. Within this dataset, the prismatic coefficient C_P shows a mild but consistent tendency: at approximately constant ∇, fuller forms (higher C_P) exhibit slightly higher R_T, whereas finer forms (lower C_P) lie slightly below the fit. The effect is secondary to the dominant volume scaling but aligns with the expectation that, for semi-displacement OPVs at fixed speed, increased longitudinal fullness raises wetted surface and wave-making near the bow and stern [78].

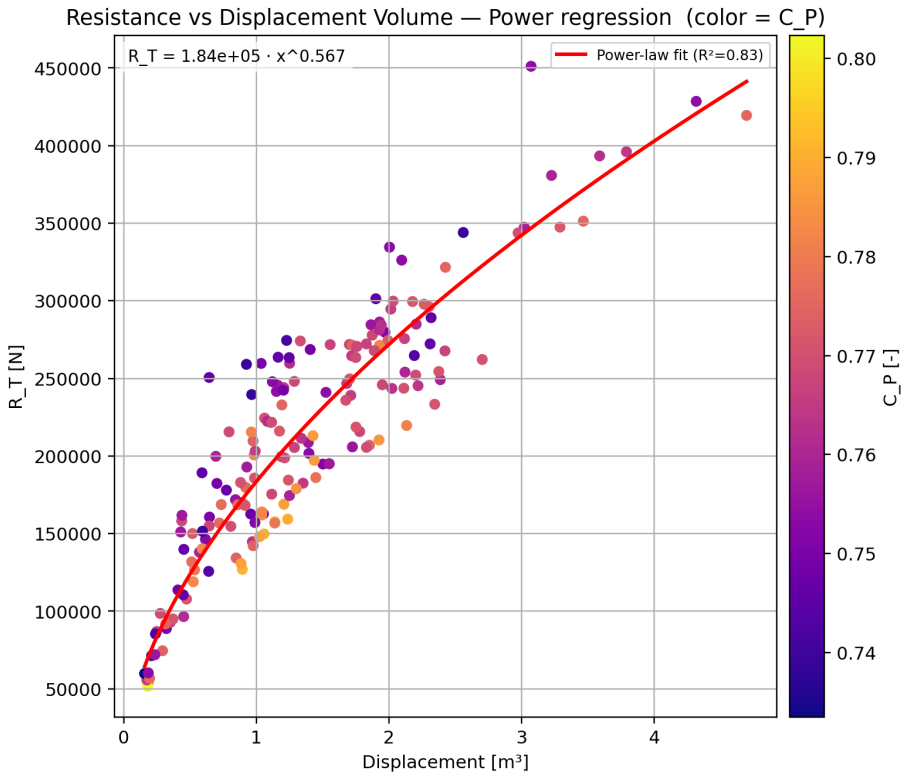

Figure 7.7: Resistance R_T versus displacement volume ∇ with colour indicating C_P. A nonlinear power-law regression confirms the volume effect; higher C_P (warmer colours) tend to lie slightly above the fit at similar ∇.

Together, these analyses confirm that the framework reproduces the three dominant resistance mechanisms:

(i) Longer hulls reduce resistance through Froude scaling,

(ii) Greater slenderness lowers wave-making resistance,

(iii) Displacement growth drives nonlinear viscous penalties, with C_P acting as a secondary modifier at fixed volume.

This alignment with classical hydrodynamic principles reinforces the validity of the framework for OPV design studies.

7.3.2. Stability Trends

The stability analysis confirms that the beam is the dominant driver of transverse stability. As shown in Figure 7.8, wider hulls systematically achieve higher SI values. This behaviour is explained by hydrostatics: increasing beam enlarges the waterplane area, thereby raising the transverse moment of inertia (I_T). This directly increases the BM and consequently the GM, improving static stability and reducing roll amplitudes. These findings are consistent with classical metacentric theory [3, 31, 78] and quantified by Gutsch et al. [30], who showed that beam growth systematically increases stiffness while lowering operability indices.

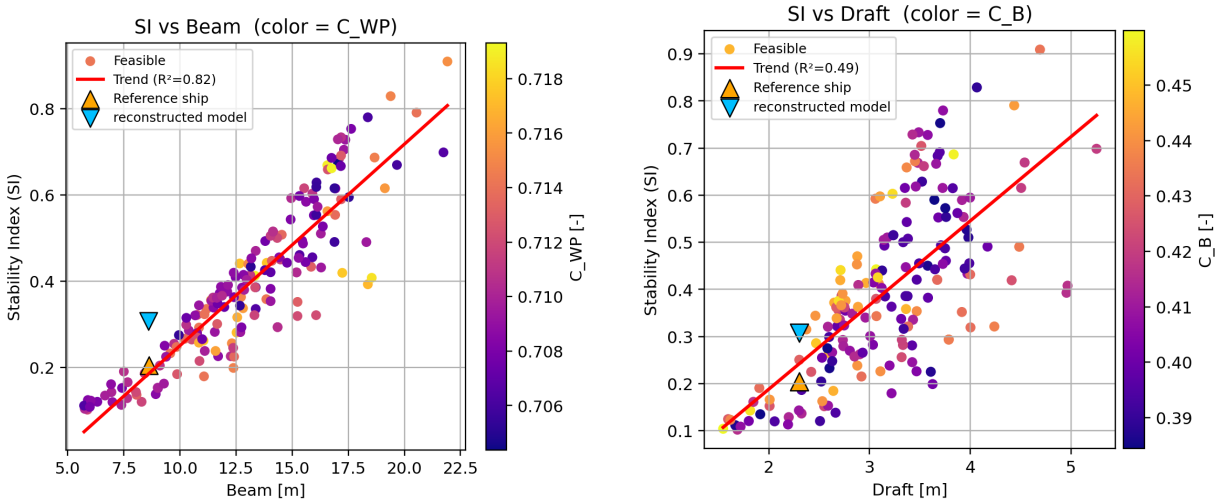

(a) SI versus beam, colour indicates C_{WP}.

(b) SI versus draft, colour indicates C_B.

Figure 7.8: Trends of SI with principal dimensions. Beam and draft both exert strong influence, with colour coding highlighting secondary effects of form coefficients.

Draft effects are also evident (Figure 7.8b), with deeper drafts contributing to higher SI through increased displacement and righting lever arm. Length effects are less pronounced in the global dataset, as they are partly masked by displacement scaling, but the general trend with L_{OA} is included in Appendix F (Figure F.4).

Overall, a strong positive correlation between beam and stability is observed ($R^2 = 0.82$), with both the reconstructed parent hull and the reference OPV lying close to this regression line, confirming the fidelity of the parametric model.

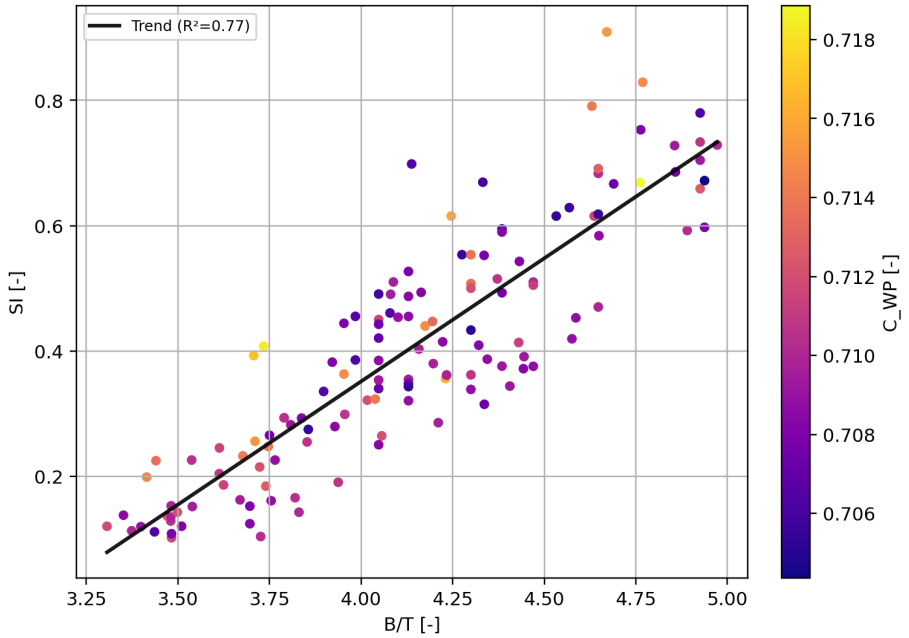

Figure 7.9: SI versus B/T ratio (colour indicates C_{WP}). A strong correlation confirms transverse proportions as a key predictor of initial stability.

The stability framework validation demonstrates compliance with IMO 2008 IS Code criteria and confirms the suitability of GM/B as a proxy metric. As detailed in Section 7.1 and Appendix F, the framework reproduces expected stability behaviour: designs with $GM/B < 0.05$ fail the IMO criterion, while higher values improve compliance but risk excessive stiffness ($T_{\text{roll}} < 6$ [s]). These results confirm the validity of the parametric model in capturing the balance between sufficient and excessive stability.

Regarding coefficients, the waterplane coefficient (C_{WP}) is a local descriptor of waterplane efficiency and directly affects BM. However, within the wide dimensional range considered here (40–90 [m]), C_{WP} alone does not provide additional explanatory power: the same value may occur for both a 50 and a 90 [m] vessel. Dimensional drivers (beam, draft, B/T) remain the primary explanatory factors.

Overall, the framework reproduces expected stability behaviour:

(i) insufficient GM/B yields IMO non-compliance,

(ii) moderate values provide balanced and acceptable stability, and

(iii) excessive values result in stiff roll responses.

The consistent beam–SI relationship strengthens confidence in the framework's ability to capture stability trends relevant for OPV scaling.

7.3.3. Seakeeping Trends

The seakeeping analysis reveals that hull proportions, particularly slenderness, are the dominant drivers of motion performance. Figure 7.10 demonstrates a strong negative correlation ($R^2 = 0.71$) between the SKI

and the L/B ratio, indicating that slender hulls, while favorable for resistance, exhibit significantly reduced seakeeping performance. This fundamental trade-off highlights the competing nature of hydrodynamic efficiency and operability in OPV design, where optimizing for fuel economy directly conflicts with motion comfort and operational capability in rough seas.

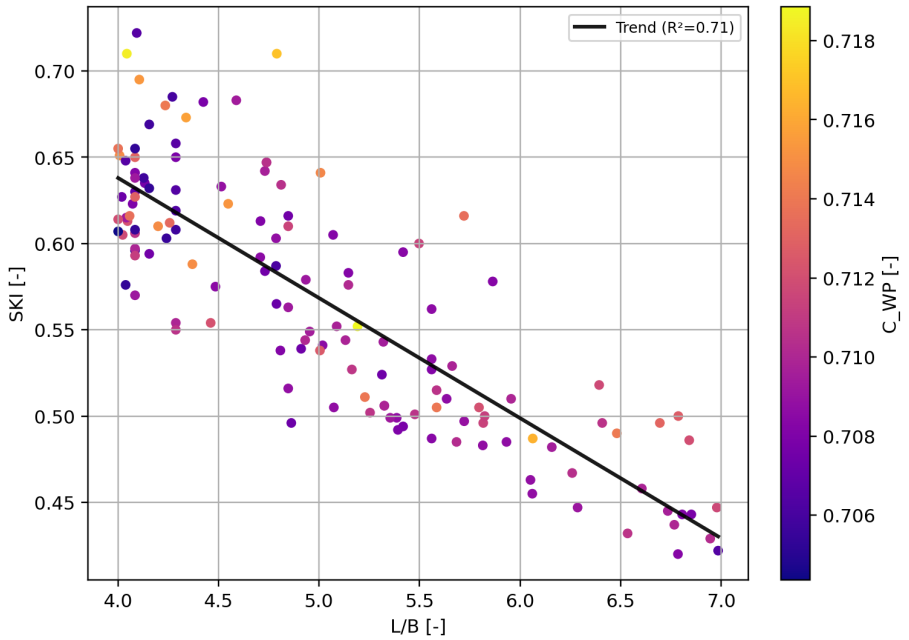

Figure 7.10: SKI versus L/B ratio (colour indicates C_{WP}). More slender hulls (higher L/B) show reduced seakeeping performance, confirming the resistance–seakeeping trade-off.

The influence of absolute dimensions on seakeeping performance presents a contrasting pattern. Figures 7.11a and 7.11b reveal that draft exhibits the strongest positive correlation ($R^2 = 0.80$), confirming that deeper hulls achieve improved seakeeping through enhanced added mass and damping effects. This relationship aligns with classical strip theory, where increased draft reduces heave and pitch motions by augmenting the vessel's hydrodynamic inertia. Beam contributes positively ($R^2 = 0.60$), though with greater scatter, reflecting complex interactions between transverse stability, roll damping, and waterplane area effects.

Most significantly, Appendix F (Figure F.5) shows that L_{OA} has only a weak correlation ($R^2 = 0.14$) with seakeeping performance. This counterintuitive result demonstrates that hull proportions dominate over absolute vessel size in governing motion behaviour—a finding with important implications for OPV scaling strategies. Unlike resistance, where length effects are paramount through Froude scaling, seakeeping performance is primarily governed by dimensional ratios rather than absolute scale.

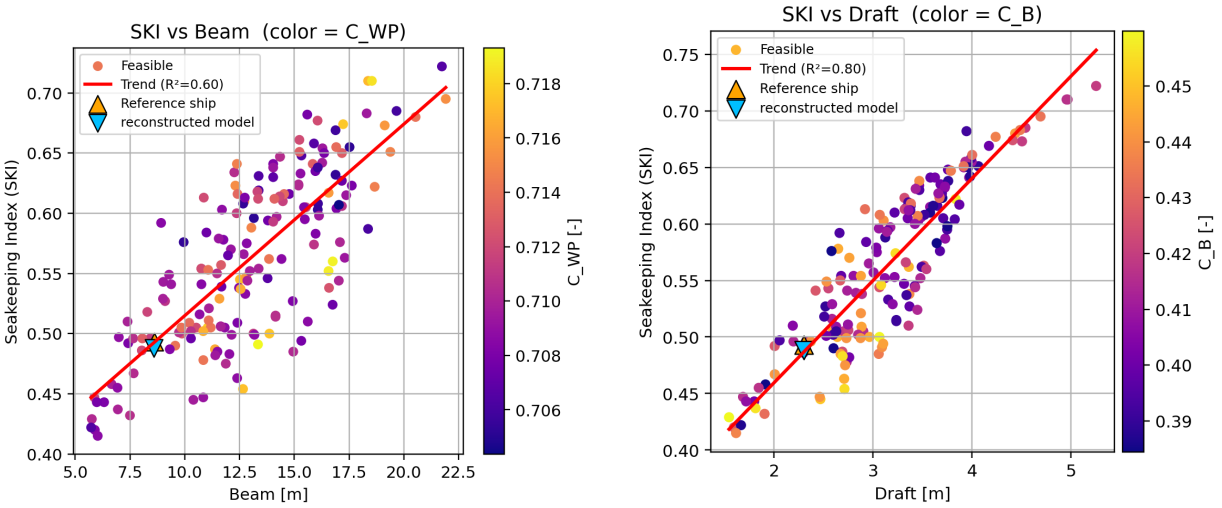

(a) SKI versus beam, colour indicates C_{WP}.

(b) SKIversus draft, colour indicates C_B.

Figure 7.11: SKI trends with principal dimensions. Beam and draft both exert strong influence, with colour coding highlighting form coefficients.

The theoretical basis for these trends can be understood through established seakeeping principles. Increasing draft enhances the vessel's added mass and damping coefficients, reducing response amplitudes across all motion modes. Greater beam improves roll stability and can provide beneficial roll damping, though this benefit may be offset by increased beam-sea excitation. The weak length correlation suggests that for the OPV size range considered, natural frequencies and encounter frequency effects are less influential than sectional properties and proportional relationships.

The C_{WP} shows secondary influence in both figures, with fuller waterplanes generally associated with reduced seakeeping performance. This reflects the increased wave excitation forces on broader waterplane areas, particularly in beam and quartering seas where waterplane shape directly affects heave and pitch coupling.

These results confirm that the framework reproduces established seakeeping scaling behaviour:

(i) L/B dominates seakeeping performance, creating a fundamental trade-off with resistance optimisation,

(ii) draft provides the strongest beneficial effect through added mass and damping enhancement.

(iii) beam contributes positively but with greater variability due to competing stability and excitation effects, and

(iv) absolute length has minimal influence, indicating that proportional scaling governs seakeeping more than dimensional scaling.

This alignment with classical seakeeping theory, particularly the dominance of sectional properties over absolute dimensions, strengthens confidence in the framework's ability to capture operability trends in OPV

scaling studies. The resistance-seakeeping trade-off quantified through the L/B relationship provides crucial guidance for mission-oriented hull optimisation, where the balance between fuel efficiency and operational capability must be explicitly managed.

7.3.4. Lightweight

The lightweight analysis confirms that the framework correctly captures fundamental scaling relationships between vessel dimensions and structural weight. Figures 7.12a and 7.12b demonstrate strong linear correlations between LWT and L_{OA} ($R^2 = 0.87$) and beam ($R^2 = 0.86$), while Appendix F (Figure F.6) shows a slightly weaker correlation with draft ($R^2 = 0.76$). These results validate the geometric scaling embedded in the weight estimation methodology and confirm that the framework reproduces expected volumetric and surface-area scaling laws.

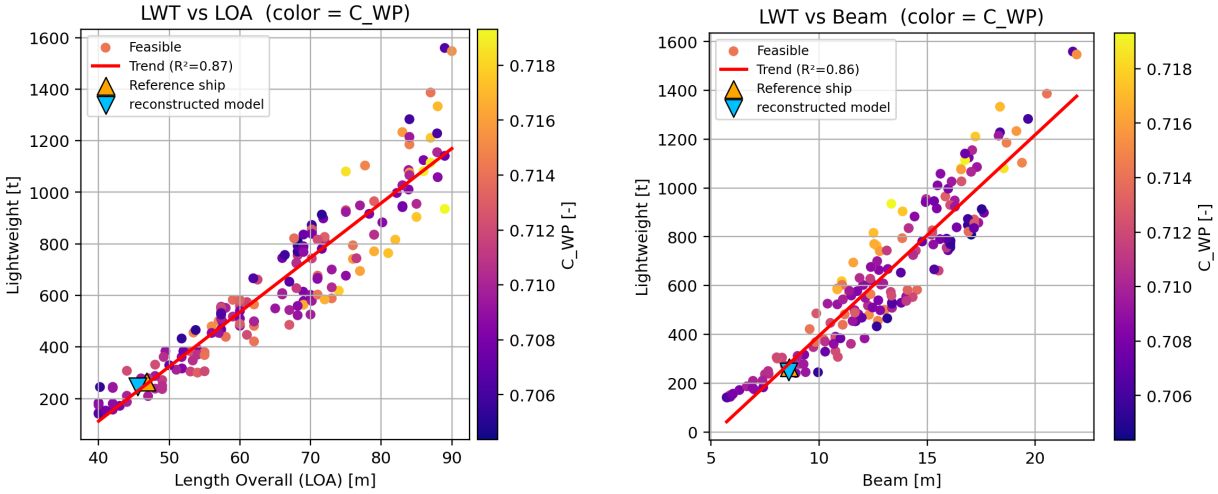

(a) LWT versus L_{OA}, colour indicates C_{WP}.

(b) LWT versus beam, colour indicates C_{WP}.

Figure 7.12: LWT trends with principal dimensions. L_{OA} and beam both drive increases in displacement weight, while colour coding highlights C_{WP}.

The near-identical correlations for L_{OA} and beam reflect the combined influence of structural steel weight, which scales with hull surface area and length, and outfit weight, which scales with deck area and internal volume. The weaker correlation with draft is consistent with naval architectural practice, where draft variations primarily affect hull plating weight but have less influence on superstructure and outfit components that comprise a significant portion of total lightweight. The strong correlations observed validate this approach and demonstrate that the parametric weight model maintains fidelity across principal dimensions.

The positioning of both the reconstructed parent hull and reference OPV close to the regression trends further validates the accuracy of the weight estimation framework. This alignment suggests that the scaling coefficients derived from the ISL OPV 45 remain applicable across the broader size range, though future work should validate these relationships against additional reference vessels to improve predictive

accuracy.

The analysis reveals several important characteristics of weight scaling in OPVs:

(i) LWT exhibits nearly linear scaling with principal dimensions, confirming the validity of dimensional-based weight estimation.

(ii) length and beam show equivalent influence, reflecting their combined role in determining structural and outfit weight,

(iii) draft exerts slightly weaker influence, consistent with its more limited impact on non-hull weight components, and

(iv) the framework maintains consistency with reference data across the design space.

However, several limitations must be acknowledged in the current weight estimation approach. The regression coefficients are derived from a single parent vessel, which may not represent the full variability in OPV construction standards, outfit levels, or structural design philosophies. Different mission requirements—such as enhanced armament, extended endurance equipment, or specialised sensor fits—would significantly alter weight distribution and scaling relationships. Additionally, the assumption of similar internal arrangements across the size range may not hold for larger vessels, where structural efficiency and outfit density typically improve with scale.

This lightweight analysis provides confidence in the framework's ability to capture first-order weight scaling effects essential for early-stage trade-off studies. The strong dimensional correlations enable reliable comparative assessment of design alternatives, though higher-fidelity weight estimation methods would be required for detailed design phases where absolute accuracy becomes critical.

7.3.5. Deadrise and Rake Angle Effects

The influence of deadrise angle on seakeeping and stability, and of rake angle on resistance and lightweight, was also explored. As shown in Figure 7.13, no consistent global trends were identified. This outcome is expected, since the effect of local hull-form parameters such as deadrise can be masked by concurrent changes in principal dimensions (length, beam, draft). These parameters should therefore be investigated under controlled, local optimisation conditions (i.e. fixed principal dimensions) to isolate their contributions.

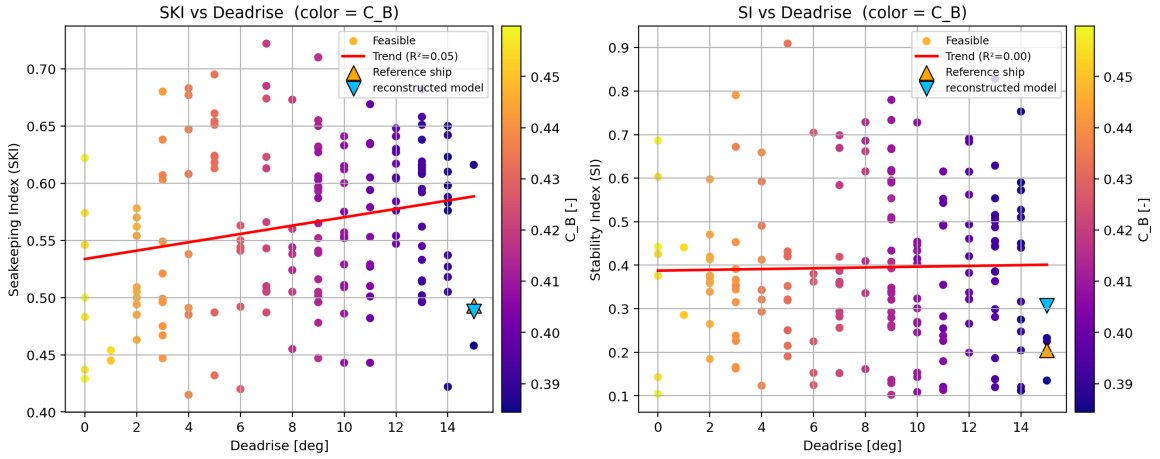

Figure 7.13: Influence of deadrise on SKI and SI. No global trend is visible, as deadrise effects are masked by variations in principal dimensions.

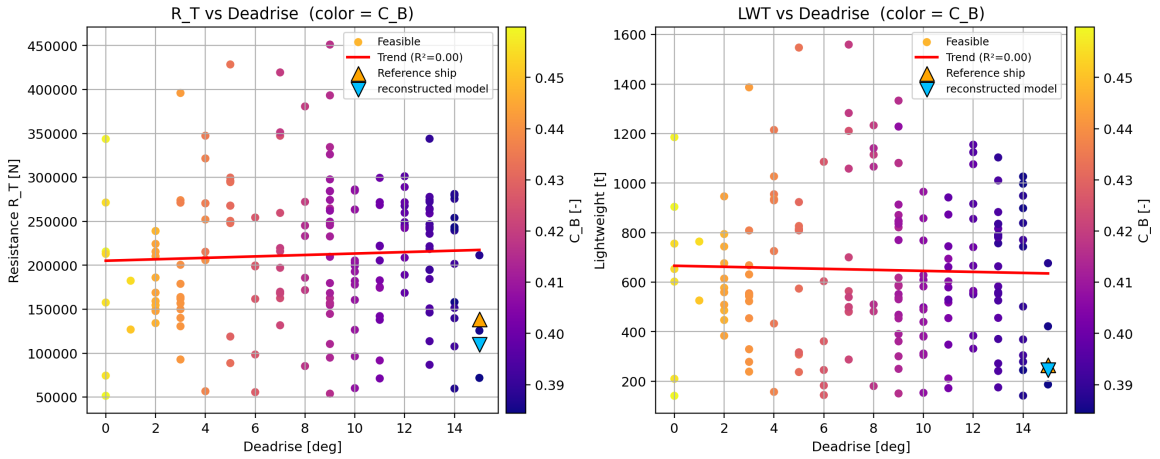

Figure 7.14: Influence of Deadrise on R_T and LWT. No consistent trend is observed, indicating that deadrise contributions are second-order compared to principal dimensions.

Similarly, Figure 7.16 indicates no clear global correlation between rake angle and either resistance or lightweight. This suggests that rake effects are second-order compared to the dominant influence of length, displacement, and block coefficient. As with deadrise, targeted local optimisation would be required to quantify rake contributions reliably. These results confirm that deadrise and rake exert only a secondary influence compared to beam and draft. Capturing such effects would require dedicated local studies or higher-fidelity methods.

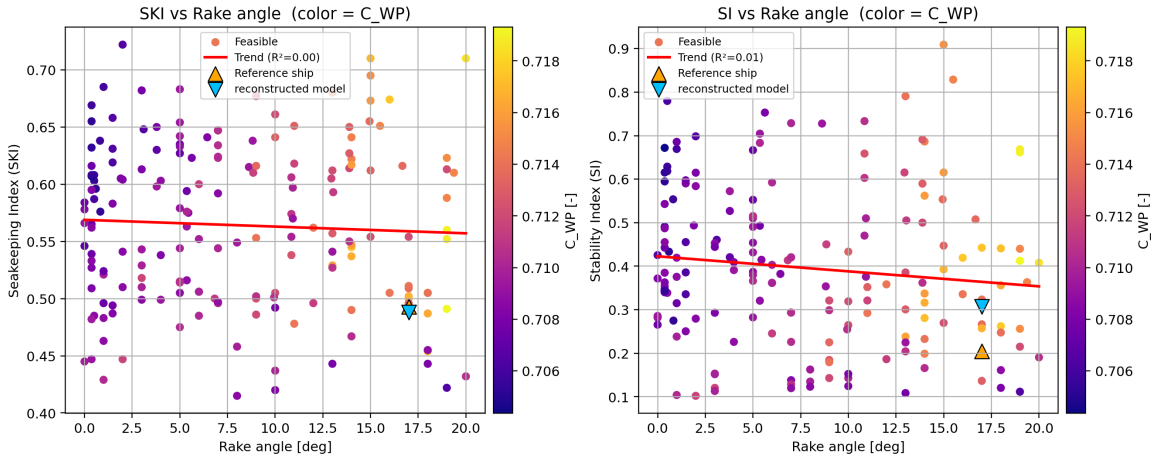

Figure 7.15: Influence of rake angle on SKI and SI. No systematic correlation is identified.

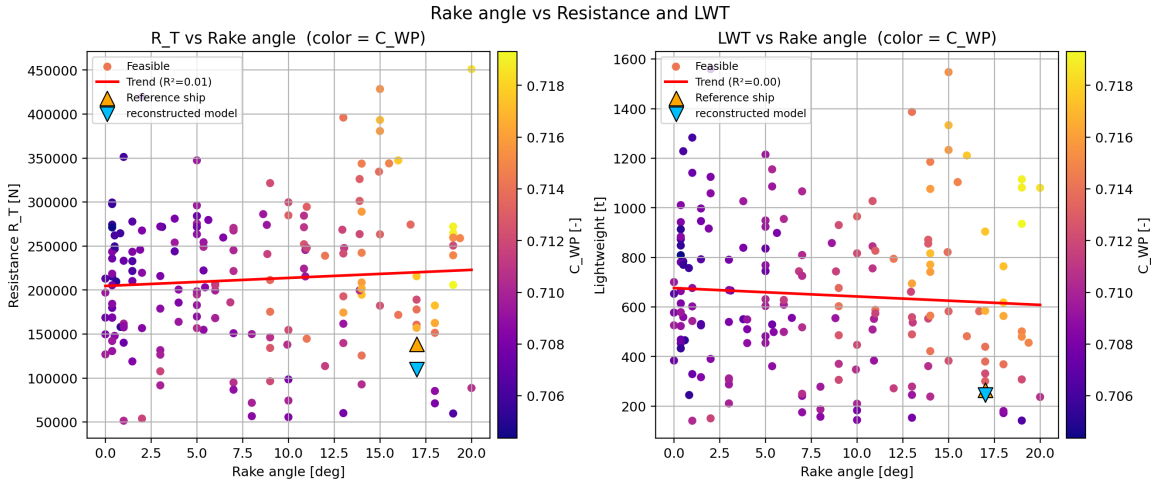

Figure 7.16: Influence of Rake angle on R_T and LWT. The absence of a global trend suggests rake is a secondary driver compared to principal dimensions.

7.3.6. Range Trade-offs

Although range was not included as an explicit optimisation objective, it was retained as a feasibility constraint (> 1500 nm). Analysing its variation across the feasible design set provides valuable insight into how endurance interacts with other objectives. Range can be interpreted as an emergent performance metric, reflecting the combined effects of displacement, resistance, and payload capacity. By projecting range onto Pareto frontiers, the trade-offs with primary objectives become visible.

Figure 7.17 presents Pareto-projected scatterplots of SKI against R_T and LWT, with points coloured by range and markers for the reference ship and reconstructed model.

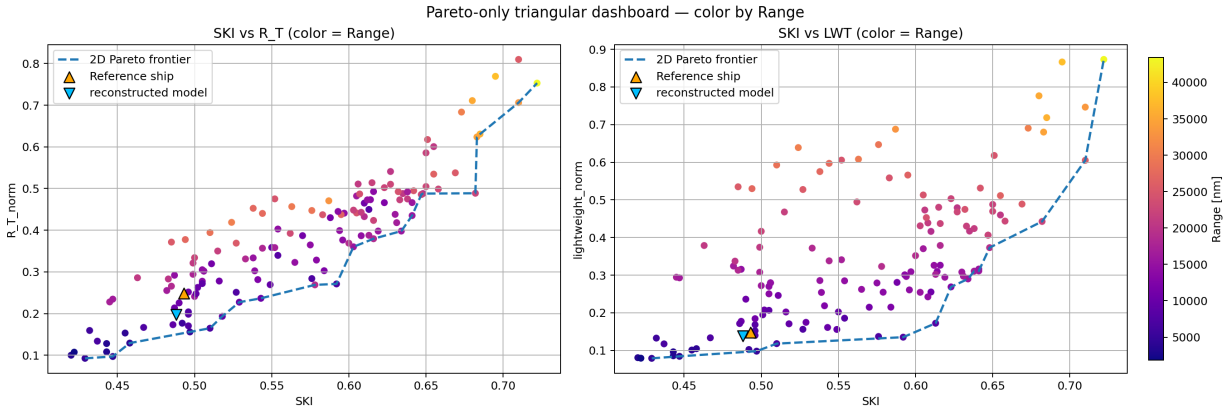

Figure 7.17: Pareto front projections of SKI versus resistance R_T (left) and SKI versus LWT (right), coloured by range. The reference ship and reconstructed model are shown for comparison.

Two main insights emerge:

- Range versus resistance (left panel): At constant SKI, increasing range requires higher resistance (moving right). At constant R_T, increasing range reduces SKI (moving down). In both cases, higher endurance shifts designs away from the Pareto frontier, confirming that range cannot be improved without sacrificing efficiency or motion performance.
- Range versus weight (right panel): At constant SKI, increasing range requires higher LWT (moving right), reflecting heavier structures to support additional endurance. At constant LWT, however, SKI can be improved without reducing range. This highlights a promising design direction: seakeeping can be enhanced without penalising endurance or weight, but extending range beyond certain limits inevitably drives the design off the Pareto frontier.

Overall, these results show that range acts as a secondary discriminator. It does not define the Pareto set directly, but it strongly conditions the balance between endurance, resistance, and seakeeping. Designers seeking an extended range must either accept higher resistance or heavier vessels, while opportunities exist to improve seakeeping without reducing endurance if weight is held constant. This confirms that range is a critical—but indirect—driver of trade-offs in OPV scaling and must be considered explicitly when selecting mission-oriented designs.

7.3.7. Effects of Variables on Objectives

To complement the trend analysis, the relationship between objectives and design variables was examined using a correlation heatmap (Figure 7.18). The heatmap compares objectives (rows: SKI, SI, R_T, LWT, Range) against principal dimensions, form coefficients, and derived ratios (columns: L_{OA}, Beam, Draft, C_P, C_B, C_{WP}, L/B, B/T, etc.). Pearson correlation coefficients ($r \in [-1, 1]$) were calculated as:

$$r_{XY} = \frac{\sum_i (x_i - \bar{x})(y_i - \bar{y})}{\sqrt{\sum_i (x_i - \bar{x})^2}\sqrt{\sum_i (y_i - \bar{y})^2}},$$

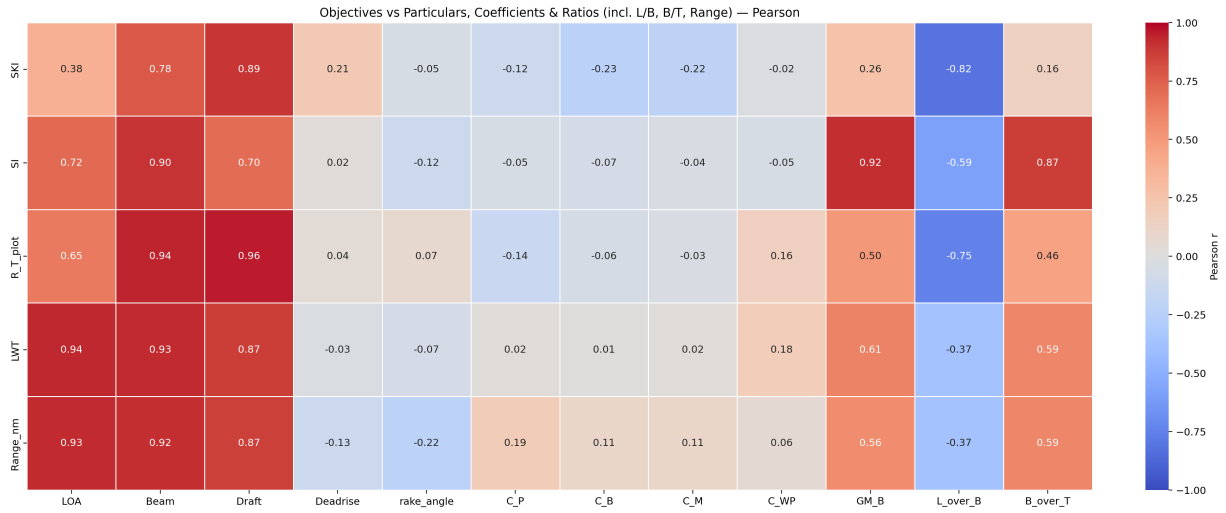

Figure 7.18: Pearson correlation coefficients between objectives and main particulars, form coefficients, and ratios. Strong positive correlations are shown in red, strong negative correlations in blue.

where values close to ± 1 indicate strong linear association, and values near zero indicate weak or no linear relationship. It is important to note that Pearson captures only linear dependencies, whereas many naval–architectural relations are nonlinear (e.g. the power-law between R_T and displacement). Therefore, the heatmap should be interpreted as a first-order diagnostic rather than a complete causal description. The underlying code in Appendix G.

The following key patterns emerge:

- Strong dimensional drivers; R_T, LWT, and range all exhibit very high positive correlation with L_{OA}, Beam, and Draft ($r > 0.85$). This reflects the dominant scale effect: larger ships are heavier, offer more displacement, and achieve longer endurance, but also incur greater resistance.
- Seakeeping; SKI correlates positively with Beam ($r = 0.78$) and Draft ($r = 0.89$), confirming that fuller cross-sectional dimensions improve motion performance. By contrast, SKI is negatively correlated with slenderness (L/B, $r = -0.82$), underlining the resistance–seakeeping trade-off.
- Stability; SI correlates strongly with Beam ($r = 0.90$) and GM/B ($r = 0.92$), consistent with hydrostatic theory. Negative correlation with L/B ($r = -0.59$) highlights how slender hulls reduce transverse stiffness.
- Secondary coefficients; Form coefficients such as C_P, C_B, and C_M show only weak to moderate correlations ($|r| < 0.25$). Their effects are largely masked by the dominant influence of principal dimensions in the explored design space.

Overall, the heatmap confirms that hull size and proportions dominate the behaviour of the objectives, while form coefficients exert secondary influence. This analysis also demonstrates the value of correlation methods: rather than examining each scatterplot separately, the heatmap provides a compact overview of how design variables systematically shape performance. At the same time, the complementary trend analysis remains essential for capturing nonlinear scaling laws that Pearson correlation cannot reveal.

7.4. Framework Application and Implications

The verification results confirm that the MOO framework consistently reproduces established hydrodynamic and hydrostatic scaling laws. Having demonstrated physical validity, the framework can now be considered a practical decision-support tool for early-stage OPV design.

Application in Early-Stage Design

The framework provides designers with a structured method to explore large design spaces rapidly. By combining Pareto fronts with constraints on stability, resistance, range, and seakeeping, the framework identifies sets of non-dominated designs that balance performance trade-offs. This approach enables systematic comparison of alternatives that would traditionally require multiple sequential analyses. In particular, it allows:

- Rapid exploration of scaling effects, such as assessing the impact of length or displacement growth on resistance and endurance.
- Quantitative trade-off analysis, for example, between seakeeping and stability when adjusting beam or GM.
- Identification of robust design ranges, where acceptable performance is achieved across multiple criteria without excessive sensitivity to a single parameter.

Operational Implications

The Pareto-optimal sets generated by the framework illustrate the design tensions faced in multipurpose OPVs. For instance, wider beams improve stability but may degrade seakeeping, while deeper drafts enhance seakeeping at the cost of resistance and displacement. The framework makes these trade-offs explicit and transparent, allowing decision-makers to prioritise criteria according to mission requirements. This is particularly valuable in OPVs, where operational profiles can vary widely between patrol, escort, and surveillance roles.

Visualisation of Feasible Substitutions

Figure 7.19 presents pairwise projections of the feasible non-dominated set within the range $40 \leq L_{OA} \leq 60$ m. Each subplot overlays: (i) the reconstructed parent hull (cyan triangle), (ii) iso–lines of constant R_T, LWT, SI, and SKI (cyan dashed), and (iii) the local two-dimensional Pareto front (green dashed). This representation highlights feasible substitutions, i.e. designs that maintain comparable performance in one objective while achieving improvements in another.

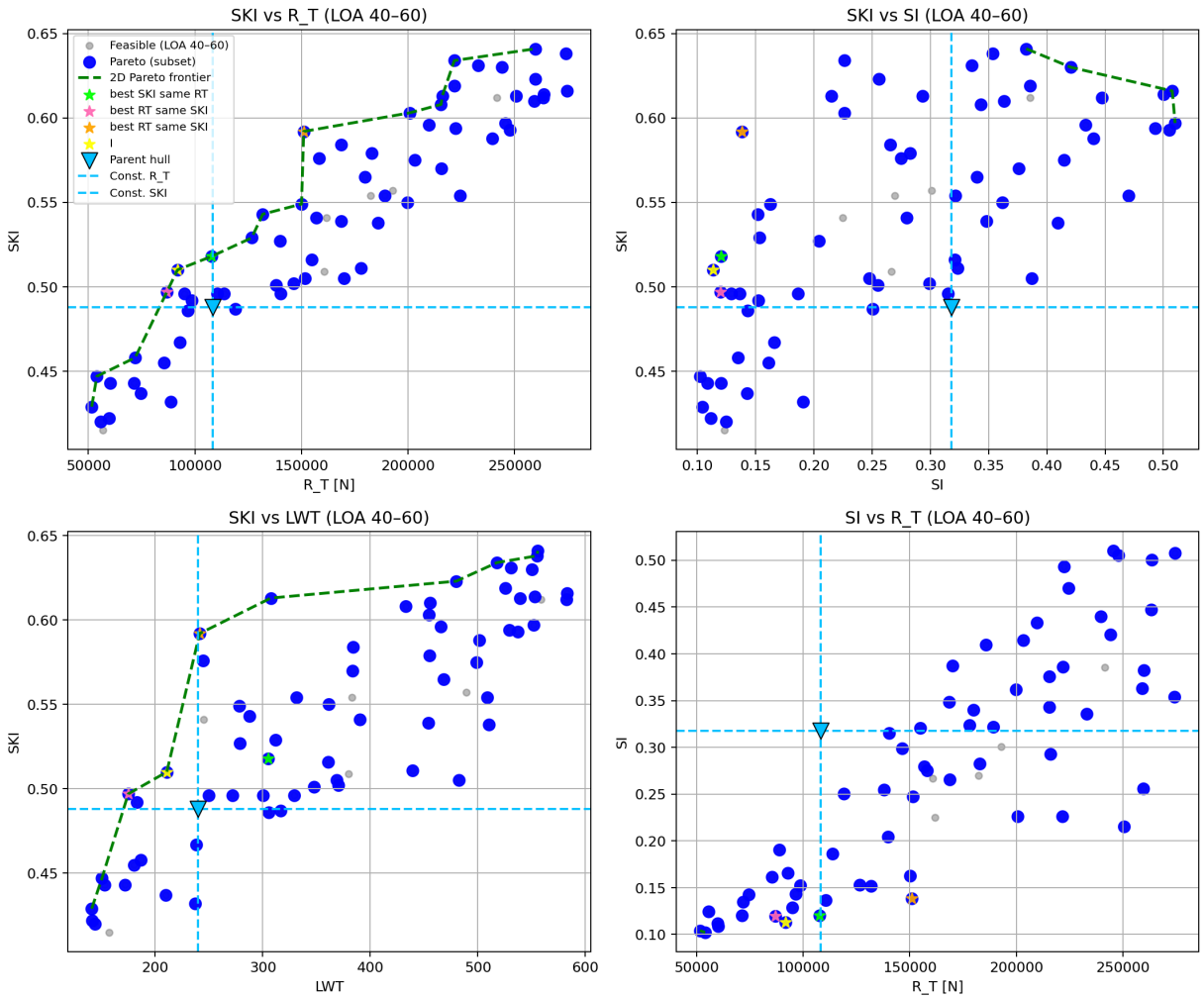

Figure 7.19: Pairwise projections of the feasible non-dominated set for $40 \leq L_{OA} \leq 60$ m. The plots show the parent hull (cyan triangle), iso–lines of constant objectives (cyan dashed), and the local 2D Pareto fronts (green dashed).

To illustrate this in detail, Figure 7.19 and Table 7.2 compare four candidate hulls against the reconstructed parent. Each candidate was selected to represent an alternative with similar performance in one metric while improving another: one with comparable resistance, one with similar SKI, one with similar LWT, and one combining improved SKI with reduced resistance.

Table 7.2: Comparison of candidate designs relative to the parent hull. Values higher than the parent hull are highlighted in green, lower in red.

Run	Parent hull	SBGO_run_1_13 (des0016)	LHS_OPV_4_8_0 (des0288)	SBGO_run_1_21 (des0018)	SBGO_run_1_04 (des0018)
L_{OA}	45.5	44	42	40	53
Beam	8.6	7.39	8.92	6.99	8.29
Draft	2.3	2.19	2.66	2.06	2.51
Depth	4.25	4.65	5.66	4.37	5.33
Deadrise	15	11	13	13	14
Rake angle	17	3	7	7	3
SKI	0.488	0.51	0.59	0.50	0.52
R_T	108198	91793	151021	86838	107766
SI	0.023	0.11	0.14	0.12	0.12
DWT	91	113.93	199.20	78.91	180.82
LWT	240	210.72	241.30	174.91	304.81
GM/B	0.1945	0.05	0.06	0.06	0.05
221a_IMO	0.21	0.06	0.07	0.06	0.06
221b_IMO	0.347	0.11	0.13	0.11	0.11
221c_IMO	0.136	0.05	0.06	0.05	0.05
222_IMO	0.788	0.31	0.39	0.32	0.33
223_IMO	0.629	0.70	0.70	0.66	0.70
224_IMO	1.615	0.37	0.49	0.43	0.42
Range	4706	6944	7380	5084	9388

Interpretation of Results

All selected candidates satisfy IMO intact stability criteria by construction. Interestingly, although the optimisation objective was formulated to maximise SI, the best overall trade-offs were achieved when SI remained close to its lower feasible bound. Excessive stiffness was shown to reduce seakeeping quality without providing further benefit to compliance. This indicates that IMO compliance alone is not sufficient: balanced performance emerges when stability is moderated rather than maximised.

Finally, all candidates demonstrated improved range relative to the parent hull. Since range is a combined function of resistance and available DWT, gains were achieved whenever R_T was reduced and/or payload fraction was increased. These findings confirm the framework's ability to reveal performance-driven substitutions and to reproduce the expected trade-offs between resistance, stability, seakeeping, and endurance.

Limitations and Further Development

While the framework captures first-order behaviour, it remains an early-stage tool. Simplifications such as the use of H&M resistance predictions and bare-hull seakeeping models mean that appendage effects, nonlinear damping, and viscous–wave interactions are not yet accounted for. Integrating higher-fidelity

methods (e.g., CFD or model testing) in later stages will refine the Pareto-selected candidates.

Implications for OPV Design Practice

By combining scaling methods with multi-objective optimisation, the framework provides a repeatable and cost-effective pathway for generating balanced OPV designs. It offers not only theoretical verification but also practical decision-support, enabling designers to identify substitutions and trade-offs that would be difficult to capture through sequential, single-objective analyses. This represents a step toward digitalised, knowledge-driven early-stage OPV design.

7.5. Test Case Conclusion

This chapter verified the behaviour of the proposed optimisation framework through a dedicated OPV scaling case study. Three key outcomes were demonstrated: convergence, trends, and application. Together, they assess the effectiveness of the framework in verifying physical consistency, capturing expected scaling behaviour, and supporting practical design decisions.

Convergence: The HV analysis confirmed stable optimisation: after approximately 25 iterations, the HV plateaued above 99% of its final value. Out of 465 candidates, 177 satisfied all feasibility constraints and 137 formed the Pareto-optimal set. Constraint filtering revealed that while 91% of designs passed the GM/B bound, only 39% satisfied the roll-period requirement, highlighting T_{roll} as a more reliable discriminator of dynamic feasibility. This supports the argument that static stability margins alone are insufficient and that dynamic criteria must be incorporated directly to ensure operational realism. In addition, normalising objectives and variables improved the definition of the Pareto front, adding non-dominated candidates that were previously masked. This shows that normalisation is essential to avoid bias when comparing heterogeneous objectives.

Trends: The framework reproduced established naval–architectural behaviour. Longer hulls increased displacement and resistance but improved stability and seakeeping, consistent with slender-body scaling. Greater beam enhanced SI but reduced SKI, reflecting the classical stability–comfort trade-off. Deeper drafts raised displacement and resistance while also improving stability.

Form coefficients (C_B, C_P, C_{WP}, C_M) showed weaker and less consistent global correlations compared to principal dimensions and derived ratios (L/B, B/T, GM/B). Their influence is partly masked by large variations in L, B, and T, and becomes clearer only in narrow-band studies. Still, secondary patterns were evident: fuller waterplanes ($C_{WP} \uparrow$) were linked to shorter roll periods and lower SKI, while higher prismatic coefficients ($C_P \uparrow$) tended to raise resistance at constant displacement. This shows that coefficients act as conditioning factors rather than dominant drivers, reinforcing the need for localised studies to isolate their influence.

Range, although not an explicit optimisation objective, emerged as a decisive secondary discriminator. Higher endurance was shown to require either increased resistance (for fixed SKI), reduced SKI (for

fixed R_T), or higher LWT (for fixed SKI). In rare cases, SKI improved without reducing range, but overall endurance strongly conditioned the feasible design space.

Correlation heatmaps confirmed that principal dimensions and derived ratios (L/B, B/T, and GM/B) exert the strongest global influence on performance, while secondary factors such as deadrise, rake, and coefficients provide nuanced effects that require targeted exploration.

Application: The framework was applied locally within the $40 \leq L_{OA} \leq 60$ m range to explore feasible substitutions. Iso-lines of constant R_T, LWT, SI, and SKI provided a transparent way to compare candidates against the reconstructed parent hull. The results showed that viable alternatives exist which maintain comparable performance in one metric while offering improvements in another. For example, designs were identified with equal R_T but higher SKI, or with equal SKI but lower LWT. This highlights the framework's strength: by presenting a structured set of trade-offs, it enables designers to select solutions that best align with mission priorities, whether endurance, comfort, or economy.

Taken together, these results confirm that the framework is:

- Robust, as convergence monitoring produced a stable Pareto set.
- Physically consistent, as the observed trends align with established naval-architectural theory.
- Insightful, as several critical trade-off patterns were revealed: the need to minimise rather than maximise SI, the importance of the roll-period (T_{roll}) constraint, the confirmation that $GM/B > 0.05$ is a valid lower bound, the necessity of normalising objectives and variables to avoid bias, and the conditioning effect of range trade-offs.
- Applicable, as the framework supports mission-oriented substitutions in OPV design.

These findings verify the framework and directly address the final part of Research Sub-question 5. Chapters 6 and 7 jointly provide the answer: Chapter 6 validates the framework against reference data, while Chapter 7 verifies its behaviour against expected physical laws and trade-offs.

8

Discussion and Conclusion

This chapter synthesises the findings of the thesis and provides final conclusions of the thesis. The discussion is structured around the research sub-questions, followed by an integrated answer to the main research question. Subsequent sections address the implications of the work, recommendations for design practice and future research, Finally a brief personal reflection.

8.1. Discussion

8.1.1. Research Sub-questions

1. **"*How do the fundamental characteristics, mission roles, and design drivers of multi-purpose Offshore Patrol Vessels (OPVs) influence their key design and mission requirements, and in turn shape overall vessel performance and operational effectiveness?*"**

   Chapter 2 confirmed that multipurpose OPVs operate across diverse mission profiles, including EEZ surveillance, environmental protection, SAR, counter-piracy, and law enforcement. These roles impose heterogeneous demands: endurance and cost efficiency favour slender hulls, while stability and seakeeping require wider beams and deeper drafts, making conflicting requirements inherent to OPV design. From this mission analysis, five key design drivers were identified: seakeeping, resistance, stability, TLCC, and operational range. In the framework, TLCC was represented by LWT as a practical early-stage proxy for cost, while range was reformulated from a DWT measure into a minimum-range constraint to ensure endurance feasibility before other trade-offs were explored. The heatmap in Figure 2.5 shows that global performance is dominated by the main particulars—length, beam, draft—together with metacentric height (GM). Beam and GM/B govern stability, draft and beam improve seakeeping, and all three dimensions drive resistance, weight, and range. Ratios further clarify trade-offs: slender hulls (L/B) reduce resistance but harm stability and seakeeping, while wider B/T ratios improve stability and range at the cost of resistance. By contrast, coefficients

(C_B, C_P, C_{WP}), deadrise, and rake angle showed only minor global influence, reflecting their role as local refinements within constrained design spaces.

2. **"*How do contemporary ship-design and scaling methodologies—including geometric, parametric, and hybrid approaches—capture the non-linear interactions between key hull parameters (length, beam, draft, block coefficient) and performance indicators (resistance, stability, seakeeping, and propulsion efficiency), and thereby support optimisation in the early stages of design?*"**

   Contemporary ship-design methodologies have increasingly shifted their focus toward optimisation in the early design stages, where multiple objectives and performance drivers must be balanced simultaneously. Scaling methods provide the foundation for this exploration and can be classified into geometric, parametric, and hybrid approaches. Pure geometric scaling preserves similarity but cannot capture the nonlinear effects of changing principal dimensions—for example, beam may improve stability while increasing resistance, and draft may enhance seakeeping at the expense of weight. Parametric scaling addresses these limitations by allowing targeted variation of individual dimensions, but exhaustive sweeps across the design space quickly become computationally expensive. Hybrid approaches combine proportional scaling with selective parametric variation, offering a balance between efficiency and the ability to reveal nonlinear interactions. In this thesis, these ideas are integrated within a Systems Engineering (SE) and Set-Based Design (SBD) framework: SE provides a requirement-driven structure where objectives, constraints, and evaluation methods are defined up front, while SBD supports the parallel evaluation of multiple candidates to avoid premature convergence. A parametric parent-hull model enables this integration by applying proportional scaling for efficiency while introducing targeted parametric variation to expose nonlinear behaviours systematically. This ensures that key performance trade-offs are identified early and that optimisation in OPV design is both efficient and robust.

3. **"*What is the current state-of-the-art in design optimisation frameworks for early-stage ship design, and based on this, what are the requirements for a Multi-Objective Optimisation (MOO)-based decision-making framework suitable for OPV scaling?*"**

   Early-stage ship design is characterised by incomplete information: detailed data on weight distribution, arrangement, and subsystems are not yet available. Optimisation under such uncertainty requires broad exploration of the design space, since focusing on one objective or variable at a time risks converging to local or sub-optimal solutions. Contemporary frameworks therefore treat early-stage design as a multi-objective exploration problem, supported by parametric modelling, systematic Design of Experiments, surrogate modelling, Pareto-based optimisation, and convergence monitoring. Building on these insights, the framework developed in this thesis links mission requirements directly to objectives and constraints, explores nonlinear parameter interactions through a hybrid SE–SBD setup, employs DoE and surrogate-assisted optimisation for computational tractability, filters infeasible candidates early, and visualises Pareto fronts to support trade-off decisions. In this

way, it fully meets the requirements for an OPV-specific, MOO-based decision-support framework.

4. **"*What components are required for the proposed framework, and how can the setup be structured to support early-stage OPV design?*"**

   The proposed framework supports early-stage OPV design by enabling both the rapid generation of candidate designs and the rapid evaluation of those candidates within a multi-objective context. It is built from three integrated components: parametric modelling, performance evaluation, and multi-objective optimisation. The framework operates on four main inputs: the parent hull as the geometric baseline, hull variables defined through a parametric model, operational conditions (sea states, headings, and speeds), and mission requirements (motion limits and minimum range). Objectives correspond directly to the key design drivers—SKI, SI, R_T, and LWT—while constraints ensure feasibility of the design space through static stability bounds, dynamic roll-period limits, and displacement consistency. These elements are embedded within a multi-objective optimisation algorithm, implemented as a surrogate-based global optimisation (SBGO) flow with a MOGA core. The parametric model enables candidate generation, the evaluation module provides consistent performance indicators, and the optimisation envelope integrates constraint filtering, surrogate modelling, and Pareto analysis. Structurally, the setup follows a sequential–parallel logic: sequential in defining mission-driven objectives and constraints (Systems Engineering), and parallel in evaluating broad candidate sets (Set-Based Design). The use of a parent hull with geometric scaling provides rapid variation, while targeted parametric scaling of selected dimensions enables systematic exploration and reduces the risk of converging to local optima.

5. **"*How can the effectiveness of an integrated scaling and mission-oriented MOO framework be verified and validated to ensure robust and reliable early-stage OPV design decisions?*"**

   For such a framework to be considered effective and reliable, it is validated against high-fidelity external reference data and verified through internal consistency checks. In this thesis, validation began with the parent hull, which was compared against available reference data, including towing tank resistance tests, seakeeping RAOs, and intact stability booklets. Demonstrating close agreement confirmed that the parametric reconstruction and evaluation methods provide a credible baseline. Verification was carried out by showing that the optimisation process converges and reproduces established naval-architectural behaviour through trend analysis. Hypervolume monitoring plateaued after approximately 25 iterations, confirming stable convergence, while trend analysis reproduced known relationships: length reducing Froude number and resistance while improving seakeeping, beam enhancing stability at the cost of seakeeping, and draft improving stability while increasing resistance. Application across the $40 \leq L_{OA} \leq 60$ m range further demonstrated that the framework could identify feasible variants satisfying IMO stability requirements while improving mission-oriented criteria such as range and comfort. Through validation of the parent hull against high-fidelity data and verification via convergence and trend analysis, the framework is shown to be a robust and reliable decision-support tool for early-stage OPV design.

8.2. Main Research Question

How can scaling and mission-oriented Multi-Objective Optimisation (MOO) be integrated into an early-stage design framework that addresses the nonlinear effects of scaling, enhances operational flexibility, and performance of multipurpose OPVs?

A design framework has been developed to support naval architects in the concept design of OPVs. The framework integrates scaling methods with multi-objective optimisation in order to quickly generate and evaluate a large number of design variants. Using a parent hull as the baseline, geometric scaling provides rapid variation, while targeted parametric scaling exposes nonlinear effects by adjusting principal dimensions. These variants are assessed against mission-oriented objectives—resistance, stability, seakeeping, and lightweight as a proxy for cost—within a constraint-driven optimisation environment. The resulting Pareto frontiers make explicit the trade-offs between competing requirements such as endurance, stability, and comfort.

In the validation and verification studies, the added value of the framework became clear. Validation against towing tank data, seakeeping RAOs, and intact stability booklets showed that the reconstructed parent hull and evaluation methods reproduce external reference data with sufficient accuracy for early-stage use. Verification through optimisation test cases confirmed both convergence and consistency with established naval-architectural trends: length reducing resistance and improving seakeeping, beam improving stability but penalising motions, and draft enhancing stability at the cost of resistance.

By achieving the above, the framework allows the naval architect to rapidly explore the design space and identify optimal trade-offs under realistic mission constraints. In the OPV case study, the framework evaluated 465 candidate designs, of which 137 formed the Pareto-optimal set. These solutions demonstrated how conflicting drivers could be balanced—for instance, by satisfying IMO stability requirements while improving range and seakeeping.

To conclude, the developed framework enables scaling and mission-oriented MOO to be effectively integrated into early-stage OPV design. It is able to reveal nonlinear interactions, ensure feasibility through constraint filtering, and provide transparent decision support via Pareto analysis. In doing so, it offers naval architects a robust and practical tool to guide OPV design under diverse and conflicting mission requirements.

8.3. Contributions

This thesis advances early-stage OPV design research by providing the following contributions:

1. Developed and demonstrated a new framework that integrates hybrid scaling with mission-oriented MOO, tailored specifically to multipurpose OPVs. The framework uniquely combines seakeeping, stability, resistance, and lightweight objectives, allowing nonlinear effects, mission constraints, and operational trade-offs to be systematically addressed in early-stage naval design.

2. Extended the application of the SKI by incorporating it as an explicit optimisation objective, combining multiple wave headings into a single metric and demonstrating its effectiveness in balancing motions against resistance, stability, and weight during OPV scaling studies.
3. Introduced the SI as an optimisation objective, based on IMO intact stability criteria, enabling stability to be treated directly as a performance driver in early-stage optimisation rather than only as a feasibility check.
4. Demonstrated that using the roll period (T_{roll}) as a dynamic stability criterion is more effective than relying solely on static GM/B limits, ensuring that overly stiff designs are constrained in a way that reflects operational realism.
5. Incorporated range as a constraint, ensuring that all feasible designs satisfy a minimum endurance requirement and remain operationally relevant.
6. Confirmed that maintaining $GM/B > 0.05$ is consistent with IMO intact stability requirements, validating its use as a lower-bound constraint in early-stage design studies.

8.4. Recommendations and Future Research

Building on the contributions of this thesis, the following recommendations are proposed to guide both the practical application and further development of the framework:

1. Building on the demonstration that T_{roll} is a more effective constraint than static GM/B limits, future frameworks should incorporate dynamic stability criteria alongside static margins to avoid overly stiff designs and ensure realistic motion behaviour.
2. Extending the use of Pareto frontiers in this work, designers are encouraged to adopt Pareto visualisation as a decision-support tool for balancing endurance, comfort, and stability under conflicting mission requirements.
3. To strengthen the validation established against towing tank and seakeeping data, future work should incorporate additional high-fidelity analyses (e.g. CFD simulations, seakeeping model tests) to further enhance the accuracy and credibility of the framework.
4. Building on the observed influence of L/B and B/T ratios in shaping performance, future studies should extend the investigated ranges—particularly at the lower bound of L/B—to broaden the design space and capture a wider spectrum of feasible OPV hull forms.
5. As this thesis treated freeboard only indirectly, introducing freeboard as a bounded design variable would allow its influence on SKI and DWT to be captured more explicitly.
6. To refine LWT estimates beyond the proxy used here, additional data points and empirical methods should be incorporated to improve predictive reliability.
7. Building on the use of the SI as an explicit optimisation objective, KG should be included as a design variable to better capture its influence on intact stability and roll behaviour.

8. The optimisation objectives can be expanded to include additional performance aspects such as manoeuvrability and damaged stability, extending the framework beyond the current scope of intact seakeeping and stability.
9. To complement the deterministic approach in this thesis, future studies should incorporate uncertainty quantification to account for variability in input parameters and improve the robustness of optimisation outcomes.
10. Sensitivity studies on coefficient variation within narrow parameter ranges should be conducted to clarify their local influence, complementing the global trends identified in this work.
11. The SI, introduced here as an objective, can be further refined to target minimum or moderate values, balancing stability with other performance drivers.
12. Finally, extending the parametric model to include superstructure effects would allow the framework to capture additional stability-related criteria, such as significant wave crest (SWC) compliance.

8.5. Conclusion

This thesis set out to integrate scaling and mission-oriented multi-objective optimisation (MOO) into an early-stage design framework for multipurpose OPVs. The work has demonstrated that this integration is feasible and effective when built around a hybrid Systems Engineering and Set-Based Design (SE–SBD) approach. By combining geometric scaling for rapid variation with targeted parametric scaling for nonlinear sensitivity, and embedding these within a constraint-driven optimisation process, the framework provides a systematic means of exploring the OPV design space.

The results showed that key performance trade-offs—between resistance, stability, seakeeping, and lightweight—can be captured explicitly in Pareto frontiers, supporting transparent decision making under conflicting mission requirements. Novel contributions included the use of the SKI across multiple headings as an optimisation objective, the introduction of the SI alongside dynamic roll-period constraints, and the incorporation of range as a feasibility requirement. Verification confirmed convergence and consistency with established naval-architectural trends, while validation against high-fidelity reference data established that the parent hull and evaluation models provide sufficient accuracy for early-stage application.

In doing so, the thesis advances OPV design research by demonstrating a practical decision-support tool that is both computationally efficient and operationally relevant. The framework enables naval architects to rapidly generate, evaluate, and compare feasible design alternatives, offering clear insights into the trade-offs that govern OPV performance. While the study was limited to a specific hull baseline and a selected set of objectives and constraints, the results provide a foundation for future research to expand the design space, refine the models, and incorporate additional performance aspects.

8.6. Personal Reflection

This thesis concludes a two-year adventure at TU Delft. Looking back on the research process, there are several aspects I would approach differently if given the opportunity.

First, closer communication with a shipyard or client would have been valuable in order to better understand practical constraints, demands, and objectives. Early alignment with stakeholders could have ensured that the framework reflected not only academic rigor but also industrial applicability.

Second, the choice of parameters and variables deserves reconsideration. While global optimisation of ship size with respect to length, beam, and draft is a useful starting point, it should be coupled with complementary factors such as GM, structural considerations, and freeboard. These influence not only stability but also seakeeping, weight, and range, and therefore directly affect design trade-offs.

From an optimisation perspective, the process would have benefited from using normalised variance for both variables and objectives from the outset. This would have improved comparability between objectives and avoided biases in Pareto-front convergence. In hindsight, the use of the Stability Index as a separate optimisation objective was redundant. It did not provide significant additional insight beyond its role as a regulatory constraint. Interestingly, lower Stability Index values often corresponded to improved seakeeping and reduced resistance, while still maintaining compliant roll behaviour and damping.

Another lesson learned concerns the treatment of roll. Roll behaviour is strongly affected by appendages such as bilge keels and stabilisers, as well as by the internal arrangement of the ship. For this reason, the optimisation of roll-related criteria in an early-stage framework has inherent limitations unless these factors are explicitly modelled.

Finally, I recognise that a more realistic strategy would have been to segment the design study into narrower size ranges—for example 40–60 m, 60–80 m, and 80–90 m. This would have yielded results more precise to each operational scale and more reflective of the practical decisions faced by designers.

In summary, this reflection highlights both the strengths of the framework developed in this thesis and the areas where it could be refined. These insights form a valuable foundation for future research, bridging the gap between academic methods and the realities of OPV design practice.

References

[1] European Security & Defence. “Offshore Patrol Vessels: The Swiss Army Knife of Modern Navies”. In: *European Security & Defence* (2023). Accessed on November 28, 2024. url: https://euro-sd.com/2023/10/articles/34029/offshore-patrol-vessels-the-swiss-army-knife-of-modern-navies/.

[2] Steven H. Cohen et al. “CONCEPTUAL DESIGN OF AN OFFSHORE PATROL BOAT”. en. In: *Naval Engineers Journal* 99.1 (Jan. 1987), pp. 70–82. doi: 10.1111/j.1559-3584.1987.tb01397.x. url: https://onlinelibrary.wiley.com/doi/10.1111/j.1559-3584.1987.tb01397.x (visited on 12/13/2024).

[3] Andrija Ljulj et al. “Multi-attribute concept design procedure of a generic naval vessel”. en. In: *Alexandria Engineering Journal* 59.3 (June 2020), pp. 1725–1734. doi: 10.1016/j.aej.2020.04.038. url: https://linkinghub.elsevier.com/retrieve/pii/S111001682030199X (visited on 02/10/2025).

[4] Paul T Schmitz. “A seakeeping performance and affordability tradeoff study for the Coast Guard Offshore Patrol Cutter”. en. Master’s thesis. Monterey, California: Naval Postgraduate School, June 2016. url: chrome-extension://efaidnbmnnnibpcajpcglclefindmkaj/https://core.ac.uk/download/pdf/45464727.pdf.

[5] David Andrews. “The expanding scope of ship design practice”. en. In: *International Marine Design Conference* (May 2024). doi: 10.59490/imdc.2024.905. url: https://proceedings.open.tudelft.nl/imdc24/article/view/905 (visited on 02/12/2025).

[6] Apostolos D. Papanikolaou. “Holistic Approach to Ship Design”. en. In: *Journal of Marine Science and Engineering* 10.11 (Nov. 2022), p. 1717. doi: 10.3390/jmse10111717. url: https://www.mdpi.com/2077-1312/10/11/1717 (visited on 02/19/2025).

[7] Onur Yurdakul et al. “A decision-making process for the selection of better ship main dimensions by a Pareto frontier solution”. en. In: *Ocean Engineering* 239 (Nov. 2021), p. 109908. doi: 10.1016/j.oceaneng.2021.109908. url: https://linkinghub.elsevier.com/retrieve/pii/S0029801821012555 (visited on 02/18/2025).

[8] David Winyall et al. “3D Hullform Modeling to Support Naval Ship Design Synthesis and Multi-Objective Optimization”. en. In: ().

[9] R. de Winter. “Efficient constraint multi-objective optimization with applications in ship design”. en. PhD thesis. Leiden University, Oct. 2024. url: https://hdl.handle.net/1887/4094606 (visited on 03/26/2025).

[10] *Israel Shipyards - Experience that empowers seagoing ventures worldwide*. url: https://www.israel-shipyards.com/naval-001.asp (visited on 02/10/2025).

[11] Andrija Ljulj et al. “Concept Design of a Hybrid Offshore Patrol Vessel”. en. In: *Journal of Marine Science and Engineering* 11.1 (Dec. 2022), p. 12. doi: 10.3390/jmse11010012. url: https://www.mdpi.com/2077-1312/11/1/12 (visited on 12/13/2024).

[12] Eddy Setyo Koenhardono et al. “Comparative of Feasibility Study Between Diesel Mechanical Propulsion System and Combination of Diesel Engine and Electric Motor Propulsion System on Offshore Patrol Vessel (OPV) 80 m”. en. In: *MATEC Web of Conferences* 177 (2018). Ed. by Suntoyo et al., p. 01011. doi: 10.1051/matecconf/201817701011. url: https://www.matec-conferences.org/10.1051/matecconf/201817701011 (visited on 03/06/2025).

[13] *Offshore Patrol Vessel*. en. url: https://www.baesystems.com/en/product/offshore-patrol-vessels (visited on 02/10/2025).

[14] *OPV ship, supply boats and research vessels*. en-US. url: https://www.kership.com/en/ships/ (visited on 02/10/2025).

[15] *ARES SHIPYARD - Vessels*. url: https://ares.global/vessels/patrol (visited on 02/10/2025).

[16] Corresponding Author. *Standard Design of Patrol Boats to Facilitate Maritime Surveillance Based on Analytical Hierarchy Process and Regression Linear*. Tech. rep. 1. 2023, pp. 2796–2807.

[17] Andy Kimber. “Designing for the Gap: The space between the OPV and the Frigate”. en. In: *Ciencia y tecnología de buques* 8.17 (July 2015), p. 19. doi: 10.25043/19098642.118. url: https://www.shipjournal.co/index.php/sst/article/view/118 (visited on 12/13/2024).

[18] Myung-Il Roh et al. *Computational Ship Design*. en. Singapore: Springer Singapore, 2018. doi: 10.1007/978-981-10-4885-2. url: http://link.springer.com/10.1007/978-981-10-4885-2 (visited on 02/26/2025).

[19] P D H Bronkhorst. “Enhancing offshore service vessel concept design by involving seakeeping”. en. In: ().

[20] Mustafa Kara. “A tool for evaluating the early-stage design of corvettes”. PhD thesis. June 2010.

[21] “Chapter 3 - Flotation and stability”. In: *The Maritime Engineering Reference Book*. Ed. by Anthony F. Molland. Oxford: Butterworth-Heinemann, Jan. 2008, pp. 75–115. doi: 10.1016/B978-0-7506-8987-8.00003-2. url: https://www.sciencedirect.com/science/article/pii/B9780750689878000032 (visited on 02/28/2025).

[22] Alan Brown et al. “Multiple□Objective Optimization in Naval Ship Design”. en. In: *Naval Engineers Journal* 115.4 (Oct. 2003), pp. 49–62. doi: 10.1111/j.1559-3584.2003.tb00242.x. url: https://onlinelibrary.wiley.com/doi/10.1111/j.1559-3584.2003.tb00242.x (visited on 12/13/2024).

[23] Anthony F. Molland et al. *Ship Resistance and Propulsion*. en. Google-Books-ID: rAAtDwAAQBAJ. Cambridge University Press, Aug. 2017.

[24] Daniele Peri. “Direct Tracking of the Pareto Front of a Multi-Objective Optimization Problem”. en. In: *Journal of Marine Science and Engineering* 8.9 (Sept. 2020), p. 699. doi: 10.3390/jmse8090699. url: https://www.mdpi.com/2077-1312/8/9/699 (visited on 02/18/2025).

[25] Wesley Wilson et al. “Hull form optimization for early stage ship design”. In: *Naval Engineers Journal* 122.2 (June 2010), pp. 53–65. doi: 10.1111/j.1559-3584.2010.00268.x.

[26] George Gougoulidis. *Energy-saving Measures for Naval Operations*. June 2015.

[27] I Lee et al. *Specialist Committee on Energy Saving Methods: Final Report and Recommendations to the 29th ITTC: Energy Saving Methods*. Tech. rep. 29th ITTC. International Towing Tank Conference (ITTC), 2021. url: https://ittc.info/media/10940/volume-ii.pdf.

[28] *Emission Standards: IMO Marine Engine Regulations*. url: https://dieselnet.com/standards/inter/imo.php (visited on 03/15/2025).

[29] *Navy Marine Emission Control Systems Market Size, 2024-2032*. en. url: https://www.gminsights.com/industry-analysis/navy-marine-emission-control-systems-market (visited on 03/26/2025).

[30] Martin Gutsch et al. “Operability robustness index as seakeeping performance criterion for offshore vessels”. en. In: *Ocean Engineering* 217 (Dec. 2020), p. 107931. doi: 10.1016/j.oceaneng.2020.107931. url: https://linkinghub.elsevier.com/retrieve/pii/S0029801820308878 (visited on 02/10/2025).

[31] Apostolos Papanikolaou. *Ship Design: Methodologies of Preliminary Design*. en. Dordrecht: Springer Netherlands, 2014. doi: 10.1007/978-94-017-8751-2. url: https://link.springer.com/10.1007/978-94-017-8751-2 (visited on 01/16/2025).

[32] Marion Zu et al. “Seakeeping criteria revisited”. en. In: *Ocean Engineering* 297 (Apr. 2024), p. 116785. doi: 10.1016/j.oceaneng.2024.116785. url: https://linkinghub.elsevier.com/retrieve/pii/S0029801824001227 (visited on 01/10/2025).

[33] *International Maritime Organization (IMO) -Ship Design and Stability*. url: https://www.imo.org/en/OurWork/Safety/Pages/ShipDesignAndStability-default.aspx (visited on 05/13/2025).

[34] P. Gualeni et al. “Parametric formulation of the floodable length curve: Application case to offshore patrol vessels”. In: *Transactions of the Royal Institution of Naval Architects Part A: International Journal of Maritime Engineering* 162 (Mar. 2020), A65–A73. doi: 10.3940/rina.ijme.2020.a1.582.

[35] Tri Rahmaji et al. “Design of Fast Patrol Boat for Improving Resistance, Stability, and Seakeeping Performance”. en. In: *Designs* 6.6 (Nov. 2022), p. 105. doi: 10.3390/designs6060105. url: https://www.mdpi.com/2411-9660/6/6/105 (visited on 03/17/2025).

[36] Daniel Savitsky. “Hydrodynamic Design of Planing Hulls”. In: *Marine Technology and SNAME News* 1.04 (Oct. 1964), pp. 71–95. doi: 10.5957/mt1.1964.1.4.71. url: https://doi.org/10.5957/mt1.1964.1.4.71 (visited on 09/10/2025).

[37] A E de Gaaij. “Applying parametric optimisation in the concept exploration phase on naval support vessels”. en. In: ().

[38] *Software | MARIN*. url: https://www.marin.nl/about/facilities-and-tools/software (visited on 09/10/2025).

[39] J. Holtrop et al. “An approximate power prediction method”. en. In: *International Shipbuilding Progress* 29.335 (July 1982), pp. 166–170. doi: 10.3233/ISP-1982-2933501. url: https://journals.sagepub.com/doi/full/10.3233/ISP-1982-2933501 (visited on 02/28/2025).

[40] *About Dakota*. en-US. url: https://dakota.sandia.gov/about-dakota/ (visited on 04/01/2025).

[41] Donald Macpherson et al. *Real Cost Savings for a Waterjet-driven Patrol Craft Design Using a CAESES-NavCad Coupled Solution*. Tech. rep.

[42] Ebru Sariöz. “Minimum ship size for seakeeping”. In: *Proceedings of the Institution of Mechanical Engineers Part M: Journal of Engineering for the Maritime Environment* 226.3 (Aug. 2012), pp. 214–221. doi: 10.1177/1475090212440068.

[43] W. R. Mccreight. “Estimating the Seakeeping Qualities of Destroyer Type Hulls.” en. In: (Jan. 1984). Number: DTNSRDCSPD107401. url: https://apps.dtic.mil/sti/html/tr/ADA139089/ (visited on 09/11/2025).

[44] A. I. Ginnis et al. “A CATIA® ship-parametric model for isogeometric hull optimization with respect to wave resistance”. In: *RINA, Royal Institution of Naval Architects - International Conference on Computer Applications in Shipbuilding 2011, Papers*. Vol. 1. 2011, pp. 9–20. doi: 10.3940/rina.iccas.2011.02.

[45] Angga Sifta Pratama et al. “FAST PATROL BOAT HULL DESIGN CONCEPTS ON HYDRODYNAMIC PERFORMANCES AND SURVIVABILITY EVALUATION”. In: *Journal of Applied Engineering Science* 21.2 (2023), pp. 501–531. doi: 10.5937/jaes0-40698.

[46] Thomas Scholcz et al. *Surrogate-Based Multi-Objective Optimisation for Powering and Seakeeping*. Sept. 2019.

[47] Ubaldo La Monaca et al. “Integrated ship design: an innovative methodological approach enabled by new generation computer tools”. en. In: *International Journal on Interactive Design and Manufacturing*

(IJIDeM) 14.1 (Mar. 2020), pp. 59–76. doi: 10.1007/s12008-019-00612-4. url: http://link.springer.com/10.1007/s12008-019-00612-4 (visited on 02/10/2025).

[48] "Chapter 5 - Powering". In: *The Maritime Engineering Reference Book*. Ed. by Anthony F. Molland. Oxford: Butterworth-Heinemann, Jan. 2008, pp. 181–343. doi: 10.1016/B978-0-7506-8987-8.00005-6. url: https://www.sciencedirect.com/science/article/pii/B9780750689878000056 (visited on 04/03/2025).

[49] Ph Rigo. "Optimization of Ship Structures". en. In: ().

[50] Stein Erikstad et al. *Design Methodology State-of-the-Art Report*. June 2022. doi: 10.5957/IMDC-2022-301.

[51] Mattia Bottero et al. "Systems Engineering for Naval Ship Design Evolution". en. In: *Journal of Marine Science and Engineering* 12.2 (Feb. 2024). Number: 2 Publisher: Multidisciplinary Digital Publishing Institute, p. 210. doi: 10.3390/jmse12020210. url: https://www.mdpi.com/2077-1312/12/2/210 (visited on 03/18/2025).

[52] David Singer et al. "What Is Set□Based Design?" In: *Naval Engineers Journal* 121 (Oct. 2009), pp. 31–43. doi: 10.1111/j.1559-3584.2009.00226.x.

[53] Stefan Harries et al. "Speed-Power Optimized AUV Design by Coupling CAESES and NavCad". en. In: ().

[54] Francisco Pérez-Arribas. "Parametric Generation of Small Ship Hulls with CAD Software". In: *Journal of Marine Science and Engineering* 11.5 (May 2023). doi: 10.3390/jmse11050976.

[55] Miguel Ángel Guerrero Sanchez et al. "Conceptual design of coastal patrol vessel (CPV) with flight deck for the reception and deployment of helicopter". en. In: *Ciencia y tecnología de buques* 14.28 (Jan. 2021), pp. 43–52. doi: 10.25043/19098642.214. url: https://shipjournal.co/index.php/sst/article/view/214 (visited on 01/16/2025).

[56] Noah J. Bagazinski et al. "ShipGen: A Diffusion Model for Parametric Ship Hull Generation with Multiple Objectives and Constraints". en. In: *Journal of Marine Science and Engineering* 11.12 (Nov. 2023), p. 2215. doi: 10.3390/jmse11122215. url: https://www.mdpi.com/2077-1312/11/12/2215 (visited on 03/22/2025).

[57] Gregory J. Grigoropoulos. "Hull Form Optimization for Hydrodynamic Performance". en. In: *Marine Technology and SNAME News* 41.04 (Oct. 2004), pp. 167–182. doi: 10.5957/mt1.2004.41.4.167. url: https://onepetro.org/MTSN/article/41/04/167/176139/Hull-Form-Optimization-for-Hydrodynamic (visited on 03/24/2025).

[58] Qian Chen et al. "Design and Optimization of Mini Underwater Robot Based on ANSYS and CAESES". en. In: *2018 2nd International Conference on Robotics and Automation Sciences (ICRAS)*. Wuhan:

IEEE, June 2018, pp. 1–5. doi: 10.1109/ICRAS.2018.8442417. url: https://ieeexplore.ieee.org/document/8442417/ (visited on 02/18/2025).

[59] Iacopo Biliotti et al. “Automatic Parametric Hull Form Optimization of Fast Naval Vessels”. en. In: (2011).

[60] Shahroz Khan et al. “A novel design framework for generation and parametric modification of yacht hull surfaces”. In: *Ocean Engineering* 136 (2017), pp. 243–259. doi: 10.1016/j.oceaneng.2017.03.013.

[61] T. Katsoulis et al. “A T-splines-based parametric modeller for computer-aided ship design”. In: *Ocean Engineering* 191 (Nov. 2019), p. 106433. doi: 10.1016/j.oceaneng.2019.106433. url: https://www.sciencedirect.com/science/article/pii/S0029801819305815 (visited on 03/24/2025).

[62] Soonhung Han et al. “Hydrodynamic hull form optimization using parametric models”. In: *Journal of Marine Science and Technology* 17 (Mar. 2012). doi: 10.1007/s00773-011-0148-8.

[63] Hui Zhou et al. “NURBS-Based Parametric Design for Ship Hull Form”. en. In: *Journal of Marine Science and Engineering* 10.5 (May 2022). Number: 5 Publisher: Multidisciplinary Digital Publishing Institute, p. 686. doi: 10.3390/jmse10050686. url: https://www.mdpi.com/2077-1312/10/5/686 (visited on 03/24/2025).

[64] J. H. Ang et al. “Hull form design optimisation for improved efficiency and hydrodynamic performance of ’ship-shaped’ offshore vessels”. In: *RINA, Royal Institution of Naval Architects - International Conference on Computer Applications in Shipbuilding 2015, ICCAS 2015 - Papers*. Vol. 2. Royal Institution of Naval Architects, 2015, pp. 71–80. doi: 10.3940/rina.iccas.2015.42.

[65] Roko Dejhalla et al. “Application of Genetic Algorithm for Ship Hull Form Optimization”. en. In: ().

[66] J. B. A. Maartens. “Hull Generation for Fast Concept Exploration”. en. In: (2020). url: https://repository.tudelft.nl/record/uuid:5718cb90-54b3-4a99-b46b-feca00c385ec (visited on 03/24/2025).

[67] Apostolos Papanikolaou. “Holistic ship design optimization”. en. In: *Computer-Aided Design* 42.11 (Nov. 2010), pp. 1028–1044. doi: 10.1016/j.cad.2009.07.002. url: https://linkinghub.elsevier.com/retrieve/pii/S0010448509001973 (visited on 12/13/2024).

[68] Marissa Renardy et al. “To Sobol or not to Sobol? The effects of sampling schemes in systems biology applications”. In: *Mathematical Biosciences* 337 (July 2021), p. 108593. doi: 10.1016/j.mbs.2021.108593. url: https://www.sciencedirect.com/science/article/pii/S0025556421000419 (visited on 03/28/2025).

[69] Brian M Adams et al. “Dakota, A Multilevel Parallel Object-Oriented Framework for Design Optimization, Parameter Estimation, Uncertainty Quantification, and Sensitivity Analysis: Version 6.16 User’s Manual”. en. In: (2022).

[70] Abdullah Konak. “Multi-objective optimization using genetic algorithms: A tutorial”. en. In: *Reliability Engineering & System Safety* (Jan. 2006). url: https://www.academia.edu/87135364/Multi_objective_optimization_using_genetic_algorithms_A_tutorial (visited on 04/11/2025).

[71] Abhishekkumar Shingala et al. “Genetic Optimisation of a Free-Stream Water Wheel Using 2D Computational Fluid Dynamics Simulations Points towards Design with Fully Immersed Blades”. en. In: *Energies* 15.10 (Jan. 2022). Number: 10 Publisher: Multidisciplinary Digital Publishing Institute, p. 3723. doi: 10.3390/en15103723. url: https://www.mdpi.com/1996-1073/15/10/3723 (visited on 04/11/2025).

[72] Nanda Yustina et al. “Surrogate Model-based Multi-Objective Optimization in Early Stages of Ship Design”. en. In: *Jurnal RESTI (Rekayasa Sistem dan Teknologi Informasi)* 6.5 (Oct. 2022), pp. 782–789. doi: 10.29207/resti.v6i5.4248. url: http://jurnal.iaii.or.id/index.php/RESTI/article/view/4248 (visited on 12/13/2024).

[73] Nir Almany. “Ship and Structural Design and Analysis of Offshore Patrol Vessel”. en. In: ().

[74] *MAN (2023) MAN 51/60DF Project Guide -Marine Four-stroke dual fuel engine compliant with IMO Tier II/IMO Tier III*. url: https://%20manes.%20com/%20appli%20catio%20ns/%20proje%20ctgui%20des/%204stro%20ke/%20Propu%20lsion/%20PG_P-II_%205160DF.%20pdf.

[75] Daniel Demko. “Tools for Multi-Objective and Multi-Disciplinary Optimization in Naval Ship Design”. en. In: ().

[76] *02 IS-Code Code on Intact Stability by IMO instruments - Netherlands Regulatory Framework (NeRF) – Maritime*. url: https://puc.overheid.nl/nsi/doc/PUC_3005_14/2/ (visited on 04/14/2025).

[77] M. Tello et al. “Seakeeping performance of fishing vessels in irregular waves”. In: *Ocean Engineering* 38.5 (Apr. 2011), pp. 763–773. doi: 10.1016/j.oceaneng.2010.12.020. url: https://www.sciencedirect.com/science/article/pii/S0029801811000060 (visited on 04/15/2025).

[78] Youngrong Kim et al. “A novel method for estimating missing values in ship principal data”. In: *Ocean Engineering* 251 (May 2022), p. 110979. doi: 10.1016/j.oceaneng.2022.110979.

[79] C.R. et al. Harris. “Array programming with NumPy”. In: *Nature* (2020).

[80] W. McKinney. “Data structures for statistical computing in Python”. In: *Proc. SciPy*. 2010.

[81] J.D. Hunter. “Matplotlib: A 2D graphics environment”. In: *CSE* (2007).

[82] M.L. Waskom. “Seaborn: statistical data visualization”. In: *JOSS* (2021).

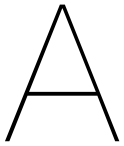

Overview of existing OPVs designs

Table A.1: Overview of existing OPVs designs [10, 13, 14, 15]

Shipyard	Vessel Name	Length (m)	Beam (m)	Draft (m)	max speed (knots)	Range (nm)	Displacement (tons)	Endurance (days)	power (kW)
ARES	ARES 51 OPV	51	9	2.5	22	3,000	270	10	2,240
ARES	ARES 55 OPV	55	9.5	2.7	23	3,500	340	12	2,500
ARES	ARES 66 OPV	66	10	3	24	4,000	400	14	3,000
ARES	ARES 72 OPV	72	11	3.5	25	4,500	450	15	3,500
ARES	ARES 160 SAR	48	8.8	2.4	22	2,800	250	8	1,800
ARES	ARES 150 BOLD	56	10	3	24	3,800	350	12	2,800
BAE	OPV 90	90	13	4	24	5,500	2,000	35	7,000
Austal	Patrol 58	58	11	3	25	4,000	350	21	4,500
Austal	Patrol 56	56	10	2.9	26	3,800	340	20	4,200
Damen	Stan Patrol 4207	43	7.1	2.4	26	1,800	240	7	4,100
Damen	Stan Patrol 5009	50	9.4	2.8	25	3,000	400	10	5,000
Damen	Stan Patrol 5509	55	9	2.7	26	3,500	450	12	5,200
Damen	Stan Patrol 6211	62	11	3.3	23	4,000	500	14	6,000
Damen	OPV 1400 Coast Guard	72	11	3.5	22	5,000	1,400	21	7,200
Damen	OPV 1800 Coast Guard	83	14	4	21	6,000	1,800	30	8,500
Damen	OPV 2200 Military	92	14	4.2	22	7,000	2,200	30	9,000
Damen	OPV 2400 Coast Guard	98	15	4.5	22	8,000	2,400	35	9,500
KERSHIP	OPV 45	46	8.4	3	22	3,200	270	10	2,500
KERSHIP	OPV 52 CG	52	9	3.2	22	3,500	440	12	3,000
KERSHIP	OPV 85 CG	84	14	4	24	8,000	1,750	35	6,000
KERSHIP	OPV 60	62	9.5	3.6	23	5,000	620	21	3,500
KERSHIP	OPV 70	65	11	3.8	24	5,000	870	21	4,000
KERSHIP	OPV 90	92	15	4.2	25	8,000	2,200	30	6,500

Shipyard	Vessel Name	Length (m)	Beam (m)	Draft (m)	max speed (knots)	Range (nm)	Displacement (tons)	Endurance (days)	power (kW)
VARD	VARD 7 043	43	8.5	2.8	24	2,500	450	10	3,200
VARD	VARD 7 055	55	10	3.2	25	3,500	600	12	3,800
VARD	VARD 7 072	72	12	3.6	24	4,500	900	14	4,500
VARD	VARD 7 080	80	12	4	24	5,000	1,200	15	5,000
VARD	VARD 7 085	85	14	4.2	23	5,500	1,500	20	5,500
VARD	VARD 7 090	90	14	4.5	22	6,000	1,800	25	6,000
DEARSAN	Tuzla Class 57m	57	9.4	2.7	25	3,000	400	10	3,500
DEARSAN	HSV 58	58	10	2.9	24	2,500	450	12	4,000
DEARSAN	MPOSV 72	72	13	3.5	23	4,500	850	14	5,000
DEARSAN	RV 70	70	12	3	22	3,800	700	12	4,200
DEARSAN	HSV 41	41	8.5	2.5	26	2,000	300	8	3,200
DEARSAN	MHV 55	55	9.5	2.8	24	3,200	450	10	3,800
DEARSAN	TS 65	65	11	3.2	22	4,000	500	12	4,500
DEARSAN	FAC 65	65	11	3	28	2,800	480	10	5,000
DEARSAN	C 74 Corvette	74	13	3.6	27	5,500	1,200	15	6,000
DEARSAN	OPV 76	76	13	3.8	24	6,000	1,500	20	5,500
Fincantieri	Musherib Class (OPV)	56	9.2	3	22	3,000	650	15	4,000
Fincantieri	Sars Turkey (OPV)	66	12	3.5	23	4,500	850	20	5,200
Fincantieri	Sirio Class (OPV)	52	10	3.2	21	3,500	700	15	3,800
Fincantieri	Falaj 2 Class (Stealth)	55	9.5	3	28	2,800	600	12	5,000
Fincantieri	Saettia MK2 (IPV)	53	9	2.8	22	3,000	500	12	4,000
Fincantieri	Saettia MK3 (IPV)	54	9.2	3	23	3,200	520	14	4,200
Fincantieri	Saettia MK4 (IPV)	56	9.4	3.2	24	3,500	550	15	4,500

Shipyard	Vessel Name	Length (m)	Beam (m)	Draft (m)	max speed (knots)	Range (nm)	Displacement (tons)	Endurance (days)	power (kW)
Fassmer	CPV 50	50	9.5	2.8	23	3,000	450	12	3,800
Fassmer	OPV 50	50	9.5	3	24	3,200	470	12	4,000
Fassmer	OPV 60	60	11	3.2	24	4,000	600	14	4,500
Fassmer	OPV 70	70	11	3.4	24	4,500	850	15	5,200
Fassmer	OPV 80	80	12	3.8	23	5,000	1,200	20	5,500
Fassmer	OPV 80 S	80	12	3.8	24	5,200	1,250	20	5,800
Fassmer	OPV 80 L	80	13	4	24	5,500	1,300	20	6,000
Fassmer	Fassmer MPV 70	70	12	3.5	22	4,500	900	15	4,800
Fassmer	SAR 46	46	8.8	2.6	22	2,800	400	10	3,500
Fassmer	CPV 40	40	8.5	2.5	25	2,500	350	8	3,200
Fassmer	MPV 70	70	11	3.3	23	4,800	950	16	5,000
Navantia	Avante 300	46	8.6	2.8	21	2,500	380	8	3,200
Navantia	Avante 1400	70	11	3.5	24	4,500	1,400	15	5,500
Navantia	Avante 1800	80	12	3.8	25	6,000	1,800	20	6,000

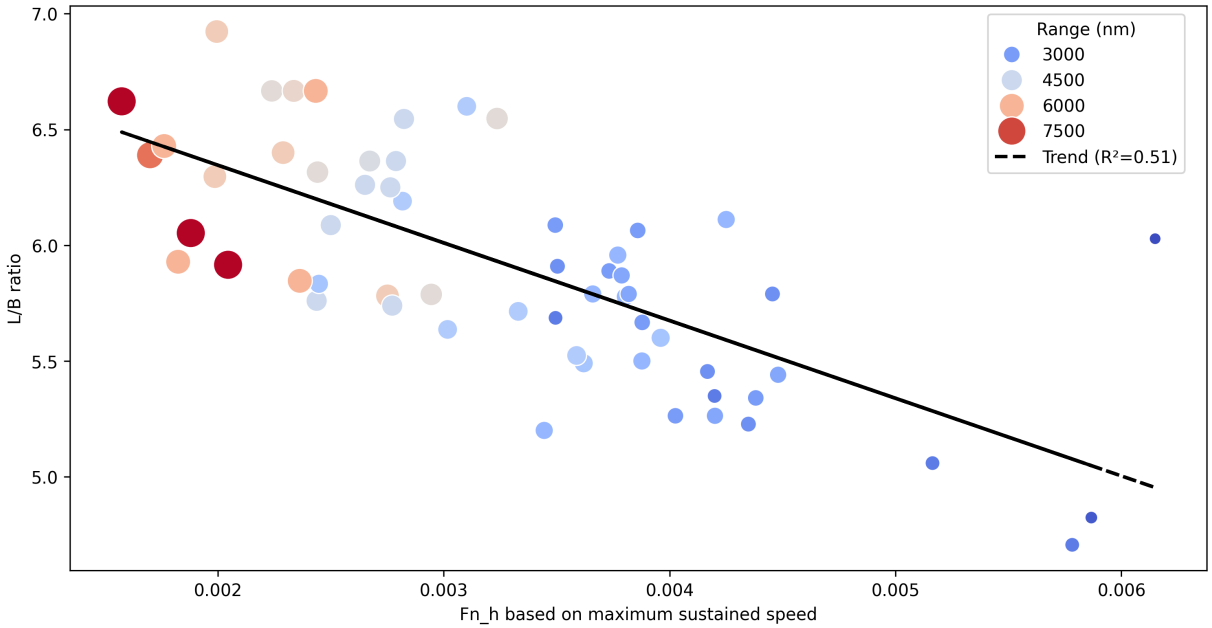

Figure A.1: Length-to-Beam (L/B) ratio versus hull-based Froude number ($F_{n,h}$) calculated at maximum sustained speed.

B

SWBS Groups and LCG, VCG Ratios

SWBS	GROUP	WEIGHT	PERCENT	LCG	LCG/LWL	VCG	VCG/D
100	HULL STRUCTURE	618.9	33.9	38.73	0.498	5.26	0.554
200	PROPULSION PLANT	152.4	8.3	46.48	0.598	3.15	0.332
300	ELECTRIC PLANT	83.4	4.6	44.3	0.570	6.06	0.638
400	COMMAND + SURVEILLANCE	53.5	2.9	36.04	0.464	9.49	0.999
500	AUXILIARY SYSTEMS	210.9	11.5	44.13	0.568	6.35	0.668
600	OUTFIT + FURNISHINGS	157.6	8.6	35.45	0.456	4.65	0.489
700	ARMAMENT	12.9	0.7	36.71	0.472	10.38	1.093
	LIGHTSHIP	1289.6	70.5	40.35	0.519	5.39	0.567
M21	PD MARGIN %2.4	30.95			**KG MARGIN%2.4**	0.12	0.014
M22	CD MARGIN %2.4	30.95			**KG MARGIN%2.4**	0.12	0.014
M11	D&B MARGIN %5.3	68.34			**KG MARGIN%5.3**	0.28	0.030
M23	CON MOD MARGIN %1.4	18.05			**KG MARGIN%1.4**	0.075	0.008
M24	GFM MARGIN %0.6	7.73			**KG MARGIN%0.6**	0.032	0.003
	LIGHTSHIP w/ MARGINS	1445.64	79.4	40.35	0.519	6.04	0.636
F00	FULL LOADS	376.1	20.6	41.24	0.531	3.11	0.327
F10	SHIP FORCE EFFECTS	13		36.53	0.470	6.78	0.714
F20	MISSION RELATED EXPENDABLES	17.9		38.86	0.500	10.02	1.055
F30	SHIP STORES	8.9		41.97	0.540	5.1	0.537
F40	FUELS&LUBRICANTS	280		41.84	0.538	2.25	0.237
F50	LIQUIDS&GASES (NON-FUEL)	56.3		39.97	0.514	4.06	0.427
F60	CARGO	0		0	0.000	0	0.000
	FULL LOAD WEIGHT	1821.74	100	40.54	0.522	5.46	0.575

Figure B.1: WMEC 270 (US Coast Guard Cutter,77 [m]) SWBS Groups and LCG, VCG Ratios [20]

C

Resistance Calculation Code in CAESES

```
// Reynolds number
double Re(Vs * LWL / nu)

// Froude number
double Fn(Vs / pow(g * LWL, 0.5))

// ITTC-1957
double ITTC(0.075 / pow(log(Re) - 2, 2))

// Frictional resistance
double R_F(0.5 * rho * pow(Vs, 2) * S * ITTC)

// --- Wave resistance helpers ---
double B_L(B / LWL)
if (B_L < 0.11)
  double C_7(0.229577 * pow(B_L, 0.33333))
elseif (B_L > 0.25)
  double C_7(0.5 - 0.0625 * B_L)
else
  double C_7(B_L)
endif

double C_1(2223105 * pow(C_7, 3.78613) * pow(T_A / B, 1.07961)
           * pow(90 - i_E, -1.37565))

if (bulb == 1)
```

```
27    double C_3(0.56 * pow(A_BT, 1.5) / (B * T_A * (0.31 * pow(A_BT, 0.5) + T_F - h_B)))
28  else
29    double C_3(0)
30  endif
31
32  double C_2(exp(-1.89 * pow(C_3, 0.5)))
33  double C_5(1 - ((0.8 * A_T) / (B * T_A * C_M)))
34
35  if (1 / B_L < 12)
36    double gamma(1.446 * C_P - 0.03 / B_L)
37  else
38    double gamma(1.446 * C_P - 0.36)
39  endif
40
41  if (C_P < 0.8)
42    double C_16(8.07981 * C_P - 13.8673 * pow(C_P, 2) + 6.984388 * pow(C_P, 3))
43  else
44    double C_16(1.73014 - 0.7067 * C_P)
45  endif
46
47  if (pow(LWL, 3) / dis < 512)
48    double C_15(-1.69385)
49  elseif (pow(LWL, 3) / dis > 1727)
50    double C_15(0)
51  else
52    double C_15(-1.69385 + (LWL / pow(dis, 1.0/3.0) - 8) / 2.36)
53  endif
54
55  double m1(0.0140407 * LWL / T_A
56            - 1.75254 * pow(dis, 1.0/3.0) / LWL
57            - 4.79323 * B / LWL
58            - C_16)
59
60  double m2(C_15 * pow(C_P, 2) * exp(-0.1 * pow(Fn, -2)))
61
62  // Wave resistance
63  double R_W1(C_1 * C_2 * C_5)
64  double R_W2(exp(m1 * pow(Fn, d) + m2 * cos(gamma * pow(Fn, -2))))
65  double R_W(R_W1 * dis * g * rho * R_W2)
66
67  // Transom resistance
```

```
double Fn_T(Vs / pow(2 * g * A_T / (B * B * C_wp), 0.5))
if (Fn_T < 5)
  double C_6(0.2 * (1 - 0.2 * Fn_T))
else
  double C_6(0)
endif
double R_TR(0.5 * rho * pow(Vs, 2) * A_T * C_6)

// Air resistance
double T_F_LWL(T_F / LWL)
if (T_F_LWL < 0.04)
  double C_4(T_F / LWL) // NOTE:      "/"
else
  double C_4(0.04)
endif
double C_A(0.006 * pow(LWL + 100, -0.16) - 0.00205
           + 0.003 * pow(LWL / 7.5, 0.5) * pow(C_b, 4) * C_2 * (0.04 - C_4))
double R_A(0.5 * rho * pow(Vs, 2) * S * C_A)

// --- (1+k) form-factor correction ---
// C_12
double T_L(T_A / LWL)
if (T_L > 0.05)
  double C_12(pow(T_A / LWL, 0.2228446))
elseif (T_L < 0.02)
  double C_12(0.479948)
else
  double C_12(48.2 * pow(T_A / LWL, 2.078) / 0.479948)
endif

double C_13(1 + 0.003 * C_stern)
double L_R((1 - C_P + (0.06 * C_P * LCB) / (4 * C_P - 1)) * LWL)

double k1(0.93 + C_12 * pow(B / L_R, 0.92497))
double k2(pow(0.95 - C_P, -0.521448))
double k3(pow(1 - C_P + 0.0225 * LCB, 0.6906))
double k(C_13 * k1 * k2 * k3)

// Appendage resistance (example)
double R_APP(0.5 * rho * pow(Vs, 2) * S_APP * (1 + k_2) * ITTC)
```

```
109  // Total resistance
110  double R_T(R_F * k + R_W + R_TR + R_A + R_APP)
```

D

Seakeeping Index (SKI) Code (Python)

```python
import pandas as pd
import os
import math
import time
import sys

# === USER SETTINGS ===
excel_file = r"OPV_design.xlsx"
output_csv = r"Single_SKU_Result.csv"
sheets_to_process = ["SS6_180", "SS6_135", "SS6_90", "SS6_45", "SS6_0"]

# Provisional maximums
provisional_max = {
    "Roll (deg)": 6,
    "Pitch (deg)": 4,
    "Vert. acc. (g)": 0.2,
    "Lat. acc. (g)": 0.2,
    "MSI (%)": 40,
    "Deck Wetness (%)": 5,
    "Slamming Probability (%)": 3
}

def compute_provisional_ski(results_dict, provisional_max):
    """Compute SKI and penalties for each component."""
    penalties = {}
    for key, max_value in provisional_max.items():
```

```
        result_value = results_dict.get(key, None)
        if result_value is None or max_value == 0:
            penalties[key.lower()] = 0.0
        else:
            penalties[key.lower()] = round(result_value / max_value, 3)
    ski = 1.0 - sum(penalties.values()) / len(provisional_max)
    ski = round(max(0.0, min(ski, 1.0)), 3)
    return ski, penalties

def process_excel_sheet(sheet_name, excel_path, freeboard, draft, loa, provisional_max):
    """Process one Excel sheet to extract raw values and compute Deck Wetness & Slamming."""
    df = pd.read_excel(excel_path, sheet_name=sheet_name)
    df.columns = df.columns.str.strip().str.lower()
    results = {}

    # Loop through each row
    for _, row in df.iterrows():
        item = str(row["item"]).strip().lower()
        rms = row.get("rms")
        m0_val = row.get("m0")

        # Roll, Pitch, Accelerations, MSI
        if "roll motion" in item and pd.notna(rms):
            results["Roll (deg)"] = rms
        elif "pitch motion" in item and pd.notna(rms):
            results["Pitch (deg)"] = rms
        elif "abs. vert. accel" in item and "bridge" in item and pd.notna(rms):
            results["Vert. acc. (g)"] = rms / 9.81
        elif "lat. (due to roll) accel" in item and "bridge" in item and pd.notna(rms):
            results["Lat. acc. (g)"] = rms / 9.81
        elif "bridge: sm" in item and pd.notna(rms):
            results["MSI (%)"] = rms

        # Deck Wetness (based on bow vertical motion)
        elif "bow: rel. vert. motion" in item and pd.notna(m0_val):
            results["bow_rel_m0"] = m0_val  # Save for Deck Wetness
            P_wet = math.exp(-((freeboard + 0.8) ** 2) / (2 * m0_val))
            results["Deck Wetness (%)"] = round(P_wet * 100, 2)

        # Slamming Probability (based on slamming location)
        elif "slamming: rel. vert. motion" in item and pd.notna(m0_val):
```

```
            results["slamming_rel_m0"] = m0_val
            term1 = (draft ** 2) / (2 * m0_val)
        elif "slamming: rel. vert. velocity" in item and pd.notna(m0_val):
            Vcr = 0.093 * math.sqrt(9.81 * loa)
            term2 = (Vcr ** 2) / (2 * m0_val)
            results["slamming_rel_m2"] = m0_val

    # Calculate Slamming Probability
    if "slamming_rel_m0" in results and "slamming_rel_m2" in results:
        term3 = term1 + term2
        P_slam = math.exp(-term3)
        results["Slamming Probability (%)"] = round(P_slam * 100, 2)
    else:
        results["Slamming Probability (%)"] = 0.0  # Default to 0 if missing

    # If Deck Wetness wasn't calculated, default to 0
    if "Deck Wetness (%)" not in results:
        results["Deck Wetness (%)"] = 0.0

    ski_value, penalties = compute_provisional_ski(results, provisional_max)
    return ski_value, penalties, results

# === Main Logic ===
try:
    ship_data_df = pd.read_excel(excel_file, sheet_name="ship_data")
    ship_data_df.columns = ship_data_df.columns.str.strip().str.lower()
    freeboard_val = ship_data_df.loc[0, "|opv|parameters|calculated|freeboard"]
    draft_val = ship_data_df.loc[0, "|opv|parameters|variables|draft"]
    loa_val = ship_data_df.loc[0, "|opv|parameters|variables|loa"]
except Exception as e:
    print(f" Could not read ship data: {e}")
    sys.exit(1)

ss6_ski_sum = 0.0
all_rows = []

for sheet in sheets_to_process:
    ski_value, penalties, raw_results = process_excel_sheet(
        sheet, excel_file, freeboard_val, draft_val, loa_val, provisional_max
    )
    ss6_ski_sum += ski_value
```

```
109
110     row = {"Sheet": sheet, "SKI": ski_value}
111     # Add raw results and penalties to the row
112     for key in provisional_max:
113         row[key] = raw_results.get(key, "N/A")
114         row[f"{key} Penalty"] = penalties.get(key.strip().lower(), "N/A")
115     all_rows.append(row)
116
117 # Compute combined SKI
118 combined_ski_ss6 = round(ss6_ski_sum / len(sheets_to_process), 3)
119
120 # Add combined SKI row
121 combined_row = {"Sheet": "Combined_SS6", "SKI": combined_ski_ss6}
122 for key in provisional_max:
123     combined_row[key] = "-"
124     combined_row[f"{key} Penalty"] = "-"
125 all_rows.append(combined_row)
126
127 # --- Save to CSV (fixed) ---
128 # Previously: output_df = pd.DataFrame([{combined_ski_ss6}]) -> malformed
129 output_df = pd.DataFrame(all_rows)
130 output_df.to_csv(output_csv, index=False)
131
132 sys.exit(0)
```

E

Hypervolume code

```python
# --- Cumulative HV across runs (constant reference point) ---

import numpy as np
import pandas as pd
import matplotlib.pyplot as plt
from pymoo.indicators.hv import HV

# Preconditions:
# - feasible_df exists (filtered)
# - ref_point_min exists (constant ref from LHS_OPV_4_8_02)

ref_min = np.asarray(ref_point_min, dtype=float)
hv_indicator = HV(ref_point=ref_min)

# Your run order (left-to-right on x-axis)
RUN_LIST = [
    "LHS_OPV_4_8_02", "dakota1_03",
    "SBGO_run_1_02","SBGO_run_1_04","SBGO_run_1_05","SBGO_run_1_07",
    "SBGO_run_1_08","SBGO_run_1_10","SBGO_run_1_11","SBGO_run_1_12",
    "SBGO_run_1_13","SBGO_run_1_15","SBGO_run_1_17","SBGO_run_1_20",
    "SBGO_run_1_21","SBGO_run_1_22","SBGO_run_1_23","SBGO_run_1_24",
    "SBGO_run_1_25","SBGO_run_1_26","SBGO_run_1_27",
    "OPV_norm_1_27","OPV_norm_1_28","OPV_norm_2_31","OPV_norm_2_32",
    "OPV_norm_2_33","OPV_norm_2_34","OPV_norm_2_35","OPV_norm_2_36","OPV_norm_2_37"
]
RUN_LIST = [r.lstrip("\\/") for r in RUN_LIST]
```

```
27
28  # Column detection
29  def find_col(df, cands):
30      for c in cands:
31          if c in df.columns:
32              return c
33      return None
34
35  RUN_COL = find_col(feasible_df, ["run","Run","RUN","seed","experiment","exp","Exp","EXP"])
36  if RUN_COL is None:
37      raise KeyError("Run column not found. Expected one of:
        ↪ run/Run/RUN/seed/experiment/exp/Exp/EXP")
38
39  # Prefer normalized objectives if present
40  OBJ_CANDIDATES = {
41      "SKI": ["SKI"],
42      "R_T": ["R_T_norm"],
43      "LWT": ["lightweight_norm"],
44      "SI":  ["SI"],
45  }
46  def choose_existing_cols(df, candidates_map):
47      chosen = {}
48      for key, cands in candidates_map.items():
49          for c in cands:
50              if c in df.columns:
51                  chosen[key] = c
52                  break
53          if key not in chosen:
54              raise KeyError(f"No column found for objective '{key}'. Tried: {cands}")
55      return chosen
56
57  col_map = choose_existing_cols(feasible_df, OBJ_CANDIDATES)
58  obj_cols = [col_map["SKI"], col_map["R_T"], col_map["LWT"], col_map["SI"]]
59
60  # Map to minimization space (+1 for min, -1 for max) in this order
61  senses = np.array([-1, +1, +1, -1], dtype=float)
62
63  def to_min_space(df, cols, senses_vec):
64      Y_raw = df[cols].apply(pd.to_numeric, errors="coerce").to_numpy(dtype=float)
65      return Y_raw * senses_vec
66
```

```python
# Build cumulative HV over runs
cum_df = pd.DataFrame(columns=feasible_df.columns)
x_labels, hv_values = [], []

for run_name in RUN_LIST:
    dfr = feasible_df.loc[feasible_df[RUN_COL].astype(str) == run_name].copy()
    if dfr.empty:
        print(f"  Skipping {run_name}: no feasible rows.")
        continue

    # Add all feasible points from this run to the cumulative pool
    cum_df = pd.concat([cum_df, dfr], ignore_index=True)

    # Compute HV of the cumulative pool in minimization space
    Y_min = to_min_space(cum_df, obj_cols, senses)
    good = np.all(np.isfinite(Y_min), axis=1)
    Y_min = Y_min[good]
    hv_val = float(hv_indicator.do(Y_min)) if Y_min.shape[0] else np.nan

    x_labels.append(run_name)
    hv_values.append(hv_val)

# Plot to match your style
plt.figure(figsize=(12,5))
plt.plot(range(len(hv_values)), hv_values, marker="o")
plt.xticks(range(len(x_labels)), x_labels, rotation=70, ha="right")
plt.xlabel("Cumulative file")
plt.ylabel("Hypervolume")
plt.title("HV Convergence (constant ref = worst + 10%)")
plt.grid(True, alpha=0.3)

# Optional: tighten y-lims with a small margin
if len(hv_values) > 0 and np.isfinite(hv_values).any():
    ymin = np.nanmin(hv_values)
    ymax = np.nanmax(hv_values)
    pad = 0.002 * (ymax - ymin if ymax > ymin else 1.0)
    plt.ylim(ymin - pad, ymax + pad)

plt.tight_layout()
plt.show()
```

F

Results from Optimization

F.1. GM/B vs IMO requirements

For completeness, Figure F.1 presents the generated design set evaluated against the IMO 2008 Intact Stability Code (Part B, Ch. 2). The individual panels correspond to criteria 221a–224. In all cases, designs with $GM/B > 0.05$ satisfy the respective IMO thresholds, confirming that the adopted lower bound is a suitable constraint for statutory compliance. However, the plots also demonstrate that while IMO criteria filter out only a small number of candidates, they do not address the dynamic stiffness effects visible in the main results (see Section 7.1). This underlines the added value of applying a direct roll-period constraint.

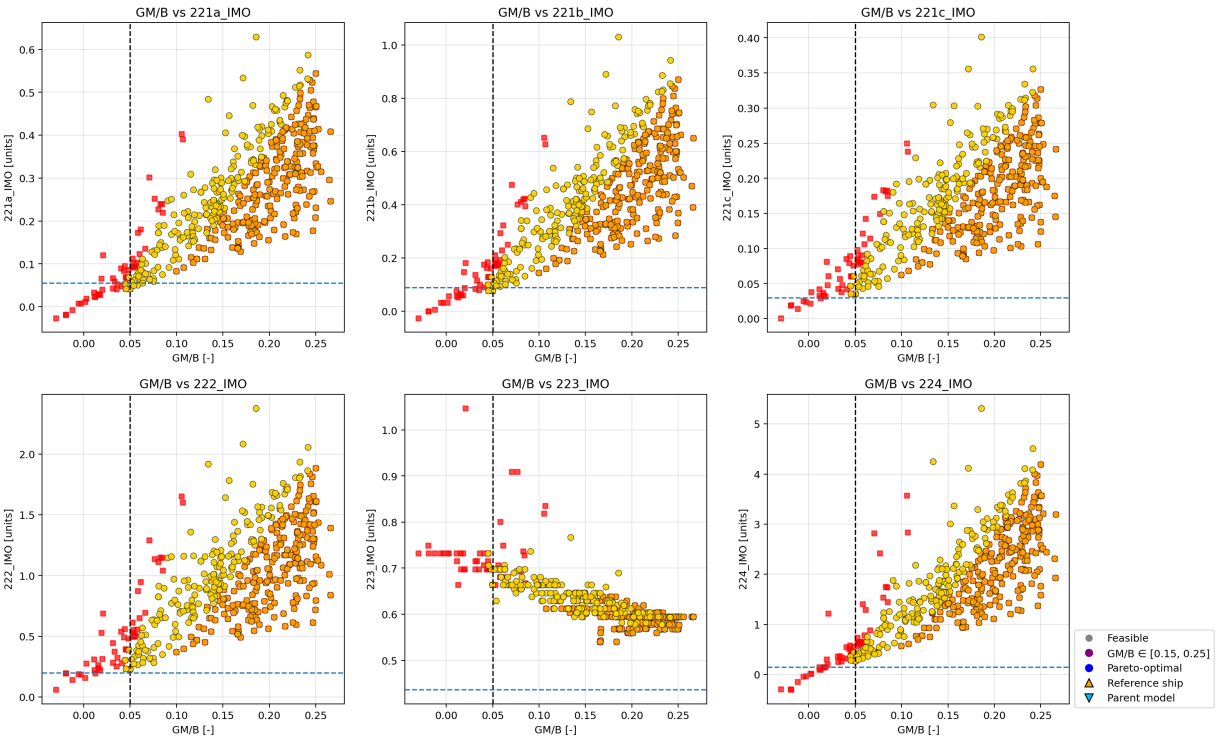

Figure F.1: Evaluation of candidate designs against IMO intact stability criteria (221a–224). All designs with $GM/B > 0.05$ comply with statutory thresholds, confirming that this bound is suitable for regulatory purposes. However, IMO compliance alone does not ensure realistic dynamic behaviour, justifying the use of roll-period constraints in the main analysis.

F.1.1. Principal variables vs objectives

This section provides supporting plots linking principal design variables (length, beam, draft) to the four main objectives (resistance R_T, lightweight LWT, stability index SI, and seakeeping index SKI). These figures complement the trend analysis in Section 7.3 by showing the raw pairwise relations across the feasible design set.

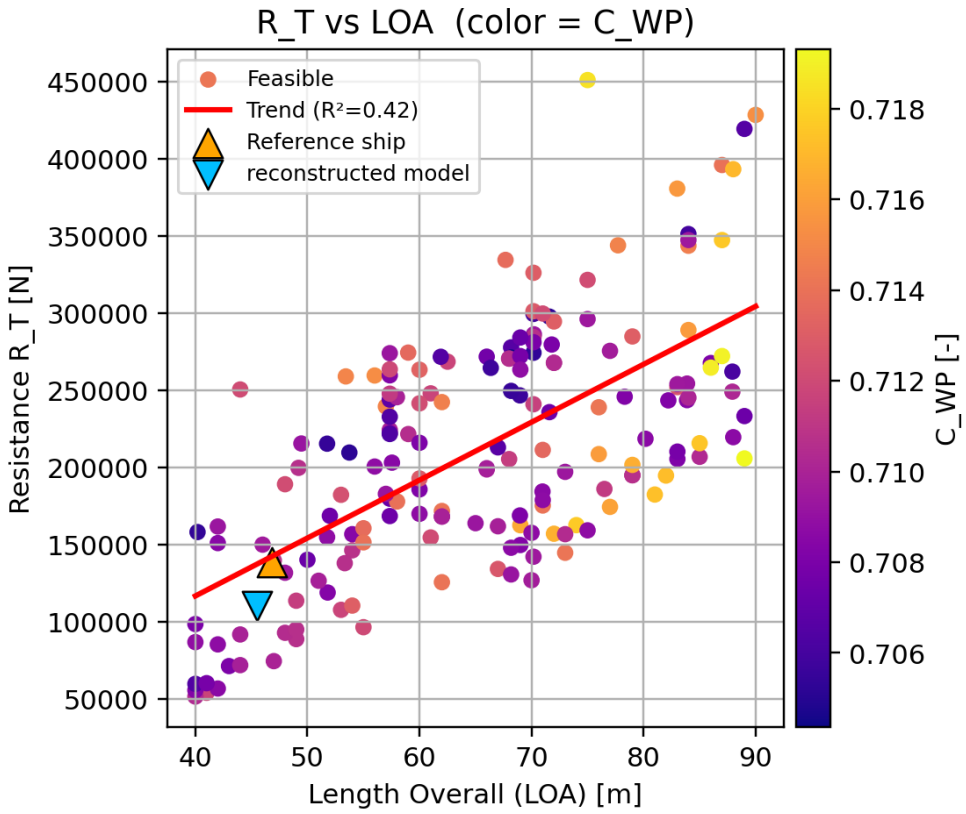

Figure F.2: Total resistance R_T versus length overall L_{OA}; colour indicates waterplane coefficient C_{WP}. At fixed speed, increasing L_{OA} changes slenderness and displacement, affecting both wave-making and frictional components.

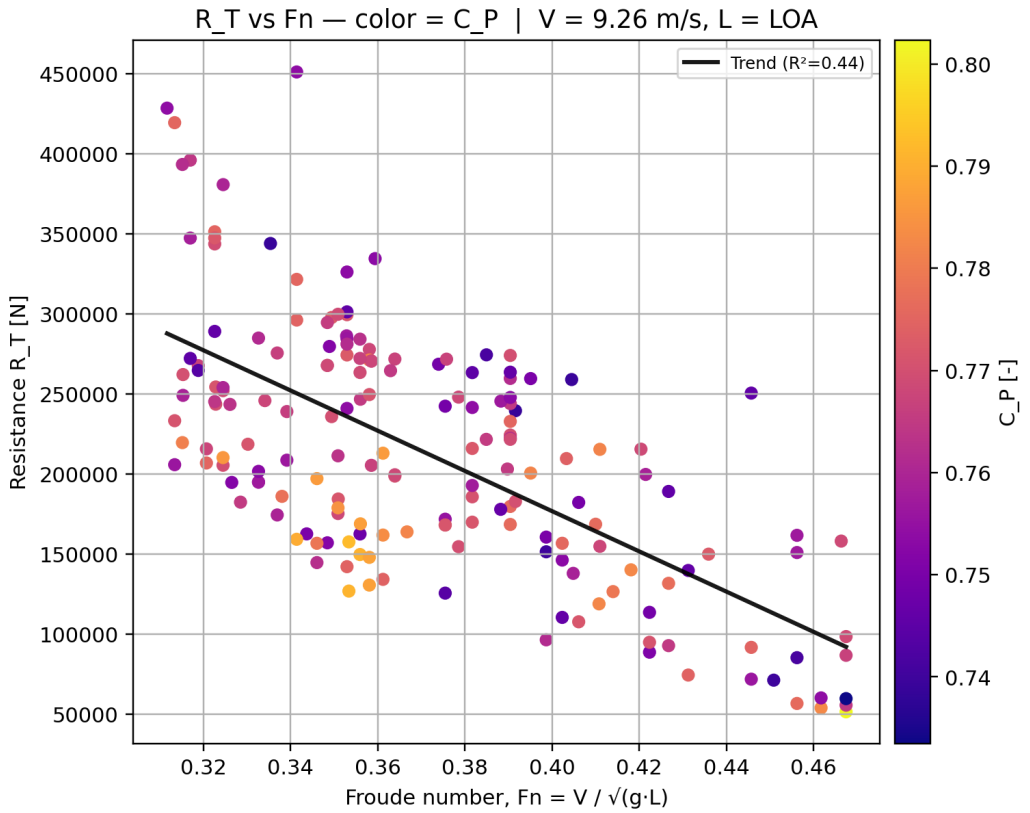

Figure F.3: Total resistance R_T versus Froude number $\mathrm{Fn} = V/\sqrt{g\,L}$ at $V = 9.26$ m s^{-1} (18 kn), with $L = L_{OA}$. Colour indicates prismatic coefficient C_P. At fixed speed, increasing L lowers Fn and is generally associated with reduced R_T (slenderness effect); the colour scale highlights the spread due to volumetric distribution (C_P). The line shows the fitted linear trend (legend reports R^2).

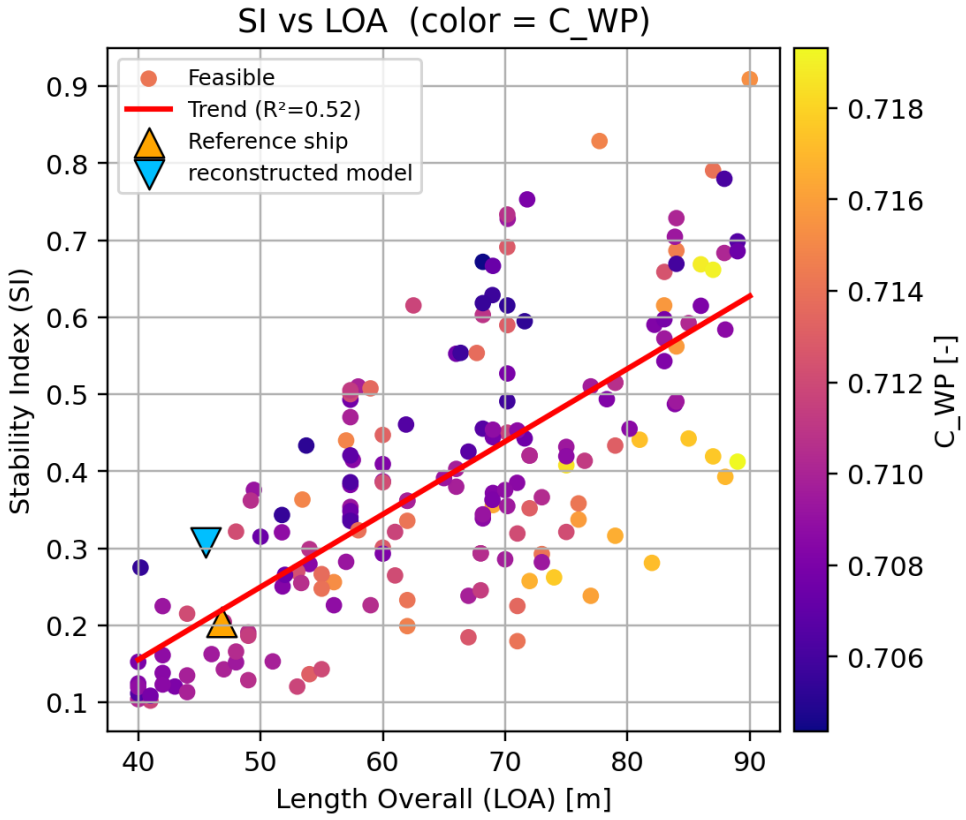

Figure F.4: Stability index (SI) versus length overall L_{OA}, colour indicates C_{WP}. Increasing length tends to improve SI, though effects are partly masked by displacement variations.

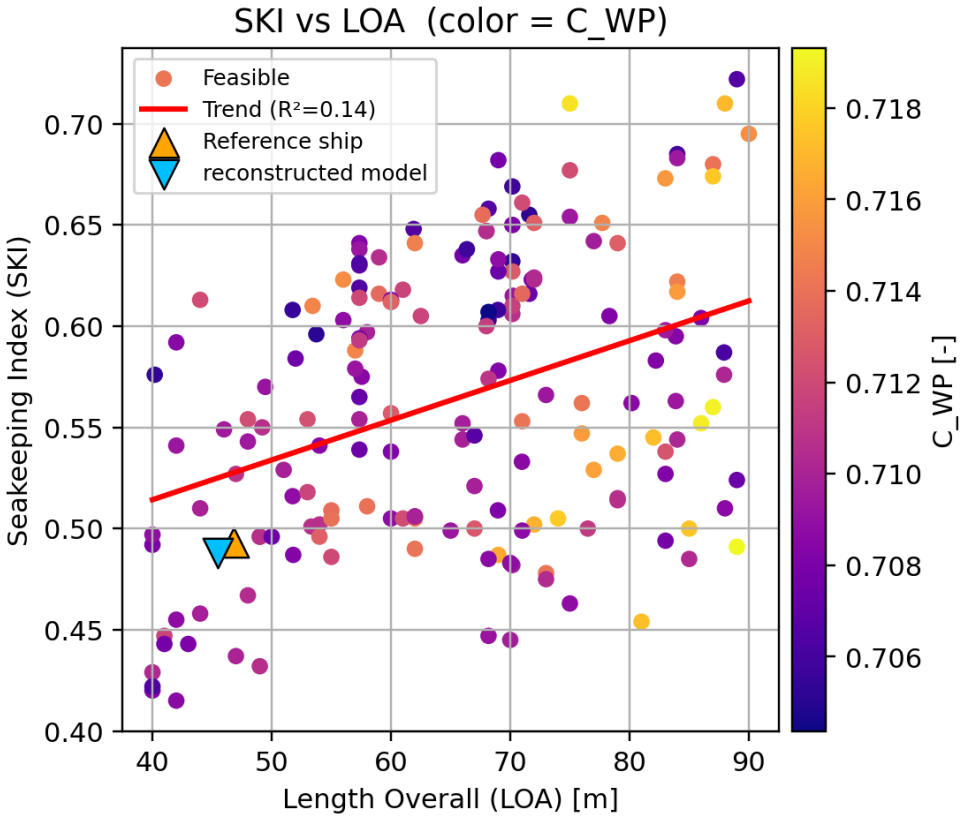

Figure F.5: Seakeeping index (SKI) versus length overall L_{OA}, colour indicates C_{WP}. Longer vessels generally achieve improved SKI, though displacement scaling partly masks the independent effect of L_{OA}.

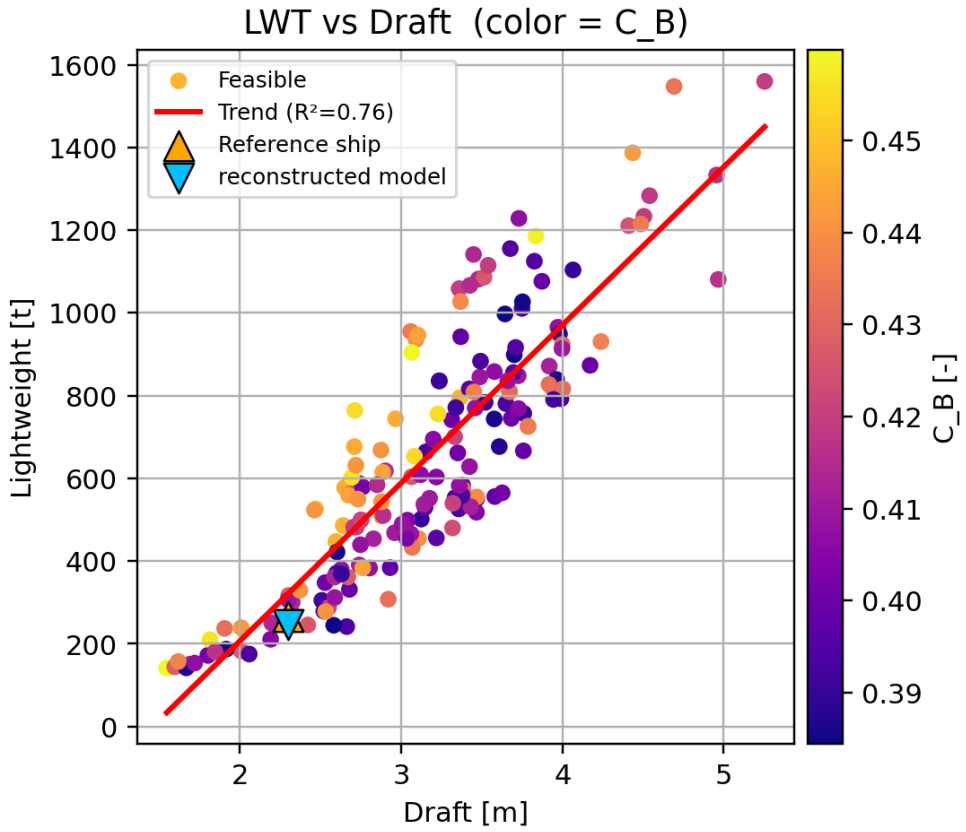

Figure F.6: Lightweight (LWT) versus draft, colour indicates C_B. Deeper drafts correspond to larger displacement and therefore higher LWT, though the effect is partly moderated by form coefficient variations.

G

Correlation Heatmap (Pearson)

G.1. Code (Python)

Dependencies: NumPy [79], pandas [80], Matplotlib [81], Seaborn [82].

```python
# === Heatmap: Objectives vs Particulars, Coefficients & Ratios (incl. L/B, B/T, Range) ===
import numpy as np
import pandas as pd
import matplotlib.pyplot as plt

# Try seaborn for the heatmap; fallback if missing
try:
    import seaborn as sns
    _HAS_SNS = True
except Exception:
    _HAS_SNS = False

# ---------- pick source DF ----------
D = (feasible_df if "feasible_df" in globals() and isinstance(feasible_df, pd.DataFrame)
     else df if "df" in globals() and isinstance(df, pd.DataFrame)
     else None)
if D is None:
    raise NameError("Need feasible_df or df in scope.")
D = D.copy()

# ---------- helpers ----------
def _num(s): return pd.to_numeric(s, errors="coerce")
```

```python

def _find_range_col(dframe: pd.DataFrame):
    for c in dframe.columns:
        lc = str(c).strip().lower()
        if lc in {"range"} or "range" in lc:
            return c
    return None

# ---------- ensure R_T_plot (Newtons) ----------
RT_FACTOR = globals().get("RT_FACTOR", 557125.1)  # R_T_norm -> R_T [N]
if "R_T_plot" not in D.columns:
    if "R_T_norm" in D.columns:
        D["R_T_plot"] = _num(D["R_T_norm"]) * RT_FACTOR
    elif "R_T" in D.columns:
        D["R_T_plot"] = _num(D["R_T"])

# ---------- add derived ratios: L/B and B/T (if inputs exist) ----------
if {"LOA","Beam"}.issubset(D.columns):
    L = _num(D["LOA"]); B = _num(D["Beam"])
    with np.errstate(divide="ignore", invalid="ignore"):
        D["L_over_B"] = (L / B).where(np.isfinite(L) & np.isfinite(B) & (B != 0))

if {"Beam","Draft"}.issubset(D.columns):
    B = _num(D["Beam"]); T = _num(D["Draft"])
    with np.errstate(divide="ignore", invalid="ignore"):
        D["B_over_T"] = (B / T).where(np.isfinite(B) & np.isfinite(T) & (T != 0))

# ---------- add Range (nm) as an objective if present ----------
rng_col = _find_range_col(D)
if rng_col is not None:
    D["Range_nm"] = _num(D[rng_col])  # assumes the stored unit is nautical miles

# ---------- define sets ----------
# Objectives (only keep those that exist)
OBJECTIVES_CAND = ["SKI", "SI", "R_T_plot", "LWT", "Range_nm"]  # <-- added Range
OBJECTIVES = [c for c in OBJECTIVES_CAND if c in D.columns]
if not OBJECTIVES:
    raise KeyError("No objectives found among: " + ", ".join(OBJECTIVES_CAND))

# Main particulars & coefficients (+ ratios)
FEATURES_CAND = [
```

```
    "LOA","LWL","Beam","Draft","Deadrise","rake_angle",
    "C_P","C_B","C_M","C_WP","GM_B",
    "L_over_B","B_over_T"
]
FEATURES = [c for c in FEATURES_CAND if c in D.columns]
if not FEATURES:
    raise KeyError("No features found among: " + ", ".join(FEATURES_CAND))

# ---------- numeric matrix ----------
USE_COLS = OBJECTIVES + FEATURES
X = D[USE_COLS].apply(_num, axis=0).dropna(how="all")

# ---------- correlations (Pearson) ----------
corr = X[OBJECTIVES + FEATURES].corr(method="pearson")
corr_obj_feat = corr.loc[OBJECTIVES, FEATURES]

# ---------- plot: Pearson heatmap ----------
fig, ax = plt.subplots(figsize=(1.2*len(FEATURES)+2.5, 0.9*len(OBJECTIVES)+2.5),
↪  constrained_layout=True)

if _HAS_SNS:
    sns.heatmap(
        corr_obj_feat, ax=ax, annot=True, fmt=".2f",
        vmin=-1, vmax=1, center=0, cmap="coolwarm",
        linewidths=0.4, linecolor="white", cbar_kws={"label": "Pearson r"}
    )
else:
    im = ax.imshow(corr_obj_feat.values, cmap="coolwarm", vmin=-1, vmax=1, aspect="auto")
    ax.set_xticks(range(len(FEATURES))); ax.set_yticks(range(len(OBJECTIVES)))
    ax.set_xticklabels(FEATURES, rotation=45, ha="right"); ax.set_yticklabels(OBJECTIVES)
    for i in range(corr_obj_feat.shape[0]):
        for j in range(corr_obj_feat.shape[1]):
            ax.text(j, i, f"{corr_obj_feat.values[i, j]:.2f}",
                    ha="center", va="center", color="black", fontsize=9)
    cbar = fig.colorbar(im, ax=ax, pad=0.02); cbar.set_label("Pearson r")

ax.set_title("Objectives vs Particulars, Coefficients & Ratios (incl. L/B, B/T, Range) -
↪  Pearson")
try:
    _save_fig(fig, "heatmap_objectives_vs_particulars_coeffs_ratios_range_pearson")
except Exception:
```

```
103         pass
104 plt.show()
```